Republic of Iraq
Ministry of Higher Education
and Scientific Research
University of Babylon
College of Science
Department of Physics

Effect of Acceptor and Donor Molecules on Some Physical Properties of Graphene Nanoribbon

A Thesis

Submitted to the College of Science , University of Babylon in Partial Fulfillment of the Requirements for the Degree of Master of Science /Science of Physics

By

Rabab Abd Al-Zahrah Muslim Abdullah

Supervised by

Asst.Prof. Dr. ***Nidhal Mohammed O. AL-Shareefi***

Prof. Dr. ***Hamid Ibrahim A. Al-Tamimi***

1443 H.D 2021A.D

بسم الله الرحمن الرحيم

﴿ يرفع الله الذين امنو منكم والذين أوتوا العلم

درجات والله بما تعملون خبير ﴾

صدق الله العلي العظيم

سورة المجادلة :الآية (١١)

Supervisor Certification

We certify that this thesis entitled (***Effect of Acceptor and Donor Molecules on some Physical Properties of Graphene Nanoribbon)***, will be prepared by **(Rabab Abdul-Zahrah Muslim Abdulla)** under our supervisions at Department of Physics, College of Science, University of Babylon as a partial requirement for the degree of Master of Science in Physics.

Signature:

Supervisor: Dr. Nidhal Mohammed O. A Shareefi
Title: Asst. Professor
Address: Department of Physics
College of Science-University of Babylon

Date: / / 2021

Signature:

Supervisor:Dr.Hamid Ibrahim Abbood Al-Tamimi
Title: Professor
Address: Department of Physics
College of Education -University of Al-zahraa for girls

Date: / / 2021

Certification of the Head of the Department

In view of the available recommendation, I forward this thesis for debate by the examination committee.

Signature:

Name: Prof. Dr. Abdulazeez O. Mousa Al-Ogaili

Title: Professor

Address: Head of the Department of Physics

College of Science - University of Babylon

Date: / /2021

Examining Committee Certificate

We certify that we have read this thesis entitled " **Effect of Acceptor and Donor Molecules on some Physical Properties of Graphene Nanoribbon** " and, as an examining Committee, examined the student " **Rabab Abdul-Zahrah Muslim Abdulla** " in its content and that, in our opinion it meets the standards of a thesis for the degree of Master of Science of Physics.

Signature:

Name: Dr. Rabab Saadon Abdoon
Title: Professor
Address: Department of Physics-College for Science- University of Babylon
Date : / / 2021
(Chairman)

Signature:

Name: Dr. Rajaa K. Mohammad
Title: Assistant Professor
Address: Department of Physics-College of Science-University of Karbala
Date : / / 2021
(Member)

Signature:

Name: Dr. Hussein Hakim Abed
Title: Assistant Professor
Address: Department of Physics-College of Science-University of Babylon
Date : / / 2021
(Member)

Signature:

Name: Dr. Nidhal Mohammed O. Al Shareefi
Title: Asst. Professor
Address: Department of Physics College of Science- University of Babylon
Date : / / 2021
(Member and Supervisor)

Signature:

Dr.Hamid Ibrahim Abbood Al-Tamimi
Title: Professor
Address: Department of Physics College of Education -University of Al-zahraa for girls
Date: / / 2021
(Member and Supervisor)

Approved by the College committee on graduate studies

Signature:

Name: Dr. Enas M . Al-Robayi
Title: Professor
Address: Dean of the College of Science-University of Babylon
Date: / / 2021

Acknowledgments

First I should like to express my deep thanks to the Almighty God, **ALLAH JALA JALALAH**, for what I have become.

I would like to express my deep gratitude and appreciation to my supervisors, **Prof. Dr. Hamid Ibrahim Abbood and Asst.Prof.Dr .Nidhal Mohammed O. AL-Shareefi** for suggesting the topic of the thesis, and continuing advice and guidance throughout this work.

I would like to express my deep appreciation to all members of my family for their material and spiritual support.

I am grateful to the Dean of the College of Science and the chairman Department of Physics for their help.

Rabab

Dedication

To…

the master of creation.... our Prophet Muhammad (Allah Blessing and Peace be upon him and his household)

To…

Light that illuminates my path of success ….

Dear father

To…

the spring of tenderness, she surrounded me with the wall of her tenderness and humiliated me with her prayers...

my dear mother

To…

the beat of my heart... and I have Adnan

To my brothers and sisters with great love

To…

the one who bore the burdens with me and kept supporting me and my life companion... my husband

To…

everyone who taught me a letter, encouraged me, and with his knowledge benefited me... I dedicate this humble effort

Rabab

Summary

The present study focuses on the study of the effect of different acceptor and donor molecules on the structural and physical properties of graphene nanoribbon (GNR) that are designed according to Aviram-Ratner model to estimate the electronic applications for the new designed structures. All the calculations were carried out by employing the functional B3LYP density functional theory with standard 6-31G basis sets.

The donors and acceptors have different values of energy gap (Eg) depending on the type of each of them. Some electronic properties such as ionization energy (IE), electron affinity (EA), softness (S), hardness (H), and electrophilic index (W) were calculated for the studied Donors, Acceptors and GNR.

Various values of ionization energy and electron affinity for the donors and acceptors under study provide the permittivity to construct the Donor-GNR-Acceptor systematically. Several structures of Donor-GNR-Acceptors were constructed. The choice of both donor and acceptor is based on the behavior for each one .

The results showed that GNR has the largest value of the energy gap compared with the designed Donor-GNR-Acceptor structures, All studied Donor-GNR-Acceptor molecules have values of electron affinity higher than for the base GNR. The variant of energy gap and electron affinity for the structures leads to different applications in electronic field.

The results showed that the hardness decreased when adding the donor and acceptor molecules to the graphene nanoribbon, in other

words, the constructed Donor-GNR-Acceptor molecules are more soft than the GNR.

The electrophilic index increased by adding the donors and acceptors molecules. The results indicated that the constructed Donor-GNR-Acceptor molecules have high activity to interact with other molecules or species in the surroundings compared with the GNR.

The effect of the presence of both donors and acceptors on the distribution of the Electrostatic Potential (ESP) was clear where, the electrostatic potential was dragged towards the areas of high concentration of charges in each Donor-GNR-Acceptor molecules. We noted that , the dipole moment for GNR is zero while the other structures have different values of dipole moment in which refers to their low symmetric distribution these structures have, and this give Doner-GNR-Acceptor structures high ability to an electron transfer in comparison with the base GNR.

As for the sensing of the graphene nanoribbon acceptor for the gas donor, the results indicate that the two structures have different energy gap and other electronic properties. This difference allows determining which of these two structures can perform in the field of reducing materials. It was noted that the sensitivity of the Donor-GNR1-Acceptor structure was low. The result also showed that the electronic transitions are almost indirect transitions in the range of visible and ultraviolet rays of electromagnetic radiation.

Contents

List of Symbols

Symbol	*Meaning*
Ψ	Wave function
$\hat{H}$	Hamiltonian operator
E	Total energy of the system
∇^2	The Laplacian operator
T	Kinetic energy of the electrons and the nuclei
V	Potential energy components
$\hat{T}_e$	Electronic kinetic energy operator
$\hat{T}_n$	Nuclear kinetic energy operator
$\hat{V}_{ne}$	The attractive interactions operator between nuclei and electrons
$\hat{V}_{ee}$	The repulsive interactions operator between the electron
$\hat{V}_{nn}$	The repulsive interactions operator between the nuclei
$Z_{A,B}$	The nuclei charge of atoms A and B
m_A	The mass of atom A
r_{AB}	The distance between nuclei A and B
r_{iA}	The distance between nucleus A and electron i
r_{ij}	The distance between electrons i and j
E_Φ	The lowest-energy eigen value
Φ	Trial function
E_0	The ground-state energy
α	Spin up
β	Spin down
F	Fock operator
j_i	The coulomb operator
k_i	The exchange operator
$C_{\mu i}$	The molecular orbital expansion coefficients
φ_i	Basis functions
ε_i	One-electron energy
ψ_i	Molecular orbital
$S_{\mu\upsilon}$	The overlap integral for atomic function μ and υ
$F_{\mu\nu}$	The elements of Fock matrix
$H_{\mu\nu}^{core}$	Core Hamiltonian

Symbol	***Meaning***
$P_{\lambda\sigma}$	The density matrix
$\mu\nu/\lambda\sigma$	The two-electron repulsion integral
$P_{\mu\nu}$	The density matrix
N	Normalization factor
Y_{im}	Angular function
ξ	Orbital exponent
M	Number of Gaussian primitives
$\rho(r)$	Electron density
K	Chemical potential
F_{HK}	Universal functional of the electron density
V_{ext}	External potential
$T[\rho]$	Kinetic energy of system
$E_{xc[\rho]}$	Exchange-correlation energy
$v_{xc}[\rho]$	Exchange-correlation potential
ε_{XC}	Exchange-correlation energy per particle
ε_c	The correlation energy
E_{gap}	Energy Gap
E_{LUMO}	the lowest unoccupied molecular orbital
E_{HOMO}	the highest occupied molecular orbital
IE	Ionization Energy
EA	Electron Affinity
E_{total}	Total Energy
K	Chemical Potential
E_F	Fermi energy
H	Chemical Hardness
S	Chemical Softness
W	Electrophilicity
μ	The total dipole moment

List of Tables

List of Figures

Chapter One
General Introduction and Literature survey

1.1 Introduction

Organic materials attracted a lot of attention in recent years due to their application diversity. It can be observed that organic molecules give up a lot of possibilities for materials research in terms of creating custom designer materials with features that closely mimic the predicted or actual behavior of individual molecules at the macroscopic and microscopic levels [1,2].

The field of functional organic materials is rapidly increasing, with the potential to replace outdated materials with newer, cheaper, and better performing materials as well as introduce new uses in the near future The successful creation of two-dimensional graphene, silicone, and germaneness has received a lot of attention due to their potential for applications in a range of disciplines [3,4].

Nanotechnology (or "nanotech") is the utilization of atomic, molecular, and supramolecular sizes for industrial applications [4,5]. The National Nanotechnology Initiative later adopted a more broader definition of nanotechnology, defining it as the manipulation of matter with at least one dimension sized between 1 and 100 nanometers [6].

Due to quantum mechanical effects are important at this quantum-realm scale, the definition has shifted from a specific technological goal to a research category that encompasses all types of research and technologies concerned with the special properties of matter that occur below the given size threshold. As a result, the plural form "nanotechnologies" as well as "nanoscale technologies" are frequently used to refer to a wide range of research and applications with a common characteristic of small size [5,6]. For its interesting features and

technological potential, the latest discovery of graphene, a single atomic plane of graphite, has piqued curiosity [7].

Graphene excellent carrier mobility and extended spin diffusion width allow for the development of promising graphene-based electronics and spintronic [7,8].

1.2 Graphene Nanoribbon

Graphene is a two-dimensional (2D) carbon allotrope. Carbon atoms are organized in a hexagonal arrangement in this substance. A single sheet of graphene is made up of a single layer of carbon atoms arranged in a honeycomb pattern. Multi-layer for graphene is made up of multiple sheets that are stacked one on top of the other until they form graphite. The three-dimensional crystal graphite is formed up of weakly connected graphene layers [9,10].

In graphene, each carbon atom is covalently connected to three other carbon atoms. Because of the strength of the covalent bonds between carbon atoms, graphene is very stable and has a high tensile strength (the force in which you can stretch something before it breaks). Because graphene is flat, every atom is on the surface and accessible from all sides, allowing for more interaction with molecules around it [8]. Furthermore, the carbon atoms are only connected to three other atoms, despite the fact that they have the ability to bond to a fourth. This aptitude, graphene's high surface area to volume ratio, paired with its tensile strength, may make it appealing for application in composite materials [11]. Graphene also has the highest electron mobility of any material known, and many studies were achieved to introduce methods to this characteristic in electronics [12,13].

Due to there was an entire community of researchers working on related materials, such as graphite, fullerenes, and carbon nanotubes, graphene was quickly recognized as a fascinating material. All of these materials (graphite = stacked graphene, fullerenes = wrapped graphene, nanotubes = rolled graphene – see Figure 1.1) are related to graphene.

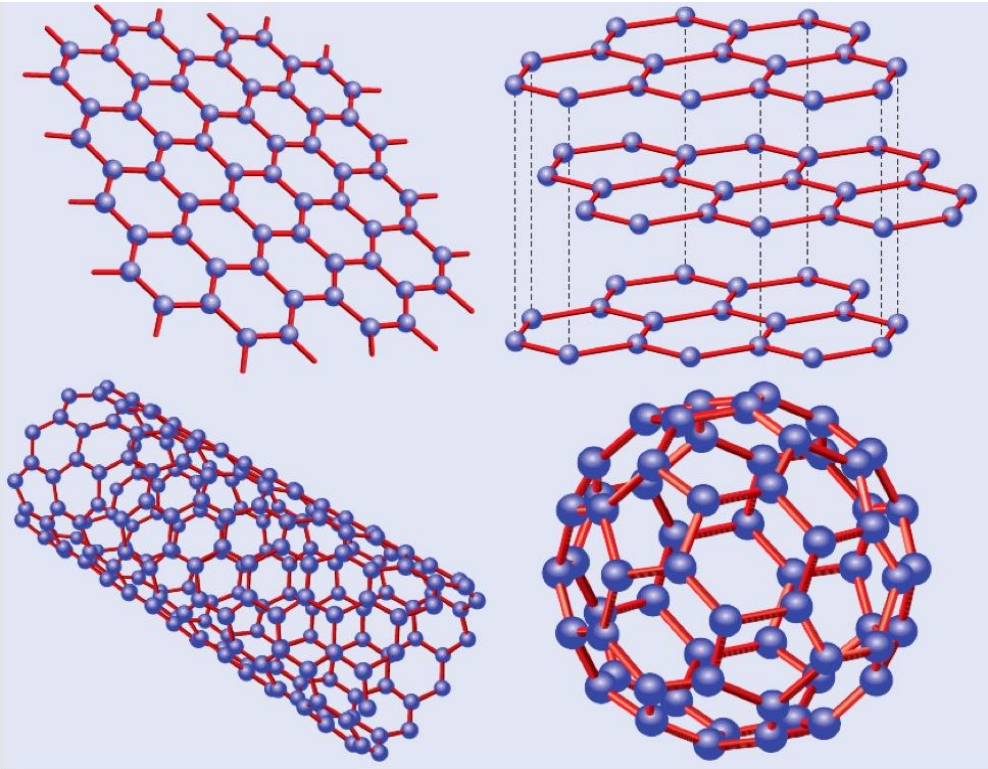

Figure (1.1): Graphene and its descendants: top right: graphene; top left: graphite = stacked graphene; bottom left: nanotube=rolled graphene; bottom right: fullerene=wrapped graphene (adapted from ref.[9]).

One of the first and most well-known instances of a two-dimensional crystal is graphene. In many aspects, two-dimensional materials and systems differ from three-dimensional materials and systems. Since its discovery in 2004, graphene has attracted a lot of academic interest as a model system for understanding two-dimensional physics and chemistry in general. It also thought to offer a lot of potential for a variety of applications [12,13].

When scientists isolated individual graphene sheets from mechanically cleaved graphite recently, they discovered remarkable electrical characteristics resulting from electron confinement in two dimensions. Researchers are rapidly approaching the goal of generating process able graphene [15,16].

Edge trapping of bonding electrons and the electron polarization are important in carbon-based nanomaterials because they can change the density of states and band gap. The electrical characteristics of graphene nanoribbons (GNRs) can also be affected by chemical edge changes. The edges of GNR are typically passivated with hydrogen atoms in order to investigate its intrinsic features [14]. Graphene nanoribbons (GNRs) are graphene strips with a width of less than 100 nanometers. Differing geometrical terminations of the graphene monolayer provide two distinct edge geometries, zigzag and armchair graphene, with vastly different electrical properties [17].

The edge structures have a big influence on the electrical states of GNRs (armchair or zigzag). Each subsequent edge segment of a zigzag edge is at an angle to the previous one. Each pair of segments in the armchair edges is a 120/-120 degree rotation of the previous pair. The edge localized state with non-bonding molecular orbitals approaching the fermi energy is provided by zigzag edges. Quantization is likely to result in significant changes in optical and electrical properties [18].

GNRs have a wide range of electronic properties, ranging from standard semiconductors to spin-polarized half metals, thanks to their diverse edge configurations, allowing them to be used as electric devices. Because GNRs have a high surface-to-volume ratio and unique edge

states, their characteristics can be altered using a variety of techniques, including doping and adsorption [19].

As finite-size models of ZGNRs, Figure 1.2 depicts a succession of Polycyclic Aromatic Hydrocarbons (PAHs). The zigzag edges on both sides of the ZGNRs studied are width = m (in the armchair direction) and width = n (in the zigzag direction) [19].

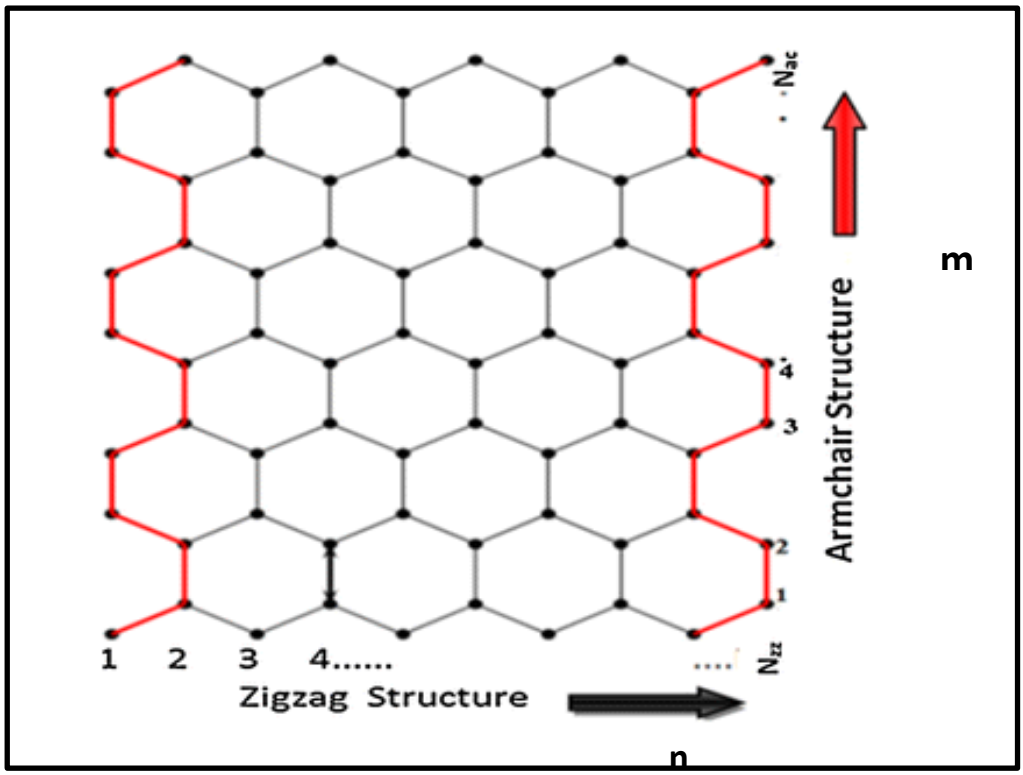

Figure (1.2): Types of graphene structures [19].

1.3 Donor and Acceptor Molecules

Donor impurity atoms contain more valence electrons than the atoms they replace in the intrinsic semiconductor lattice. Donor impurities "donate" their extra valence electrons to the conduction band of a semiconductor, providing extra electrons to the intrinsic semiconductor. Excess electrons raise the electron carrier concentration (n_0), creating the semiconductor n-type [1].

In the intrinsic semiconductor lattice, acceptor impurity atoms have less valence electrons than the atoms they replace. They "accept" electrons from the valence band of the semiconductor. The intrinsic semiconductor receives more holes as a result of this. Excess holes raise the semiconductor's hole carrier concentration (p+), resulting in a p-type semiconductor [2].

In semiconductor physics, an acceptor is a dopant atom that can form a p-type area when added to a semiconductor, these types of materials as shown in the Figure (1.3) [20].

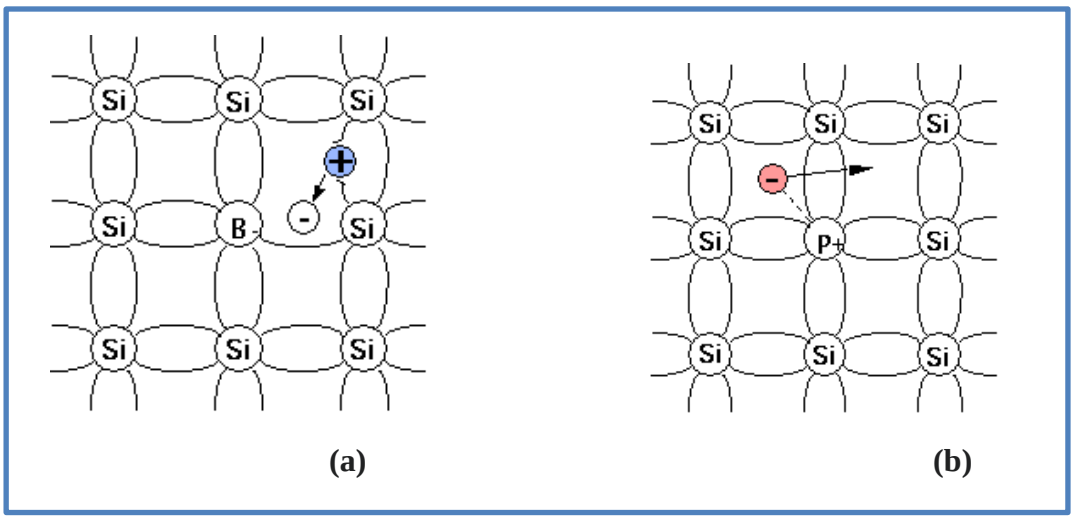

Figure (1.3): (a) Boron atom acting as an acceptor in the simplified 2D silicon lattice, (b) Phosphorus atom acting as a donor in the simplified 2D silicon lattice [20].

For example, silicon (Si), has four valence electrons, needs to be doped as a p-type semiconductor, elements from group III like boron (B) or Aluminum (Al), having three valence electrons, can be used. The latter trivalent impurities are another name for elements. Indium (In) and gallium (Ga) are two more trivalent dopants [21].

The three valence electrons of boron make covalent connections with three of the Si neighbors when substituting for a Si atom in the

crystal lattice, but the link with the fourth neighbor remains unfulfilled. The acceptor, which was previously electro-neutral, becomes negatively charged (ionized) [22]. The electrons from surrounding bonds are drawn to the unsatisfied bond. An electron from an adjacent bond will jump to repair the unsatisfied bond at normal temperature, leaving a hole (a place where an electron is deficient) [23].

To repair this dissatisfied bond, the hole will attract an electron from an adjacent bond. As a result of this chain-like mechanism, the hole moves around the crystal, carrying a current and so acting as a charge carrier [24]. A donor is a dopant atom in semiconductor physics that, when introduced to a semiconductor, can generate an n-type area [25].

When Si with four valence electrons needs to be doped as an n-type semiconductor, elements from group V such as phosphorus (P) or arsenic (As) with five valence electrons can be utilized. A pentavalent impurity is a dopant that has five valence electrons. Antimony (Sb) and bismuth (Bi) are two more pentavalent dopants [26].

Four of the valence electrons of phosphorus form covalent bonds with nearby Si atoms when a Si atom is substituted in the crystal lattice, but the fifth one stays weakly bonded. The donor, which was previously electro-neutral, becomes positively charged (ionized). The fifth electron is liberated at normal temperature, allowing it to wander around the Si crystal and carry a current, and therefore acting as a charge carrier [26,27].

1.4 Graphene Applications

Graphene is a carbon-based material that is comparable to graphite but has properties that make it extremely light and strong. A sheet of graphene measuring one square meter weighs 0.77 milligrams. Its tensile

strength is 200 times that of steel, and its density is comparable to carbon fiber. All of this allows it to withstand large bending pressures without cracking. It is one of the most electrically and thermally conductive materials, making it ideal for electronics and a variety of other sectors. Its uses are essentially limitless, and it has the potential to transform a wide range of fields, including electronics, computing, building, and even health [28,29].

Graphene is a game-changing substance that has the potential to open up new industries and perhaps replace existing technologies and materials. The whole potential of graphene may be realized when it is employed both to improve existing materials and to transform them. Transportation, medical, electronics, energy, military, and desalination are the most common use sectors [30].

Modify the structure and properties of graphene where, given the wide spectrum of industries where graphene research is having a significant influence, "No other material has properties as similar to graphene," says an international research team, which has proven a revolutionary method for modifying graphene's structure and properties. This method depended on a chemical reaction known as photocycloaddition, which uses ultraviolet (UV) light to modify the bonds between atoms [30].

- **Enhance the strength of other Materials:**

Graphene is the world's strongest substance, and it can be used to make other materials stronger. Adding even a trace amount of graphene to plastics, metals, or other materials can make them much stronger - or lighter. These graphene-enhanced composite materials can be used in

aerospace, building materials, mobile devices, and a variety of other applications [30].

- **Thermal Applications:**

Graphene is the most heat conducting material ever discovered. Due to graphene is both strong and light, it's an excellent material for heat-spreading applications like heat sinks and heat dissipation films. This could be beneficial in both microelectronics and mobile devices, such as thermal foils [30].

- **Graphene Can Boost the Nonlinear Generation of Light**:

Structures created around a single layer of graphene allow for powerful optical nonlinearities that can convert light, according to an international research team lead by the University of Vienna. The findings are expected to pave the way for the development of a new class of ultra-small tunable nonlinear devices [30].

- **Covid-19 and Graphene:**

The graphene market and industry have been severely impacted by the Coronavirus outbreak. Graphene has already attracted a lot of attention before the pandemic because of its promising antibacterial characteristics and established antiviral potency. However, the recent urgency to put these traits to good use in combating the Coronavirus cannot be denied [30]. The pneumonia outbreak of coronavirus disease 2019 (COVID-19) represents a global issue. The dimensional material graphene has captured much attention due to promising antimicrobial applications and has also demonstrated antiviral efficacy. In response to this global outbreak, we summarized the current state of knowledge of graphene and virus interaction as well as possible successful applications to fight COVID-19. Antibody-conjugated graphene sheets can rapidly detect targeted virus

proteins and can be useful for large population screening, but also for the development of environmental sensors and filters, given the low cost of graphene materials. Functionalized graphene has demonstrated a good viral capture capacity that, combined with heat or light-mediated inactivation, could be used as a disinfectant. Graphene sensors arrays can be implemented on standard utility textiles and drug efficacy screening. Thanks to its high versatility, we foresee that graphene may have a leading role in the fight against COVID-19 [110].

1.5 Aviram and Ratner Model

Aviram and Ratner proposed the first theoretical prediction to manufacture electrical devices using single molecules in 1974, demonstrating that rectification characteristics can be achieved with a single organic molecule .

The Aviram-Ratner molecular rectifier consists of two parts, the donor and the acceptor connected by a bridge part, as shown in Figure (1.4-a). The donor and the acceptor parts in the molecule are isolated by presence of a bridge in the structure. In molecular rectifier, it is required for the donor to have a low ionization energy and the acceptor has to show a high electron affinity [31].

(a)

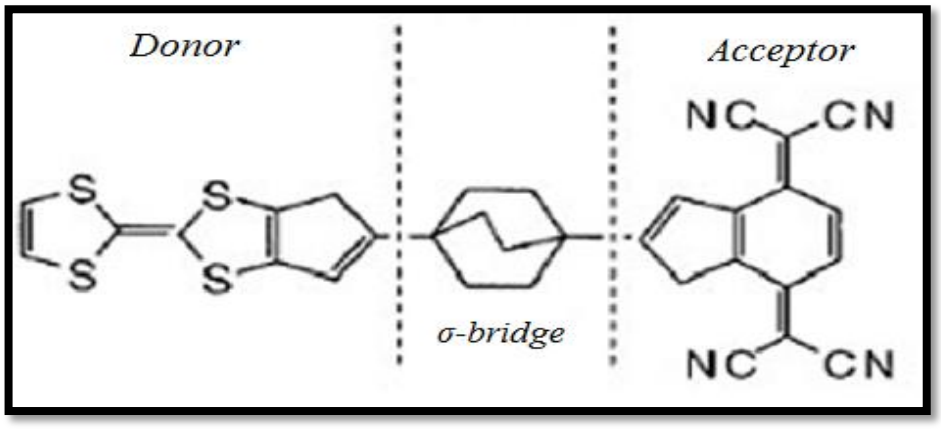

Figure (1.4-a) : The Aviram – Ratner molecular rectifier [31].

When the molecular rectifier is aligned between two metallic electrodes, then the electronic device is designed. When a voltage is not applied to the device, the HOMO–LUMO stands for highest occupied molecular orbital–lowest unoccupied molecular orbital (HL) are distributed in relation to the electrodes as illustrated in Figure(1.4-b). orbitals A and B are the HOMO and LUMO of the acceptor, respectively, orbitals C and D are the HOMO and LUMO of the donor , respectively. E_1 and E_2 are the two electrodes and $\emptyset$ is the electrodes' function of work. It is required for orbital B to be totally or partially empty, it should also be located at or slightly above the fermi energy level of the electrode E_1. Orbital C should lie below orbital B [31].

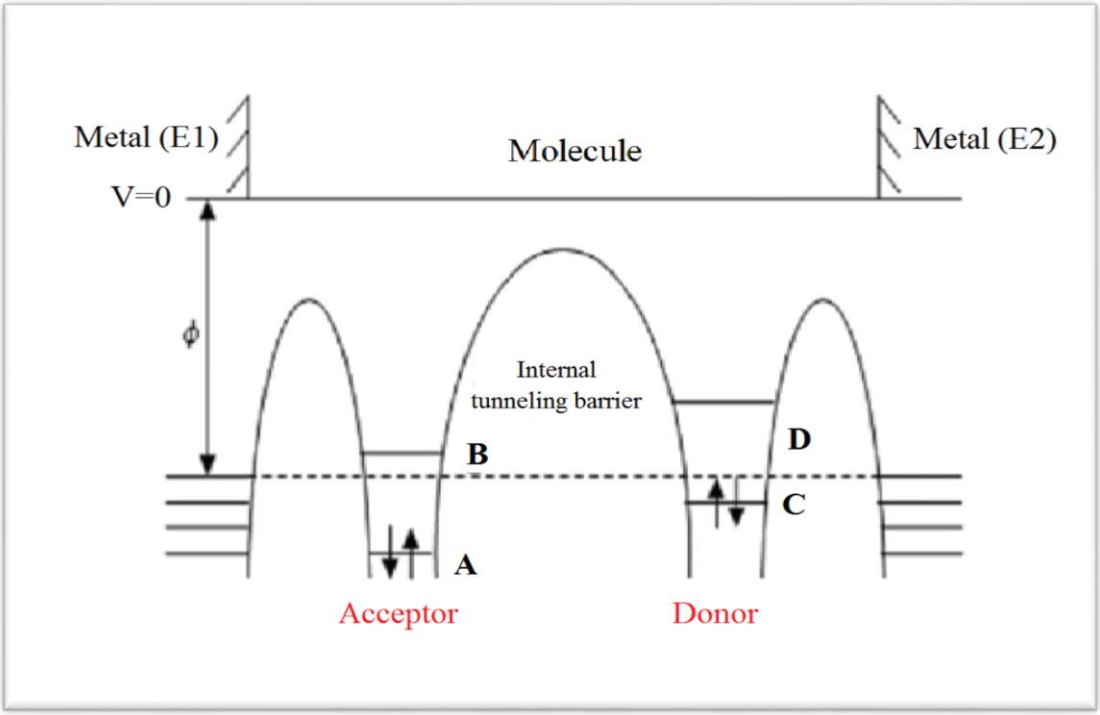

Figure (1.4-b): Molecular orbital distribution of a rectifier with metal electrodes without applied voltage [14].

1.6 Literature Survey

Graphene has been the subject of numerous theoretical and experimental studies. As a result, some have been selected and classified into theoretical and experimental backgrounds.

1 . Huda Bukheet Hassan, in 2014 [32]**,** studied the electronic characteristics of the donor-bridge-acceptor molecule system, the energies were determined using the theoretical B3LYP/6- 31G (d, p) density functional theory. Under the orbital-vertical theory, the electronic states of the system were computed using Koopman's theorem. The results demonstrated that the functional theory utilized to describe the researched molecular system has been proven to be valid in computing the HOMO and LUMO energies, and that it is acceptable for researching the geometry optimization for organic molecular systems. In distinct regions of the Donor-Bridge-Acceptor molecule system, there are localized orbitals that satisfy crucial requirements for the Doner-Bridge-Acceptor system to reveal model new electronic properties as an Aviram-Ratner.

2. Ramla A. A and H. I. Abbood, in 2014 [33], studied the structural parameters of the donor-bridge-acceptor molecular system, the energies were determined using the B3LYP/6-31G (d,p) density functional theory. Under the orbital-vertical theory, the electronic states of the system were computed using Koopman's theorem. They demonstrated that the functional used in the description of the studied molecular system has been proven to be valid in calculating the HOMO and LUMO energies, and that it is suitable for studying the geometry optimization for the organic molecular system. They also demonstrated that there are localized orbitals in various parts of the D-B-A molecular system that satisfy important properties for the D-B-A system to show rectification.

3. Jaafar T. A. and H. I. Abbood, in 2014 [34], using the Aviram–Ratner model, researchers designed a donor-bridge-acceptor molecular system and calculated geometrical parameters and energies for the D-B-A and its components. They demonstrated that substituents added to the phenyl ring changed the LUMO-HOMO energy gap for the examined structures, resulting in new electronic materials, and that the D-B-A molecular system had an appropriate tiny energy gap. The polarizability studies revealed that this novel molecular system is more reactive in charge transfer.

4.Timothy H. Vo *et al.,* in 2014[35], theoretical investigations show that narrow graphene nanoribbons with atomically perfect armchair edges and widths of 2 nm have a bandgap similar to that of silicon (1.1 eV), making them potentially useful for logic applications. Ribbons with a width of >10 nm are often produced using various top–down fabrication methods, which offer little control over their edge structure. They developed a revolutionary bottom-up technique that delivers gram amounts of high-aspect-ratio graphene nanoribbons with atomically smooth armchair edges that are only 1 nm wide. These ribbons exhibit a huge electronic bandgap of 1.3 eV, which is much greater than any value previously reported in experimental studies of graphene nanoribbons made using a top–down technique. These synthetic ribbons could have lengths of >100 nm and self-assemble into highly organized few-micrometer-long 'nanobelts,' which can be viewed using conventional microscopy techniques and could be used to fabricate electronic circuits.

5. Mikko M. Ervasti *et al.,* in 2015 [36], studied theoretically the atomic structure and energetics of silicon and silicon-nitrogen impurities in graphene. Using density functional theory, get insight into the atomic

structures of the impurities, evaluate their formation energies and assess their abundance in realistic samples, find that nitrogen, as well as oxygen and hydrogen, are trapped at silicon impurities, considerably altering the electronic properties of the system. Furthermore, show that nitrogen doping can induce local magnetic moments resulting in spin dependent transport properties, even though neither silicon nor nitrogen impurities are magnetic by themselves.

6. Kaled jabbar Mutashar and Hamid I . Abbood, in 2015 [37], calculated theoretically the structural and electrical properties of donor-Nano bridge-acceptor molecular systems, as well as the effect of Nano bridge length on molecular systems developed using the Aviram-Ratner model. All calculations are performed using the B3LYP hybrid functional density functional theory, which relies on the Koopman's theorm to discover the influencing elements of ionization energy and electron affinity values, and then investigates several key electronic properties. The suggested nanobridge, connecting the donor and acceptor, is suitable to construct the D-nB-A molecular systems. The density functional theory calculations presented a good results of total energies of all D-nB-A molecular systems calculated from the summation of the total energies of the component for each D-nB-A molecular system. The results of the relaxation of the studied molecular systems showed that the large basis sets used in the description of the studied structures are significant but it requires a large time in complete the relaxation.

7. Gorchakov's N. *et al.* in 2016 [38], induced charge transfer in organic materials is a crucial phenomenon in a wide range of biological and technological applications. DBA molecules are utilized as model systems in a variety of theoretical and experimental studies to comprehensively examine and uncover the fundamental principles of charge transfer.

Despite its commendable achievements, experimental work, in particular, is prone to oversimplification and unproven assumptions.

8. Govindasamy Jayamurugan *et al.*, in 2016 [39], studied the rectification in Langmuir–Blodgett (LB) films and designed and synthesized of Aviram–Ratner-Type Dyads they created Aviram–Ratner-type molecular rectifiers with an anilino-substituted extended tetrarchy anoquino dime thane (exTCNQ) acceptor and designed and synthesized them, The s-spacer bicycle is used to covalently bind [2.2.2]octane (BCO) to a tetrathiaful Valene (TTF) donor moiety. X-ray research shows that the stiff BCO spacer keeps the TTF donor and exTCNQ acceptor moieties away.

9. Oleg V. Kozlova *et al.*, in 2017 [40], investigated donor materials for organic solar cells should combine high stability and facile synthesis with good device performance to succeed in practical applications. TPA-TDCV- Ph, a novel small-conjugated molecule that fits those requirements, is presented here. A push-pull molecule with diphenylamine donor and phenyldicyanovinyl acceptor groups is produced using a three-step synthesis that is appropriate for both solution processing and vacuum deposition.

10. Thomas J. Sisto *et al.*, in 2017 [41], reported a novel chemical architecture for the effective production of donor-acceptor, cove-edge graphene nanoribbons and their solar cell characteristics. These nanoribbons are soluble, long (5 nm), and atomically accurate. The fusing of electron-deficient perylene diimide oligomers with an electron-rich alkoxy pyrene component is the basis for the design. The cove-edge structure of these nanoribbons results in a significant degree of bending along the long axis, whilst this technique of alternating electron rich and

electron poor units promotes a visible light fusion reaction in >95 percent yield.

11. Pour, M. M. *et al.*, in 2017 [42], indicated the nanoribbons made of narrow, atomically perfect graphene show considerable potential for electrical and optoelectronic applications, yet previously reported nanoribbon-based devices have poor currents and mobility. They looked at the idea of lateral extension of graphene nanoribbons to improve their electrical conductivity in this work. They began by designing a laterally stretched form of a traditional chevron graphene nanoribbon. The lateral extension of these novel graphene nanoribbons resulted in a decrease in their electronic bandgap and an enhancement in the electrical conductivity of nanoribbon-based thin films, according to our research. This study shows the methodology for designing new atomically precise graphene nanoribbons with improved properties, their bottom-up synthesis, characterization, processing and implementation in electronic devices.

12. Liu, Yu-Min *et al*. in 2018 [43], investigated the conjugation of nanographenes (NGs) with electro-active molecules can establish donor-acceptor π-systems in which the former generally serve as the electron-donating moieties due to their electronic-rich nature. In contrast, here we report a series of reversed donor-acceptor structures are obtained by C–N coupling of electron-deficient perchlorinated NGs with electron-rich anilines. Selective amination at the vertexes of the NGs is unambiguously shown through X-ray crystallography. By varying the donating ability of the anilino groups, the optical and assembly properties of donor-acceptor NGs can be finely modulated. The electron-deficient concave core of the resulting conjugates can host electron-rich guest molecules by

intermolecular donor-acceptor interactions and gives rise to charge-transfer supramolecular architectures.

13. Thomas J. Sisto *et al.,* In 2019 [44], suggested a new chemical architecture for the effective production of donor–acceptor, cove-edge graphene nanoribbons and their characteristics in solar cells was disclosed in this communication. These nanoribbons are soluble, long (~5 nm), and atomically accurate. The fusing of electron-deficient perylene diimide oligomers with an electron-rich alkoxy pyrene component is the basis for the design. The cove-edge structure of these nanoribbons results in a significant degree of bending along the long axis, whilst this technique of alternating electron rich and electron poor units promotes a visible light fusion reaction in >95 percent yield. The backbone's stiffness results in a strong absorption edge at the longest wavelength. These nanoribbons are exceptional electron acceptors, and organic photovoltaics fabricated with the ribbons show efficiencies of ~8% without optimization.

14. Akihiro Shimizu *et al.,* in 2020[45], developed and synthesized conjugated zwitterions made of electron-donating anions, such as phenoxide and anthroxide, and electron π -accepting cations, such as pyridinium and acridinium, to generate relatively tiny donor–acceptor compounds with minimal $\Delta E_{\mathrm{H-L}}$ values.

15. Khalid Jabbar Mutashar, in 2020 [46], used the density functional theory to investigate the structural, electronic, and spectroscopic features of the D-B-A molecule system. For describing the structures under investigation, the B3LYP hybrid functional was combined with the huge basis sets 6-31G. For all calculations, the Gaussian 09 software package was used. The Koopmans theorem was used to calculate the electronic

properties. He found that the Donor-Bridge-Acceptor system under investigation has a sufficient gap, and orbitals at various points in the molecular system can give the system new electronic features. The TD-SCF / DFT approach was used to calculate the transition states.

16. Xijiao Mu *et al.,* In 2020 [47], studied theoretically the one-photon (OPA) and two-photon (TPA) absorption and transition characteristics of the porphyrin and fullerene donor–acceptor systems linked by thiophene oligomers. A variety of 2D and 3D visualization methods were utilized to investigate the transition features of OPA and TPA. They found that The both super exchange charge transfer without thiophene oligomers and sequential charge transfer through thiophene oligomers throughout the OPA and TPA transitions of this D–A system.

17. Xiangjian Wan *et al.,* in 2020 [48], found among various types of active layer materials, molecules with A–D–A (acceptor–donor–acceptor) architecture have demonstrated much great success in recent years. Thus, in this review, we will focus on A–D–A molecules used in OPVs from the viewpoint of chemists. Notably, the chemical structure–property relationships of A–D–A molecules will be highlighted and the underlying reasons for their outstanding performance will be discussed. The device stability correlated to A–D–A molecules will also be commented on. Finally, an outlook and challenges for future OPV molecule design and device fabrication to achieve higher performance will be presented.

1.7 The Aim of This Study

The main object of this study is to design some molecular systems as Donor-Graphene nanoribbon-Acceptor, to modify the physical properties of graphene nanoribbon via the addition of various acceptor and donor molecules, and draw a new map for energy band gap to determine their significant application in molecular electronics field, and then simulate the sensitivity of the effective structure for some important gases are (sarin, hydrogen sulfide and ammonia).

Chapter Two
Theoretical Part

2.1 Introduction

The Schrödinger equation is Newton's second law with a quantum counterpart in classical mechanics [49]. Given a set of known initial conditions, Newton's second law predicts a physical system's final trajectory over time. The Schrödinger equation is a mathematical formula that describes how a wave function changes over time, which is the quantum-mechanical characterization of a physically isolated system [50,51].

The quantum mechanical wave function contains all of the information about a system. Schrödinger equation can be solved exactly to obtain the wave function of a simple 2-D square potential or even a hydrogen atom. The system's allowable energy states can then be determined. Unfortunately, solving Schrödinger equation for an N-body system is impossible. Evidently, certain approximations are required to make the task solvable, albeit difficult. The most basic definition of DFT is as follows: A method for obtaining an approximation solution for Schrödinger equation of many-body system [52].

Researchers can employ simulations to design and tune target molecules while lowering the costs of experiments, which is very valuable when screening high-energy materials (HEM). Molecular modeling is a set of strategies for using computer to investigate chemical problems [53,54].

Molecular mechanics (MM) methods, semi empirical (SE) methods, ab initio approaches, and density functional theory (DFT) methods are the four primary methodologies that computational chemists and physicians might use [55,56].

DFT is a quantum mechanical approach used in physics and chemistry to study the electronic structure of many-electron systems,

particularly molecules. It is based on a strategy of describing electron correlation via a generic functional of the electron density [57]. In computational physics and chemistry, DFT is one of the most prominent and helpful methodologies. DFT is now one of the most essential tools for calculating metal, semiconductor, and insulator ground state properties [58].

2.2 Schrodinger Equation

In quantum mechanics, Schrödinger's equation used to describe the state of the system. It is given by the relation.

$$H\,\psi(x) = E\,\psi(x) \qquad (2.1)$$

The operators on the left express the Hamiltonian H acting on ψ(x), which represents the time independent Schrödinger equation. (Time-independent Schrödinger equation)

where $H = -\ \frac{\hbar^2}{2m}\ \nabla^2 + V(x)$ is the Hamiltonian

The following is the time-dependent form of Schrödinger equation [59]:

$$i\hbar\frac{\partial}{\partial t}\Psi(\vec{r},t) = -\frac{\hbar^2}{2m}\nabla^2\Psi(\vec{r},t) + V(\vec{r},t)\Psi = H(\vec{r},t)\Psi(\vec{r},t) \qquad (2.2)$$

As

$$\hat{H}\Psi(\vec{r},t) = E\Psi(\vec{r},t) \qquad (2.3)$$

∇^2 :The Laplacian Operator

Where Ψ is the wave function, $\hat{H}$ is the Hamiltonian operator, and E is the eigen value of the system. The Hamiltonian operator, H consists of two terms the kinetic energy operator of the electrons and the nuclei (T) and potential energy components operator (V) as follows:

$$\hat{H} = \hat{T} + \hat{V} \qquad (2.4)$$

The total Hamiltonian of the molecular system $\hat{H}$ containing M nuclei and N electrons can expressed as follows [60, 61]:

$$\hat{H} = -\frac{1}{2}\sum_{i=1}^{N}\nabla_i^2 - \sum_{A=1}^{M}\frac{1}{2m_A}\nabla_A^2 - \sum_{i=1}^{N}\sum_{A=1}^{M}\frac{Z_A}{r_{iA}} + \sum_{i=1}^{N}\sum_{j>i}^{N}\frac{1}{r_{ij}} + \sum_{A=1}^{M}\sum_{B>A}^{M}\frac{Z_A Z_B}{r_{AB}} \quad (2.5)$$

$$\hat{H}_{total} = \hat{T}_e + \hat{T}_n + \hat{V}_{ne} + \hat{V}_{ee} + \hat{V}_{nn} \quad (2.6)$$

In equations (2.5) and (2.6), the total kinetic energy is the sum of the electronic ($\hat{T}_e$) and nuclear ($\hat{T}_n$) kinetic energies, the total potential energy are the sum of three components, the attractive interactions between nuclei and electrons ($\hat{V}_{ne}$), the repulsive electron-electron interactions ($\hat{V}_{ee}$) and the repulsive interactions between the nuclei ($\hat{V}_{nn}$). $Z_{A,B}$ are the nucleic charge of atoms A and B, m_A is the mass of atom A, r_{AB} is the distance between nuclei A and B, r_{iA} is the distance between nucleus A and electron i and finally r_{ij} is the distance between electrons i and j, $r_{ij} = |\vec{r}_i - \vec{r}_j|$.

According to the Born-Oppenheimer Approximation, the electronic and nuclear motions in molecules may be separated, and the entire wave function of a molecule takes the form [61-63]:

$$\Psi_{total} = \Psi_{electronic} \times \Psi_{nuclear} \quad (2.7)$$

Because the nucleus is significantly heavy than electrons, nuclear motion is substantially slower than electrical motion. It's possible that it is fixed. The kinetic energy of nuclei is removed, and the potential energy of nuclei-nuclei is assumed to be constant. So that, the kinetic energy of nuclei and the potential energy of nuclei-nuclei can be eliminated from

the Hamiltonian operator, and the Hamiltonian operator $\widehat{H}$ is simplified as the following:

$$\widehat{H}_e = \widehat{\mathrm{T}}_e + \widehat{V}_{ne} + \widehat{V}_{ee} \qquad (2.8)$$

2.3 Hartree-Fock methods

This system employs the time–independent Schrödinger equation. Calculating the multi- electron wave functions is required to solve Schrödinger equation for all electrons in the system. Many simultaneous differential equations must be solved to solve the Schrödinger equation for all electrons in the system [61,64].

In 1928, Hartree used an iterative self-consistent field "SCF" method to achieve this simplification. Hartree simplified the problem by assuming that the many-electron wave functions would be in a uniform system, the product of a collection of single-electron wave functions, with these wave functions being simple plane waves. It was able to proceed using the variation principle after making this assumption $[60, 61]$, if a system is characterized by a collection of unknown parameters, the set of parameter values that accurately characterizes the system′s ground state and total energy can be written as [54-61]:

$$E\phi = \frac{<\phi|\hat{H}|\phi>}{<\phi|\phi>} \geq E_{\circ} \qquad (2.9)$$

Where Eϕ is the lowest- Energy eigenvalue of the trial function, ϕ trial function and $E_{\circ}$ is the ground-state energy. The wave function of Hartree–Fock approach is complicated than the Hartree product wave function but it can be written in a compact way as a slater determinant. Since electrons are fermions having a spin of $(\frac{1}{2})$ the total electronic wave function will be antisymmetric with respect to the interchange of

any two–electron coordinates [65,66]. The determinant considers the spin of all the electrons and the Pauli Exclusion Principle and the electrons have a spin up ($+\frac{1}{2}\ or\ \alpha$) or spin down ($-\frac{1}{2}\ or\ \beta$).The slater determinant for N- electron system [54,68].

$$\Psi = \frac{1}{\sqrt{N!}}\begin{vmatrix} \psi_1(1)\alpha(1) & \psi_1(1)\beta(1) & \psi_2(1)\alpha(1) & \psi_2(1)\beta(1)\dots & \psi_N(1)\alpha(1) & \psi_N(1)\beta(1) \\ \psi_1(2)\alpha(2) & \psi_1(2)\beta(2) & \psi_2(2)\alpha(2) & \psi_2(2)\beta(2)\dots & \psi_N(2)\alpha(2) & \psi_N(2)\beta(2) \\ . & . & . & . & . & . \\ \psi_1(N)\alpha(N) & \psi_1(N)\beta(N) & \psi_2(N)\alpha(N) & \psi_2(N)\beta(N)\dots & \psi_N(N)\alpha(N) & \psi_N(N)\beta(N) \end{vmatrix} \tag{2-10}$$

Where Ψ, is the electronic wave function, α and β spin of electrons and $\frac{1}{\sqrt{N!}}$ is a normalizations factor [13]. Using the iterative process of the self–consistent field producer yields the molecular orbitals to solve the Hartree–Fock equation $\Psi\ (r_i)$ [54,69].

$$\hat{F}\Psi_i(\vec{r}) = \epsilon_i\Psi_i(\vec{r}) \tag{2.11}$$

Where F delineates the Fock operator, for closed shell systems.

$$\hat{F} = H^{core}(1) + \sum_{L=1}^{n/2}\left(2\hat{J}_l - \hat{K}_l\right) \tag{2.12}$$

The one-electron Hamiltonian is the first operator of the Hartree-Fock Hamiltonian for an electron moving in the field of the bare nuclei $\hat{J}_l and\ \hat{K}_l$ it is effects on $\Psi_i\ (\vec{r})$ the exchange operator K_l is:

$$\hat{K}_l\Psi_i(r) = \int \frac{\Psi_l^*(r)\Psi_i(r)}{\left|\vec{r}-\vec{r}\right|}\ d\acute{v}\Psi_l(r) \tag{2.13}$$

And Coulomb operator, $\hat{J}_l\ is$:

$$\hat{J}_l\Psi_i(\vec{r}) = \int \frac{\Psi_l^*(\vec{r})\Psi_l(\vec{r})}{\left|\vec{r}-\vec{r}\right|}\ dv\Psi_i\ (\vec{r}) \tag{2.14}$$

A further restriction involves expanding the molecular orbitals in terms of basis functions φ_i , linear combinations of one-electron functions

according to the linear combination atomic orbital (LCAO) method Thus an individual molecular orbital is defined as[51,54,70]:

$$\Psi_i = \sum_{\mu=1}^{N} C_{\mu i}\phi_\mu \qquad (2.15)$$

$C_{\mu i}$ represents the constants of molecular orbital expansion, To be normalized, the basis functions ϕ_μ are chosen.

Within the set of constraints, the precise energy $E_\circ$ of the system's ground state, or the exact solution of the Schrodinger equation [69].

$$E(\phi_1, \phi_2, \dots\dots\dots, \phi_n) \geq E_\circ \qquad (2.16)$$

The equality sign shall be applied only in case Ψ is the exact ground state function.

2.4. Roothaan-Hall Equations

Clemens C. J. Roothaan and George G. Hall independently created the method in 1951, and it is frequently referred to as the Roothaan-Hall equations. These equations are a non-orthonormal basis set of Gaussian or Slater type with a form of the Hartree-Fock equation. It refers to molecules or atoms with closed shells in which all molecular or atomic orbitals are filled [65].

$$\sum_{\nu=1}^{N}\left(F_{\mu\nu} - \varepsilon_i S_{\mu\nu}\right) C_{\mu\nu} = 0 \qquad \mu = 1,2,3, \dots\dots, N \qquad (2.17)$$

Where ε_i is the one-electron energy of a molecular orbital ψ_i. $S_{\mu\nu}$ and $F_{\mu\nu}$ are the overlap matrix and the Fock matrix [65]:

$$S_{\mu\nu} = \int \phi_\mu^*(1)\phi_\nu(1)dx_1 dy_1 dz_1 \qquad (2.18)$$

And $F_{\mu\nu}$ describes the elements of (NxN) Fock matrix.

$$F_{\mu\nu} = H_{\mu\nu}^{core} + \sum_{\lambda=1}^{N}\sum_{\sigma=1}^{N} P_{\lambda\sigma}[(\mu\nu/\lambda\sigma) - 1/2\,(\mu\nu/\lambda\sigma)] \qquad (2.19)$$

$P_{\lambda\sigma}$ in equation (2.19) represents the density matrix and (μν/λσ) are the two-electron repulsion integrals [61]:

$$(\mu\nu/\lambda\sigma) = \iint \phi_{\mu}^{*}(1)\phi_{\nu}(1)\left(\frac{1}{r_{12}}\right)\phi_{\lambda}^{*}(2)\phi_{\sigma}(2)dx_1dy_1dz_1dx_2dy_2dz_2 \qquad (2.20)$$

The matrix $H_{\mu\nu}^{core}$ stands for the energy of a single electron in a field of pure nuclei.

$$H_{\mu\nu}^{core} = \int \phi_{\mu}^{*}(1)H^{core}\phi_{\nu}(1)dx_1dy_1dz_1 \qquad (2.21)$$

$$H^{core}(1) = -\frac{1}{2}\left(\frac{\partial^2}{\partial x_1^2} + \frac{\partial^2}{\partial y_1^2} + \frac{\partial^2}{\partial z_1^2}\right) - \sum_{A=1}^{M}\frac{Z_A}{r_{1A}} \qquad (2.22)$$

The restricted open shell Hartree-Fock (ROHF) approach [73], uses a single set of molecular orbitals with doubly and singly occupied orbitals.

Different spatial orbitals are given to α and β electrons using the unconstrained Hartree-Fock (UHF) method. The previously doubly occupied orbital 1 is split into two different orbitals Ψ_i^{α} and Ψ_i^{β} which are described by two sets of coefficients [66]:

$$\Psi_i^{\alpha} = \sum_{\mu=1}^{N} C_{\mu i}^{\alpha}\phi_{\mu} \quad ; \quad \Psi_i^{\beta} = \sum_{\mu=1}^{N} C_{\mu i}^{\beta}\phi_{\mu} \qquad (2.23)$$

The coefficients are varied independently and lead to modified Roothaan-Hall equations according to the UHF theory [62].

$$\sum_{\mu=1}^{N}\left(F_{\mu\nu}^{\alpha} - \varepsilon_i^{\alpha}S_{\mu\nu}\right)C_{\mu\nu}^{\alpha} = 0 \qquad (2.24)$$

$$\sum_{\mu=1}^{N}\left(F_{\mu\nu}^{\beta}-\varepsilon_{i}^{\beta}S_{\mu\nu}\right)C_{\mu\nu}^{\beta}=0 \qquad \mu=1,2\ldots N \tag{2.25}$$

The Fock matrices for the associated Fock matrices are defined by [66, 74]:

$$F_{\mu\nu}^{\alpha}=H_{\mu\nu}^{core}+\sum_{\lambda=1}^{N}\sum_{\sigma=1}^{N}\left[\left(P_{\lambda\sigma}^{\alpha}+P_{\lambda\sigma}^{\beta}\right)(\mu\nu/\lambda\sigma)-P_{\lambda\sigma}^{\alpha}(\mu\nu/\lambda\sigma)\right] \tag{2.26}$$

$$F_{\mu\nu}^{\beta}=H_{\mu\nu}^{core}+\sum_{\lambda=1}^{N}\sum_{\sigma=1}^{N}\left[\left(P_{\lambda\sigma}^{\alpha}+P_{\lambda\sigma}^{\beta}\right)(\mu\nu/\lambda\sigma)-P_{\lambda\sigma}^{\beta}(\mu\nu/\lambda\sigma)\right] \tag{2.27}$$

And the density matrix $P_{\mu\nu}$ divided into two parts:

$$P_{\mu\nu}^{\alpha}=\sum_{i=1}^{\alpha ooc}C_{\mu i}^{\alpha *}C_{\nu i}^{\alpha} \quad ; \quad P_{\mu\nu}^{\beta}=\sum_{i=1}^{\beta occ}C_{\mu i}^{\beta *}C_{\nu i}^{\beta} \tag{2.28}$$

Where α_{occ} and β_{occ} denote the involved occupied orbitals.

2-5. Basis Set

A basis set is a group of related items functions that characterize the form of an atom's orbitals. The exceptions include a few methods that define the basis set as an essential component of the technique, and some semi empirical techniques that use a predetermined basis set. A basis set must be specified when ab initio or density functional theory computations are performed. Linear combinations of basic functions and angular functions are used to generate molecule orbitals and full wave functions. The correctness of the results is mostly determined by the type of calculation used and the basis set chosen [62, 69].

2.5.1 Slater Type Orbitals (STO's)

With a discontinuous behavior, functions of the Slater kind describe a correct behavior near the nucleus at r. The orbitals of the Slater type have the following shape [75, 76]:

$$\chi^{STO} = Nr^{n-1}e^{-\xi r}Y_{lm}(\theta,\varphi) \qquad (2.29)$$

Where n is a fundamental quantum number and ξ is a constant related to the nucleus' effective charge. The angular part of the wave function is described by Y_{lm} which is a spherical harmonic.

2.5.2 Gaussian Type Orbitals (GTO's)

Due to highly efficient techniques exist for calculating the many-center integrals analytically, the Gaussian type orbitals (GTOs) HF basis function and related functions approaches is popular. In terms of Cartesian coordinates, Gaussian type orbitals are expressed as [62,69]:

$$\chi^{GTO} = Nx^{lx}y^{ly}z^{lz}e^{-\xi r^2} \qquad (2.30)$$

A normalization factor is denoted by the letter N. The total of lx, ly and lz determines the type of orbitals. ξ the orbital exponent is a number that represents the size of an orbit. Show ξ is the resulting function is compact large or diffuse small, and dependence r^2 in the exponential is a weakness of the GTO's with regard to the slater-type orbitals STO's.

One of the drawbacks of STO's is that integrals with multiple centers such as coulomb and HF-exchange terms are difficult to compute with STO's. As a result, it has no bearing on the situation modern wave Quantum chemistry codes based on functions. As a result, for Coulomb and other computations HF-exchange terms the analytical solution is

available for the Gaussian functions. A contracted GTO basis set, in which several primitive Gaussian functions are mixed to give a contracted Gaussian function (CGF), is commonly used to improve GTO basis sets. [66]:

$$\chi_j^{CGF} = \sum_i^M C_{ij}\chi_a^{GTO} \quad (2.31)$$

The number of Gaussian primitives utilized in a linear combination is denoted by M. The basis sets used in Gaussian are classified into: minimal basis sets, split valence sets, polarization and diffuse functions and others [54,64].

2.5.2.1 Minimal Basis Sets

STO-3G is a minimum basis set that includes all orbitals up to and including valence, the smallest number of basis functions required to describe the ground states of the constituent atoms of a molecule (1s, 2s and 2p on carbon atom). Core and valence orbitals are made up of the same number of Gaussian primitives in these basis sets, [74,78].

2.5.2.2 Split-Valence Basis Sets

For each valence orbital, split-valence basis sets use multiple basis functions with various orbital exponents, but only one for each core orbital. The valence orbitals are represented by two or more basis functions, while the inner-shell atomic orbitals are represented by one basis function (Pole basis sets) [61,79]. Increasing the amount of basic functions employed per orbital is an easy way to enlarge a basis set. Each valence orbital in the valence double-zeta (VDZ) basis set has two basis functions, whereas the valence triple-zeta (VTZ) basis set has three, and so on. For example, the 6-31G basis set employs a split-valence of 3 and 1 primitive for the valence orbitals and a set of 6 primitives contracted to

one basis function for each core orbital. While split valence basis sets provide a better description of molecular orbitals due to their ability to accommodate changing atom sizes, they are unable to create a balanced basis set of their own [80].

2.6 Density Functional Theory

One of the most helpful methods for calculating the electronic structure of atoms, molecules, and solids is density functional theory DFT [81]. Electronic structure methods that use the electron density is calculated using the Thomas – Fermi and Thomas – Fermi – Dirac models, which have been shown to be ineffective since they cannot produce a lower total energy for a molecule than for separated atoms. Hohenberg–Kohn solved the challenge by offering two key findings [81, 82]. To begin, the ground state electron density defines the Hamiltonian, and hence the ground state electronic wave function, as well as all other aspects of the system. Second, given the correct ground state density, the genuine density functional for electronic energy takes its lowest.

The Hohenberg-Kohn results reduced the task of solving the many-body Schrödinger equation to reduce the density functional. Kohn – Sham technique is a well-known work that has been widely adopted for a variety of applications [82].

The quantum mechanical method of DFT is frequently used to study the electronic structure of many-electron systems in physics and chemistry it is now one of the most essential tools for calculating metal, semiconductor, and insulator ground state parameters. In computational physics and computational chemistry, DFT is one of the most common and useful approaches [83].

DFT now the most successful method of computing matter's electronic structure. It can be used to atoms, molecules, solids, and nuclei. It predicts a wide range of molecular properties, structures, vibrational frequencies, atomization energies, ionization energies, electronic, magnetic properties, and reaction routes, among other things [84]. In 1927, the functional the Thomas-Fermi model, devised by Thomas and Fermi, was the forerunner to density theory. Thomas and Fermi estimated an atom's energy by describing its kinetic energy as a function of electron density and combining this with the classical equations for nuclear-electron and electron-electron interactions, both of which can be expressed in terms of electron density[59,62].

The properties of a many-particle system are derived using DFT as a function of electron density (r). The number of electrons per unit volume at a certain state is called electron density. It is dependent only on three coordinates regardless of the number of electrons of the system, so [61]:

$$N = \int \rho(\vec{r}) d\vec{r} \qquad (2.32)$$

The primary notion of DFT is based on the ground state energy, and the electron density is the sole determinant of all other ground state electronic properties. In addition, the electronic density for low total energy corresponds to the exact ground state of the system. The density functional theory is founded on two fundamental theorems, according to Hohenberg and Kohn in 1964 [85,86].

Theorem I: A many-electron system's ground state energy is a unique, universal functional of ground state electron density (r).

Theorem II: For a many-electron system, the ground state electron density (r) minimizes the functional of ground state energy.

The ground state energy is central to DFT, and the electron density is the sole determinant of all other ground state electronic parameters. DFT is now one of the most important methods for determining the characteristics of metals, semiconductors, and insulators in their ground states [61].

2.6.1 Hohenberg–Kohn Theorems

Hohenberg and Kohn proved two important theorems in 1964.Underpin density functional theory [64]. The energy functional $E_\circ$ for the ground state is as follows [74]:

$$E_V[\rho] = \int \rho\,(\vec{r}) V_{ext}(\vec{r}) d\vec{r} + F_{HK}[\rho] \qquad (2.33)$$

Where $F_{HK}[\rho]$ is to be calculated a functional of $\rho(\vec{r})$that incorporates kinetic energy and all electron-electron interactions and $V_{ext}(r)$ is the external potential. The variation of ground state energy satisfies the following principle [69,74]:

$$\delta\{E_V[\rho] - K[\int \rho(\vec{r}) d\vec{r} - N]\} = 0 \qquad (2.34)$$

Which gives

$$K = \frac{\delta E_V[\rho]}{\delta\rho(r)} = V_{ext}(\vec{r}) + \frac{\delta F_{HK}[\rho]}{\delta\rho(r)} \qquad (2.35)$$

Where K is the chemical potential, $F_{HK}[\rho]$ is a universal functional and is independent of the external potential $V_{ext}(r)$. From equation.(2.33) and equation (2.34), Hohenberg-Kohn theorem was first proposed aimed to treat the non-spin polarized electron state and later has been extended to spin–polarized state, finite temperature and relativity conditions [64]. Hohenberg–kohn theorems proposed a basic idea that the electron density

in the ground state is the foundation of constructing all the ground state physics for a many–electron system.

However, these theorems did not give the concrete expression of energy functional $F_{HK}[\rho]$, in which kinetic functional and exchange–correlation functional were not known. At the same time, one had no idea how to construct a many–electron system's ground state electron density $\rho(\vec{r})$ [62,64].

2.6.2 Kohn-Sham Equations

Hohenberg and Kohn established two fundamental theorems in 1964 [66,74] that underpin density functional theory:

$$F_{HK}[\rho] = T[\rho] + \frac{1}{2} \iint \frac{\rho(\vec{r})\rho\left(\vec{\vec{r}}\right)}{\left|\vec{r}-\vec{\vec{r}}\right|} d\vec{r}\, d\vec{\vec{r}} + E_{xc}[\rho] \qquad (2.36)$$

Where T$[\rho]$ is the kinetic energy of system, the second term is the classical coulomb energy, the third term $E_{xc}[\rho]$ is the exchange correlation energy which describes the non–classical interaction of electrons including all the many–body effects.

However, one could not carry out a first principle calculation because the concrete expression of functional $T[\rho]$ and $E_{xc}[\rho]$ were not given. In order Kohn and Sham presented a solution to this problem, a method through supposing a non- interacting many–electron system which has the same electron number N and ground state electron density$\rho(\vec{r})$ under an external potential $V_{ext}(\vec{r})$ with those of an interacting many-electron system. The basic idea is as follows. For anon–interacting system $\rho(\vec{r})$ can be expressed by a set of auxiliary orthogonal functions $\Psi_i(\vec{r})$ as [67]:

$$\rho(\vec{r}) = \sum_i \Psi_i^*(\vec{r})\Psi_i\,(\vec{r}) \qquad (2.37)$$

With $\langle \Psi_i | \Psi_j \rangle = \delta_{ij}$ the Kohn–Sham kinetic energy was given by:

$$T_{ks}[\rho] = -\frac{\hbar^2}{2m} \int \sum_{i=1}^{N} \Psi_i^*(\vec{r})\, \nabla^2 \Psi_i(\vec{r}) dr \qquad (2.38)$$

∇^2 : The Laplacian operator

Considering the many-body interaction, the true kinetic energy $T[\rho]$ in equation (2.38) is not equal to $T_{ks}[\rho]$. The difference between $T[\rho]$ and non–interacting electron system $T_{ks}[\rho]$ can be combined with non-classical energy $E_{Nc}[\rho]$ of interacting electron system as [67,85]:

$$E_{\times c}[\rho] = E_{Nc}[\rho] + T[\rho] - T_{ks}[\rho] \qquad (2.39)$$

Where $E_{Nc}[\rho] = V_{ee}[\rho] - J[\rho]$

and the ground state energy functional can be written as:

$$E_V[\rho] =$$

$$T_{ks}[\rho] + {}^1\!/_2 \iint \frac{\rho(\vec{r})\rho(\vec{\vec{r}})}{|\vec{r}-\vec{\vec{r}}|} d\vec{r}\, d\vec{\vec{r}} + E_{\times c}[\rho] + \int \rho(\vec{r}) V_{ext}(\vec{r}) d\vec{r} \qquad (2.40)$$

Applying the vibration principle to Eq. (2.40)

$$\frac{\delta}{\delta \Psi_i^*(r)} \{E[\rho] - \int d\vec{r} \sum \epsilon i\, \Psi_i^*(\vec{r}) \Psi_i(\vec{r})\} = 0 \qquad (2.41)$$

The Kohn – Sham equations:

$$\left\{ -\frac{\hbar^2}{2m} \nabla^2 + \int \frac{\rho(\vec{\vec{r}})}{|\vec{r}-\vec{\vec{r}}|} d\vec{\vec{r}} + V_{\times c}[\rho] + V_{ext}(\vec{r}) \right\} \Psi_i(\vec{r}) = \epsilon_i \Psi_i(\vec{r}) \qquad (2.42)$$

Where

$$V_{\times c}[\rho] = \frac{\delta E_{\times c}[\rho]}{\delta \rho(\vec{r})} \qquad (2.43)$$

Is the exchange–correlation potential which has been modified to include all the difference between the interacting and non-interacting kinetic energy in equation (2.39). It should be noted that the Kohn-Sham equation has to be calculated self–consistently considering that the wave function $\Psi_i(\vec{r})$ influenced by the electron density $\rho(\vec{r})$ which is included in Hamiltonian. Through solving a set of Kohn-Sham equations (2.41) self- consistently, one can obtain the total energy of system [67,85].

$$E = \sum_{i}^{N} f_i \varepsilon_i - \frac{1}{2}\iint \frac{\rho(\vec{r})\rho(\overrightarrow{r'})}{|\vec{r} - \overrightarrow{r'}|} d\vec{r} d\overrightarrow{r'} + E_{XC}[\rho] - \int d\vec{r}\, \rho(\vec{r}) V_{ext}(\vec{r}) \qquad (2.44)$$

The total energy is not equal to the summation of single electron energy ϵ_i. The excitation energy from (i) state to (j) state is not simply $\epsilon_i - \epsilon_j$ and thus the physics of Kohn-Sham equation is not equal to that of Schrodinger equation [66].

2.6.3 The Local (Spin) Density Approximation (L(S)DA)

The simplest approximation to the exchange–correlation E_{XC} [(r)] is the local density approximation (LDA) [56,61], which assumes that the system is a homogeneous electron gas and that the exchange–correlation E_{XC} [(r)] is only dependent on the local value of electron density. As a result, the exchange– correlation E_{XC} [(r)] can be stated in a straightforward manner [69]:

$$E_{XC}^{LDA}[\rho] = \int \rho(\vec{r})\, \varepsilon_{XC}\big(\rho(\vec{r})\big) d\vec{r} \qquad (2.45)$$

The approximation of local spin density (LSDA) defines the exchange correlation potential in terms of the density of α and β spins and was developed for calculating the properties of open-shell systems [66].

$$E_{XC}^{LSDA}[\rho_\alpha, \rho_\beta] = \int \rho(\vec{r}) \varepsilon_{XC}(\rho(\vec{r})_\alpha, \rho(\vec{r})_\beta) d\vec{r} \quad (2.46)$$

Where E_{XC} is the per-particle energy of exchange-correlation. In several cases, such as equilibrium structures, vibrational frequencies, and dipole moments, the LSD approximation outperforms the HF approximation.

The LSDA, in general, gives valid information for systems that closely approximate a uniform electron gas, i.e., those in which the density fluctuates slowly with position. In actuality, atomic and molecular systems do not have uniform electron densities, necessitating the use of more complicated models [66].

2.6.4 The General Gradient Approximation

For the exchange-correlation energy, generalized gradient approximations (GGAs) outperform atoms, molecules, and solids are described using the local spin density (LSD) method. Suggest a basic GGA derivation in which all parameters are fundamental constants (except from those in LSD) [69].

$$E_{XC}^{GGA}[\rho_\alpha, \rho_\beta] = \int f(\rho_\alpha, \rho_\beta, \nabla\rho_\alpha, \nabla\rho_\beta) d\vec{r} \quad (2.47)$$

This functional is often superior than the LSDA since it accounts for density change in regard to position (E_{XC}) is frequently expressed as the sum of an exchange to make the problem easier to understand. (E_X) and correlation (E_C) terms [66]:

$$E_{XC} = E_X + E_C \quad (2.48)$$

The exchange-energy functional can then be produced by replacing the HF orbitals with Kohn-Sham orbitals, and approximate solutions for (E_C) are sought. Various exchange and correlation

functionalities have been independently created and can be coupled in a variety of ways. B3LYP, for example, is a well-known (GGA) functional that combines Becke's 1988 exchange functional with the Lee-Yang-Parr correlation functional [79].

2.6.5 The Hybrid Functional

Hybrids are particularly useful for a term used to describe a wide range of molecular properties. Calculating the exact (Hartree-Fock)exchange in large molecules and solids, on the other hand, is time consuming, especially for systems with metallic characteristics for the exchange interaction, a new hybrid density functional was constructed based on a screened coulomb potential, which circumvents this bottleneck. Becke's exchange functional from 1988 is used in the most popular hybrid functional, B3LYP (E_X^{B88}) and the correlation functionals of Lee Yang and Parr (E_C^{LYP}) as LSDA exchange and correlation functional gradient adjustments [69,73,86]

$$E_{\times c}^{B3LYP} = (1-a)E_{\times}^{LSDA} + aE_{\times}^{HF} + bE_{\times}^{B88} + CE_c^{LYP} + (1-C)E_c^{LSDA} \quad (2.49)$$

The three parameters are , a=0.20, b=0.72 and c=0.81. Here :

a: stated the exact amount of exchange

The contributions of exchange and correlation are controlled by b and c, respectively.

2.7 Structural and Electronic Properties

2.7.1 HOMO, LUMO and Energy Gap

The two most important molecular orbitals MOs, which reside at the outmost limits of the electrons of the molecules, are the highest

occupied molecular orbital HOMO and the lowest unoccupied molecular orbital LUMO. The energy difference between the HOMO and LUMO orbitals is known as the band gap [85,87].

$$E_g = E_{LUMO} - E_{HOMO} \quad (2.59)$$

The energy gap is used to determine a molecule's chemical reactivity and stability as well as to control how it interacts with other species. A soft molecule with a small band gap is frequently associated with high chemical reactivity, low stability, and a small band gap [87]. When an electron moves from the ground state to a higher energy level, it fills vacant molecular orbitals and is referred to as the excited state [89,90].

The LUMO eigenvalue is affected by orbital relaxation to a substantial extent. Aside from the issue of relaxation's effect on the validity of KT, there has been considerable debate on the physical importance of the KS orbitals of DFT used inside the KS framework [91,92].

2.7.2 Total Energy, Ionization Energy and Electron Affinity

The sum of a system's total kinetic and potential energy is called total energy. Due to the effective forces' resultant is zero, an optimized molecular system must have the lowest total energy value. This indicates that the molecular system is at equilibrium[90].

An atom's or molecule's ionization energy (IE) is the smallest amount of energy needed to separate an electron from its nucleus ground state. Ionization potentials of small atoms or molecules tend to be higher [91,93,94].

Energy +X $(g) \rightarrow X^+(g) + e^-$ (2.50)

X stands for an atom or a molecule. The amount of energy produced when an electron adds to an atom or molecule and forms a negative ion is called the electron affinity EA of an atom or molecule [90,91,94]:

$$X(g) + e^{-} \rightarrow X^{-}(g) \quad (2.51)$$

The IE and EA can be calculated as [36,43,44]:

$$IE = E_{cation} - E_n \quad (2.52)$$

$$EA = E_n - E_{anion} \quad (2.53)$$

Where E_n , E_{cation} , E_{anion} are the total energies of the ground state of a neutral molecule, cation and anion, respectively.

In this study, the IE and EA are estimated according to Koopmans theorem as [94,95]:

$$IE = -E_{HOMO} \quad (2.54)$$

$$EA = -E_{LUMO} \quad (2.55)$$

Where E_{HOMO} and E_{LUMO} are the HOMO and LUMO energies, respectively.

2.7.3 Fermi energy

The Fermi energy is the fundamental variation principle of DFT. The fleeing trend of a cloud of electrons is measured using Fermi energy. It is a constant throughout all space and may be determined using the equation below [96]:

$$E_F = \left[\frac{\partial E}{\partial N}\right] v_{(\vec{r})} \quad (2.56)$$

Where E is the energy and N is the number of electrons.

Experimentally, Fermi energy is related to IE and EA, as in the following equation [96,97]:

$$E_F \approx \frac{1}{2}(E_{HOMO} + E_{LUMO}) \approx -\frac{1}{2}(IE + EA) \quad (2.57)$$

2.7.4 Electrochemical Hardness

The electrochemical hardness H under minor chemical perturbations, indicates the resistance of the electron cloud of atoms, ions, or molecules to deformation or polarization. Using the density functional theory as a starting point, [98]:

$$H = \frac{1}{2}\left[\frac{\partial \mu}{\partial N}\right]_{V(\vec{r})} \quad (2.58)$$

The hardness is central of the energy gap between HOMO and LUMO, molecule has large energy gap called hard molecule. In terms of IE and EA, the hardness is calculated as [62, 63]:

$$H = \frac{(IE - EA)}{2} \quad (2.59)$$

For a constant external voltage V(r), the electrochemical hardness is the second derivative of electronic energy with respect to the number of electrons N in DFT [65].

$$H = \frac{1}{2}\left[\frac{\partial^2 E}{\partial N^2}\right]_{V(\vec{r})} \quad (2.60)$$

2.7.5 Electronic Softness

The energy gap of a molecule is related to its electrical softness; a soft molecule has a small energy gap, and its electron density changes more easily than a hard molecule soft molecules will be more reactive than hard molecules because a small energy gap equals small excitation

energies to the manifold of excited states. The electronic softness is calculated using the following formula [65].

$$S = \frac{1}{2H} = \left(\frac{\partial^2 N}{\partial E^2}\right)_{V(r)} = \left(\frac{\partial N}{\partial \mu}\right)_{V(r)} \quad (2.61)$$

2.7.6 Chemical Potential (K)

The link between electronic chemical potential and two known parameters, ionization energy and electron affinity, is as follows [99, 100]:

$$K = (IE+EA) / 2 \quad (2.62)$$

2.7.7 Electrophilicity index

The electrophilicity index is a measurement of energy loss as a result of maximum electron flow between the donor and acceptor. The electrophilicity index (W) is calculated as follows [86]:

$$W = K^2 / 2H \quad (2.63)$$

The electrophilicity is formed up from the electronic structure of molecules, independent of the nucleophilic, where K is the electronic chemical potential. Electrophiles are organisms that become stable when they get an increased quantity of electronic charge from their surroundings [86].

2.7.8 Total Dipole Moment

The first derivative of the energy with respect to an applied electric field is the dipole moment (μ). It is a three-dimensional vector that represents the asymmetry in molecule charge distribution. Debye is the measurement unit for dipole moment and it equal to (3.336×10^{-30}

coulomb * meter) in quantum mechanical description of dipole moment, the charge is a continuous distribution that is a function of (r), and the dipole moment for neutral system is calculated from the atomic charges and the lone pairs as : for neutral system is calculated from the atomic charges and the lone pairs as :

$$\mu_i = ce \sum_A (Q_A i_A) + 2cea_o \sum_A P(s - p_i)_A \; D(A), i = x, y, z \tag{2.64}$$

Where c is the speed of light, e is the charge of an electron, and is the total electron density $\Sigma(Q_A i_A)$ is bond dipole, is Bohr radius, (a_o) Bohr radius, $\mathrm{P}(\mathrm{s} - p_i)_A$ D(A) is the one center two electron integral, and is the one center electron density matrix element. The dipole moment in total is [101]:

$$\mu = \mu_x + \mu_y + \mu_z \tag{2.65}$$

2.7.9 Polarizability

The tendency of an atom's or molecule's electron shell to be deformed under an electric field is known as polarizability. With increasing volume, an atom's or ion's electron cloud becomes more diffuse and its outer electrons become more loosely connected, making it easier to deform. As a result, larger atoms and molecules have a higher polarizability[108].Because polarization functions often, this leads to more precise calculated geometries and vibrational frequencies, they are frequently used. Polarization functions must be introduced to the basis set to improve outcomes [109]. Polarization functions are d-type and f-type functions for heavy atoms, and p- and d-type functions for hydrogen and helium atoms, are examples of higher angular momentum functions. By

enabling the orbital form to fluctuate, the flexibility of the basis set is increased (polarized in one direction). The use of polarization functions can be beneficial Hydrogen-bonding and proton transfers are important systems in which hydrogen is engaged. The reason for this is that employing extended split valances with polarization basis sets 6-31G (d, p)[100], the s orbital will be deformed from its typical spherical shape.

2.8 Software

All calculations in this study have been performed by using the Nanotube modeler, Gauss View Program, Gaussian 09 package of Programs, Gauss View 5.0.8, Gauss Sum 3.0 and other assistant programs. These programs are described as below:

2.8.1 Nanotube modeler

The structure under study (graphene nanoribbon) can be generated by the Nanotube modeler program. To calculate the physical properties of the structure, it would use the Gaussian 09 and Gaussview 5 is used [102].

2.8.2 Gaussian 09 (G09) Program

Gaussian program is a computational software package initially published by John Pople in 1970. Gaussian program is a software suite for quantum mechanics at the highest level. The number "09" refers to the year in which the software was released [102].

All of the major molecular modeling approaches, such as molecular mechanics, ab-initio, semi-empirical, HF, and DFT, can be run using Gaussian. Furthermore, with this application, excited state

computations can be performed using a variety of methods[104]. The name Gaussian comes from the use of Gaussian Type Orbitals, which Gaussian's creator, John Pople, is utilized to solve the computational challenges that Slater Type Orbitals brought up.

The software is compatible with almost any computer platform, including Microsoft Windows. In addition, Web-based interface tools such as Web MO can be used to access it. Gaussian is the most sophisticated program offered to instructors and student researchers through the North Carolina Schoo Computational, Chemistry server [103].

2.8.3 Gauss View Program

Gaussian View was created to import the input files for the Gaussian program and to display the output files for the Gaussian program in a three-dimensional image. Gaussian View is not a calculation program, but it simplifies the work on the Gaussian program and provides three major benefits to the users. First, allow the user to draw molecules, including the large ones, as well as rotate, transfer, and change their size with ease, and use the mouse. Second, the Gaussian view allows for various Gaussian calculations to be performed, as well as complicated input preparation for everyday tasks and advanced methods. Third, the Gaussian view allows for the examination of Gaussian calculations using a number of geometrical tools, including the balanced molecular patterns electronic density surfaces [103,104].

2.8.4 GaussSum 3.0

The GaussSum 3.0 is a software application recorded by Noel O'Boyle. GaussSum 3.0 uses the plotting program (Gnuplot17) for picture graphs. The GaussSum is that can examines the output of widely computational physics and chemistry program (such as Gaussian 09 Program) [103,105].

GaussSum can get ready more information such as a geometry optimization, plot the density of states (DOS) spectrum, source information on the UV-Vis. Transition states, scheme abstracting data on IR and Raman vibrations and visualizing the IR and Raman spectra, which may be scaled using generic or particular scaling factors[106].

Chapter Three
Results
and Discussion

Results and Discussion (Part one)

3.1 Introduction

In this chapter, it will be an interest to understand the effect of different acceptor and donor molecules on the structural and physical properties of graphene nanoribbons to estimate the electronic applications for the new designed structures. Ground state calculations are performed using Becke's three parameters exchange Lee-Yang-Parr correlation functional B3LYP density functional theory with standard 6-31G basis sets, and excited state calculations are performed using the time dependent TD-SCF density functional theory with the same level of density functional theory.

Figure 3.1 shows the optimized structural orientation of different molecules represents the acceptors (labelled A1 to A5) and donors (labelled D1 to D5), and the relax structure of graphene nanoribbon GNR. Graphene nanoribbon in present section was constructed with length 14.65 nm and width 7.12 nm. The conformation search shows the minimum energy for the molecules is having all aromatic types of arrangement of donor and an acceptor with graphene nanoribbon parts.

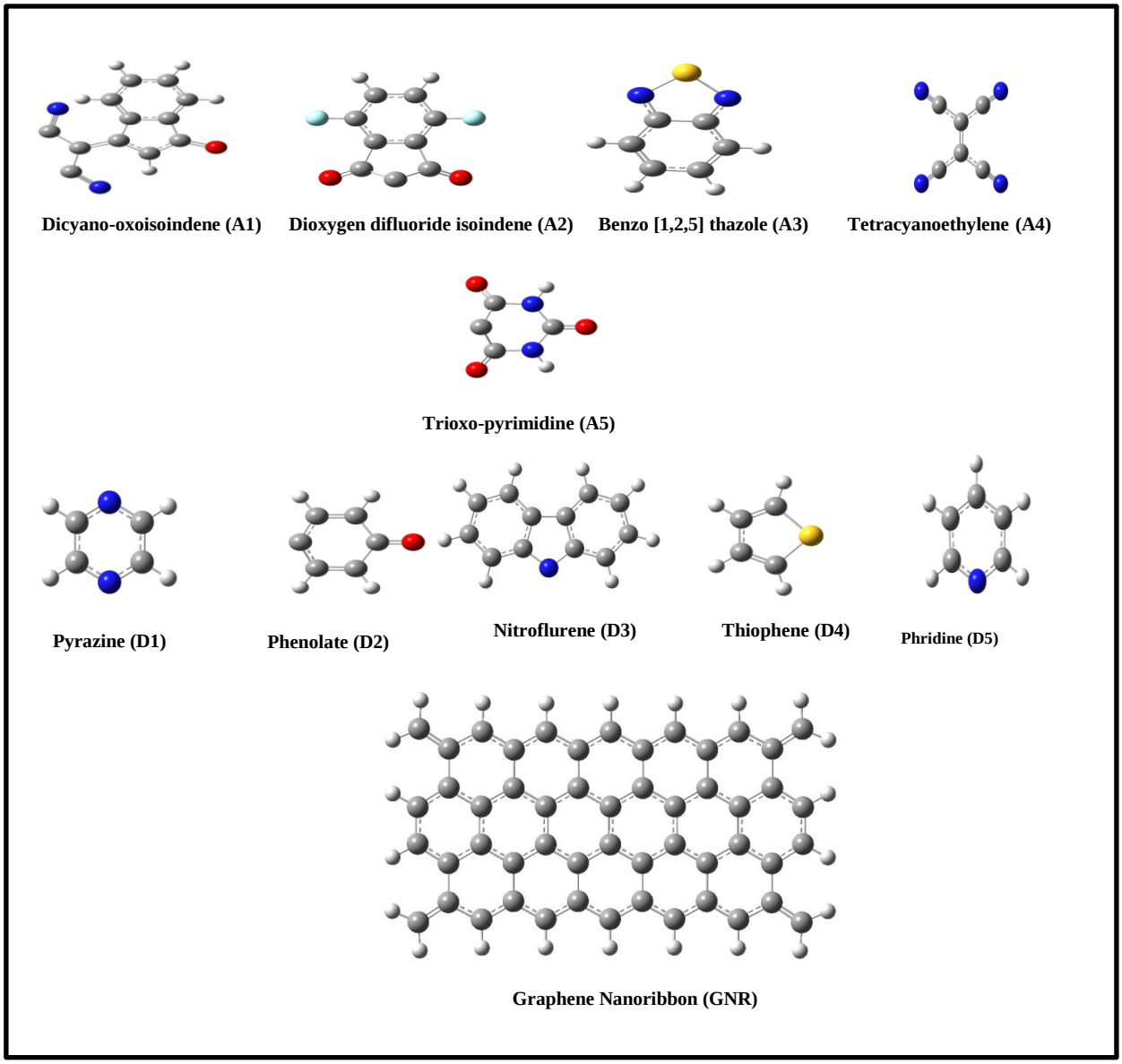

Figure (3.1): Proposed structures of accepters and donors, Graphene nanoribbon. Note/Atoms by colors:Gray=Carbon, Red=Oxygen, Blue=Nitrogen, White=Hydrogen and yellow=Sulfur.

Table 3.1: Bond lengths in nm and angles in degrees for donors and acceptors.

	Bond Length(Å)		**Bond Angle (degree)**		**Bond Angle (degree)**	
	Bond	**value**	**Angle**	**value**	**Angle**	**value**
A1	C=C	1.500	C-C-C	115.406 - 117.935	C=C-C	121.174 – 122.833
	C-C	1.358	C-C=O	120.3154 – 121.895	C-C-O	112.582- 126.242
	C=O	1.254	C-C=C	121.761	C-O-C	118.783
	C-H	1,095	C-C-H	115.888 – 116.069	O-C-H	110.56 4- 104.913
	O-C	1.459	C=C-H	122.894	H-C-H	109.993- 110.353
A2	**Bond**	**value**	**Angle**	**value**	**Angle**	**value**
	C..C	1.358- 1.425	C..C..C	119.620- 120.282	C-C=O	129.541- 133.818
	C-H	1.082	C..C-C	108.811- 131.360		
	C-C	1.469- 1.514	C..C-F	119.089 - 120.614		
	C-N	1.377	C..C-H	119.212- 120.766		
	C=O	1.234	C-C-C	96.369- 109.645		
A3	**Bond**	**value**	**Angle**	**value**	**Angle**	**value**
	C-C	1.465	C-C- C	119.602	C=C- C	121.722
	C..C	1.442	C-C- N	116.161	N-S-N	95.237
	C..N	1.335	C…C- N	116.161 - 124.236	C-N-S	106.219
	C=C	1.369	C..C-H	118.4735 - 118.888		
	C-H	1.085	C..C=C	118.675 – 121.722		
	S-N	1.789	C=C-H	119.804- 122.436		

A4	**Bond**	**value**	**Angle**	**value**	**Angle**	**value**
	N≡C	1.173	C=C..C	121.310		
	C=C	1.377	C..C=C	117.378		
	C..C	1.427	N≡C..C	179.586		
A5	**Bond**	**value**	**Angle**	**value**	**Angle**	**value**
	C-C	1.460	C-C=O	126.075	C-N-H	116.410-118.624
	C=O	1.235 -1.241	C-C-N	109.490	C-N-C	124.773
	C-N	1.413	O=C-N	122.876-124.269		
	H-N	1.014	N-C-N	114.241		
D1	**Bond Length (nm)**		**Bond Angle (degree)**		**Bond Angle (degree)**	
	Bond	**Value**	**Angle**	**Value**	**Angle**	**Value**
	C..C	1.398	C..C-H	121.437		
	C-H	1.084	C..C..N	121.651		
	C..N	1.352	H-C..N	116.911		
D2	**Bond**	**Value**	**Angle**	**Value**	**Angle**	**Value**
	C=C	1.381	C=C..C	114.61		
	C..C	1.407	C=C-H	121.924 - 122.109		
	C-H	1.085	C=C-C	120.773		
	C-C	1.468	C-C-H	117.215		
	C=O	1.265	C-C=O	121.376		
D3	**Bond**	**Value**	**Angle**	**Value**	**Angle**	**Value**
	C..C	1.404	C - C -C	105.105-134.779		
	C-H	1.085	C-C-N	112.307-126.637		
	C -N	1.396	C-C-H	119.267-121.0789		
D4	**Bond**	**Value**	**Angle**	**Value**	**Angle**	**Value**
	C = C	1.316 - 1.364	C=C-H	122.951-129.346	C-C-H	123.325
	C - H	1.078-1.083	C=C-S	111.552	C-C-C	113.725
	C - S	0.803	H-C-S	119.102	C-S-C	89.449
	C -C	1.441	C-C=C	113.724		

	Bond	Value	Angle	Value	Angle	Value
D5	C..C	1.353 - 1.398	C..C-H	120.993		
	C-H	1.085	C..C..N	123.953		
	C..N	1.353	C..C..C	118.684		
GNR	**Bond**	**Value**	**Angle**	**Value**	**Angle**	**Value**
	C..C	1.397 - 1.428	C..C..C	122.0498-123.306	H-C-H	116.2465
	C-H	1.086	C..C-H	117.984-118.709		
	C=C	1.3764	C..C=C	119.535		
	C-C	1.456-1.484	C=C-H	120.207		

Since the two rings junction (donor and acceptor with graphene nanoribbons) are predisposed to interior rotations, a ground state scan with full minimization of the molecules are carried out to obtain the true optimized parameters. These parameters included the bond lengths in nm and bond angles in degrees, as shown in Table 3.1.

3.1.1 Ground State Energies

Table 3.2 illustrates the results of the relaxation for donors, acceptors and graphene nanoribbon obtained from the full minimization at DFT-B3LYP/6-31G level of theory included the total energy E_T in a.u, high occupied molecular orbital energy E_{HOMO}, lower unoccupied molecular orbital energy E_{LUMO} and energy gap E_g in eV.

Total ground state energy for the molecules in Table 3.2 is only dependent on the number of electrons in the molecules, it is the summation of energies for all atoms in each molecule.

Table 3.2: E_T, E_{HOMO}, E_{LUMO} and E_g for donors, acceptors and GNR.

Molecule	E_T (a.u)	E_{HOMO} (eV)	E_{LUMO} (eV)	E_g (eV)
A 1	-644.754	-7.18779	-3.31076	3.877023
A2	-693.923	-7.39051	-4.72791	2.662596
A 3	-738.564	-6.72629	-2.80056	3.925731
A4	-447.375	-9.16058	-1.03483	4.199474
A5	-488.522	-7.98752	-5.36029	2.627222
D 1	-1994.93	-6.70452	-1.59348	5.111042
D 2	-306.03	-6.092	-4.06369	2.028308
D 3	-516.693	-6.72629	-0.99402	4.718387
D 4	-552.932	-8.23895	-0.40653	6.08057
D 5	-248.216	-6.65772	-0.69606	5.961658
GNR	-1994.37	-3.87457	-3.47022	0.404355

The calculated energies for the two frontier molecular orbitals HOMO and LUMO were computed from the self-consistent field SCF as a linear combination of atomic orbitals. The energy gap in Table 3.2 was calculated as a distance between the two frontier orbitals or the difference LUMO-HOMO, GNR has 0.404 eV, while the donors and acceptors have different values of energy gap in order depending on type of each one. It is necessary to select a number of donors/acceptors with various values of energy gap to determine significantly the application for the designing Donor-GNR-Acceptor structures [in follow sections of this thesis].

3.1.2 Some Electronic Properties

There are many electrical properties, that calculated in this study, are presented in the flowing:

3.1.2.1 Ionization Energy and Electron Affinity

Some electronic properties such as ionization energy IE and electron affinity EA in eV were calculated for the studied donors, acceptors and GNR from the SCF calculations by employing the Koopmans theorem and they are listed in Table 3.3.

Table 3.3: The ionization energy, electron affinity in eV for donors, acceptor and GNR.

Molecules	IE (eV)	EA (eV)
A1	7.187786	3.310762
A2	7.390508	4.727911
A 3	6.726287	2.800556
A4	9.160583	4.96111
A5	7.987517	5.360295
D1	6.704518	1.593476
D2	6.091999	4.063691
D3	5.712405	0.994018
D4	6.487102	0.406532
D5	6.657715	0.696057
GNR	3.874574	3.470219

As seen in Table 3.3, all donor molecules have lower values of ionization energy in comparison with acceptor molecules which refer that the donors have high ability to donate an electron and become cations, D3 has the lowest energy of ionization compared with the other donor molecules. On the other hand, A5 acceptor has the highest value of an electron affinity in compared with the other acceptor molecules, that means A5 appear high ability to accept an electron to become anion. In

general, low ionization energy for a molecule of high capability for it to donating electrons, and large electron affinity for a molecule high capability for it to accepting electrons. Various values of ionization energy and electron affinity for the donors and acceptors under study provide the permittivity to construct the Donor-GNR-Acceptor systematically.

3.1.2.2 Global Quantum Chemical Parameters

The calculated values of quantum chemical parameters included electrochemical hardness H in eV, electronic softness S in $(eV)^{-1}$ and electrophilic index W in eV of donor, acceptor and GNR are illustrated in Table 3.4. As known, the softer molecule, the smaller separation between conduction band and valence band, and therefore, the small excitation energy for an electron to transfer. Additionally, the hard molecule requires high excitation energy for an electron transfer.

Table 3.4:The electrochemical hardness H, electronic softness S and electrophilic index W of the molecules Acceptor and donor .

Molecules	H (eV)	S $(eV)^{-1}$	W(eV)
A1	1.938512	0.25793	26.70773
A2	1.331298	0.665649	24.43865
A3	1.962865	0.25473	22.26889
A4	2.099737	1.049868	52.34177
A5	1.313611	0.656806	29.25479
D1	2.555521	1.277761	21.9956
D2	1.014154	0.507077	13.07473
D3	2.359194	0.211937	13.26342
D4	3.040285	0.164458	18.06013
D5	2.980829	0.167739	2.267741
GNR	0.202178	0.101089	1.363335

As seen in Table 3.4 all donors have accepted values of hardness except D4 molecule, it has 3 eV, while the five acceptors have less than or equal 2 eV hardness, that means they all have suitable ability for accepting an electron. A4 molecule has the highest value of softness in comparison with the other acceptors due to the presence of tetra cyanide in A4 of four nitrogen atoms. On the other hand, D1 or so called pyrazine has the higher value of softness compared with other donors due to the presence of two nitrogen atoms in the ring. Table 3.4 showed all donors and acceptors have large values of electrophilic index, they are all can interact with the surrounding molecule (GNR of small value of electrophilic index of 1.36 eV).

3.1.3 Molecular Polarizability

The related ground state properties like the total dipole moment in Debye and the average molecular polarizability α_{ave} in a.u., with its components α_{xx}, α_{yy} and α_{zz} of the studied donors, acceptors and GNR. are presented in table two notes can observe in Table 3.5 two notes can observe in Table 3.5, the first is $\boldsymbol{\alpha}_{xx} < \boldsymbol{\alpha}_{yy} < \boldsymbol{\alpha}_{zz}$ which agreed with the literatures , the second is the molecular polarizability depends only on the type of atoms that the molecules constructed from.

Table 3.5: Total dipole moment and polarizability for donor, acceptor and GNR.

Molecules	Total dipole moment (Debye)	Polarizability (a. u)			
		α_{xx}	α_{yy}	α_{zz}	α_{ave}
A1	4.537	41.243	171.724	221.04	144.669
A 2	5.4616	36.463	120.133	130.796	95.79733
A3	2.3381	30.538	88.801	137.926	85.755
A4	0.0007	28.586	102.987	107.125	79.566
A5	2.1485	27.899	73.829	82.162	61.29667
D1	0.0002	18.881	53.044	65.982	45.969
D2	3.1411	22.91	68.756	104.429	65.365
D3	2.3381	37.652	132.055	239.022	136.243
D4	1.0166	21.243	59.693	66.447	49.12767
D5	2.4849	18.751	61.464	68.035	49.41667
GNR	0.000	131.144	1530.172	1279.221	980.179

Table 3.5 showed also the GNR has high symmetric distribution in space with zero total dipole moment due to the GNR lie under the D6h/C1 point group. Donor molecules have different values of dipole moment due to their symmetrical distribution in space. D1 donor has low dipole moment equals 0.0002 Debye with D2h/C1 high symmetric compared with the other donors, while D2, D3 and D4 donors have relatively large values of dipole moment due to that they are asymmetrical shapes with C2v/C1 point group. On the other hand, all acceptor molecules have high values of dipole moment except A4 molecule has high symmetry due to its symmetric distribution under D2h/C1 point group, other acceptors have low symmetric distribution under C2v/C1 point group except A1 under the point group Cs/C1. The results enable us to decide to construct different structures of Donor-GNR-Acceptor molecules depending on selectively donors and acceptors.

3.2 Donor-GNR-Acceptor

Centered on above results in previous sections, Depending on the previous results several structures of Donor-GNR-Acceptors were constructed. The choice of both donor and acceptor is based on the behavior for each one.

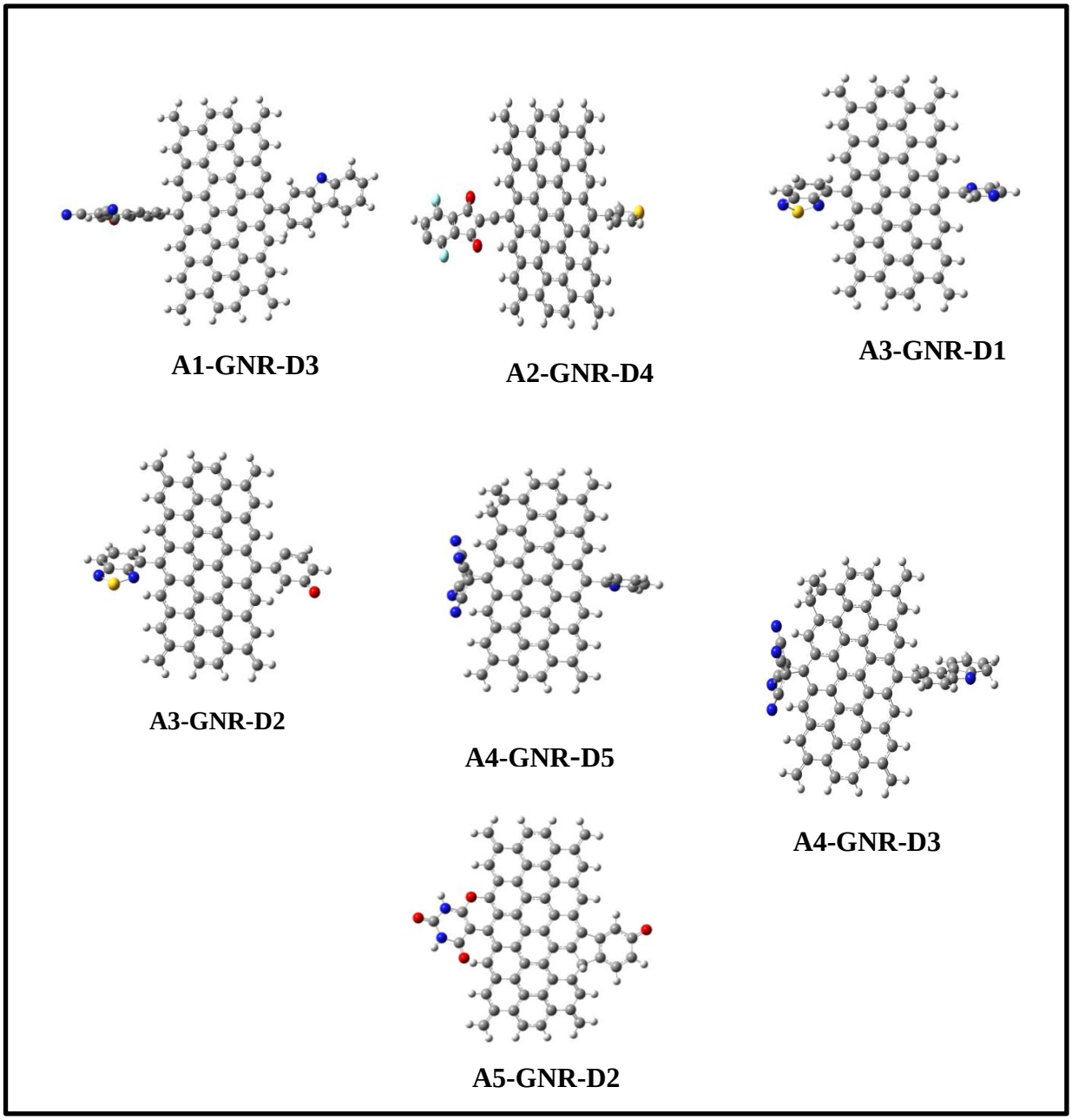

Figure (3.2): Proposed structures of Acceptor-GNR-Donor molecules. Atoms colors: Gray=Carbon, Red=Oxygen, Blue=Nitrogen, White=Hydrogen, Yellow=sulfur.

The relax structure of the group of mentioned Donor-GNR-Acceptor was drawn in Figure 3.2. The structures are optimized at B3LYP/6-31G level using density functional theory and the conformation search displays the minimum energy for each structure approaching the absolute ratio of potential to kinetic energy below 0.0056.

3.2.1 Some Electronic Properties

There are many electrical properties, that calculated in this study, are presented in the flowing:

3.2.1.1 Ground State Energies

Table 3.6 shows the SCF calculations from the relaxation of molecules in Figure 3.2 obtained from the full minimization at DFT-B3LYP/6-31G level of theory, these calculations included the total energy E_T in a.u., high occupied molecular orbital energy E_{HOMO}, lower unoccupied molecular orbital energy E_{LUMO}, Fermi energy E_F and the energy gap E_g in eV.

Table 3.6: SCF calculations from the relaxation of studied Structures.

Structures	E_T (a. u)	E_{HOMO} (eV)	E_{LUMO} (eV)	E_F (eV)	E_g (eV)
GNR	-1994.37	-3.87457	-3.47022	-3.6724	0.404355
A1-GNR-D3	-3153.33	-4.77852	-4.3943	-4.58641	0.384219
A2-GNR-D4	-3276.95	-4.36029	-4.15458	-4.25743	0.205715
A3-GNR-D1	-2994.76	-3.93743	-3.55185	-3.74464	0.38558
A3-GNR-D2	-2688.75	-3.97063	-3.69607	-3.83335	0.274559
A4-GNR-D5	-2786.8	-4.18777	-3.85662	-4.02219	0.331158
A4-GNR-D3	-2957.82	-3.94505	-3.6811	-3.81308	0.263947
A5-GNR-D2	-3036.56	-4.11294	-3.76519	-3.93906	0.347757

It is clear from Table 3.6 that the total energy of the studied structures is approximately the summation of the total energy of its components. One can find conclude the following formula:

$$E_T\,[\text{molecules}] \simeq E_T(\text{donor}) + E_T(\text{graphene nanoribbon}) + E_T(\text{acceptor}) \quad (3\text{-}1)$$

Final total energy for each structure obtained from the SCF in above equation and listed in Table 3.6 was determined by the optimization steps according to the number of iterations in each cycle through the solution of SCF equation, these iterations are limited due to the types of both donors and acceptors in the structures.

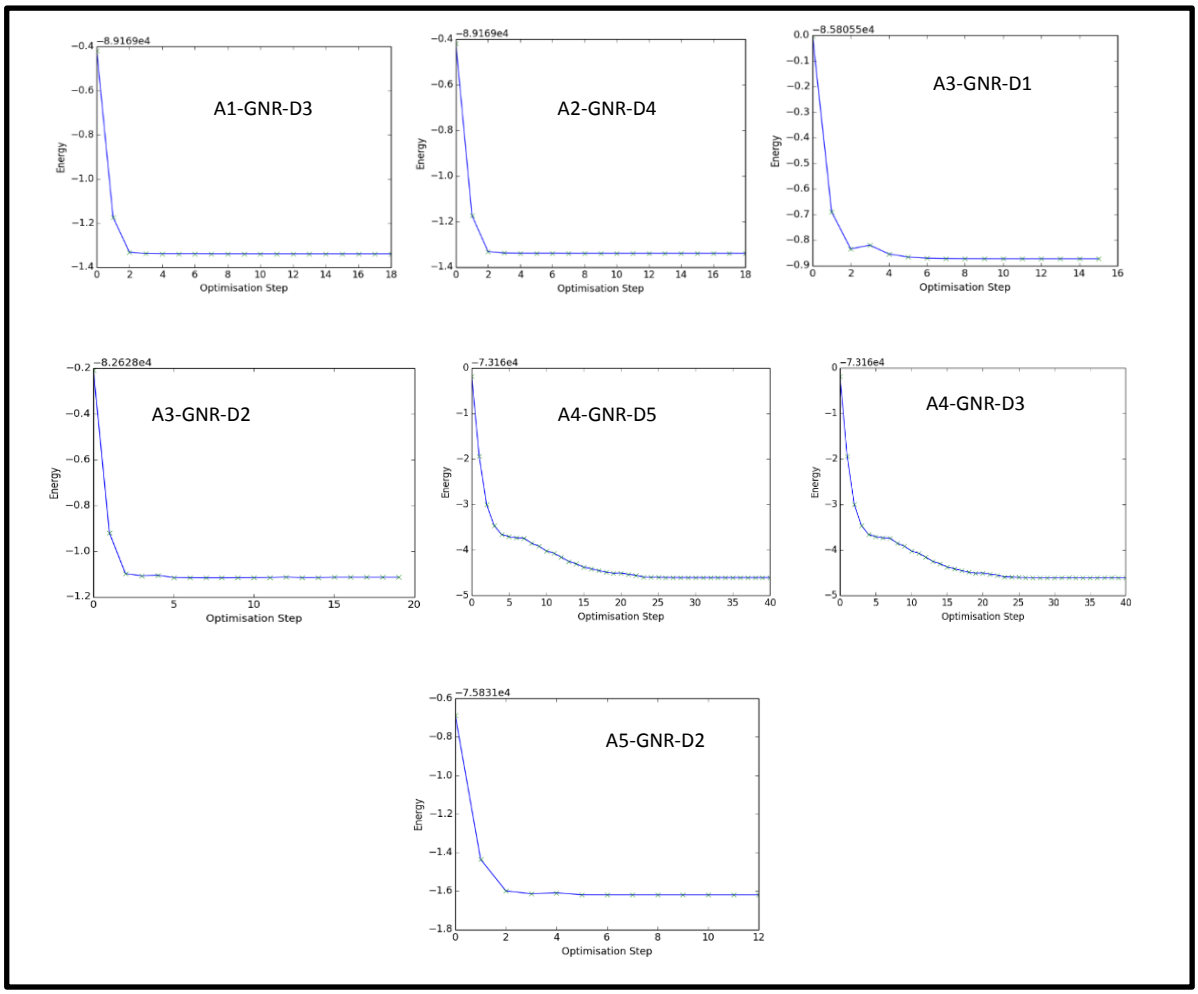

Figure (3.3): SCF energy as a function of optimization steps for Acceptor-GNR-Donor structures.

Therefore, Figure 3.3 was drawn to illustrates the variation of the relationship between the SCF total energy and the number of optimization steps for the studied structures.

Figure 3.4 shows the values of energy levels $\mathbf{E_{HOMO}}$ and $\mathbf{E_{LUMO}}$ for the structures. As noticed in Table 3.6, there are difference values of energy of the two frontier molecular orbitals for the studied structures. These frontier orbitals represent the two edges of valence and conduction bands and they are built according to linear combination of atomic orbitals. The distribution of HOMO and LUMO shapes for the structures studied in this thesis was illustrated in figure 3.5, where the green color represents the positive charges and the red color represents the negative charges.

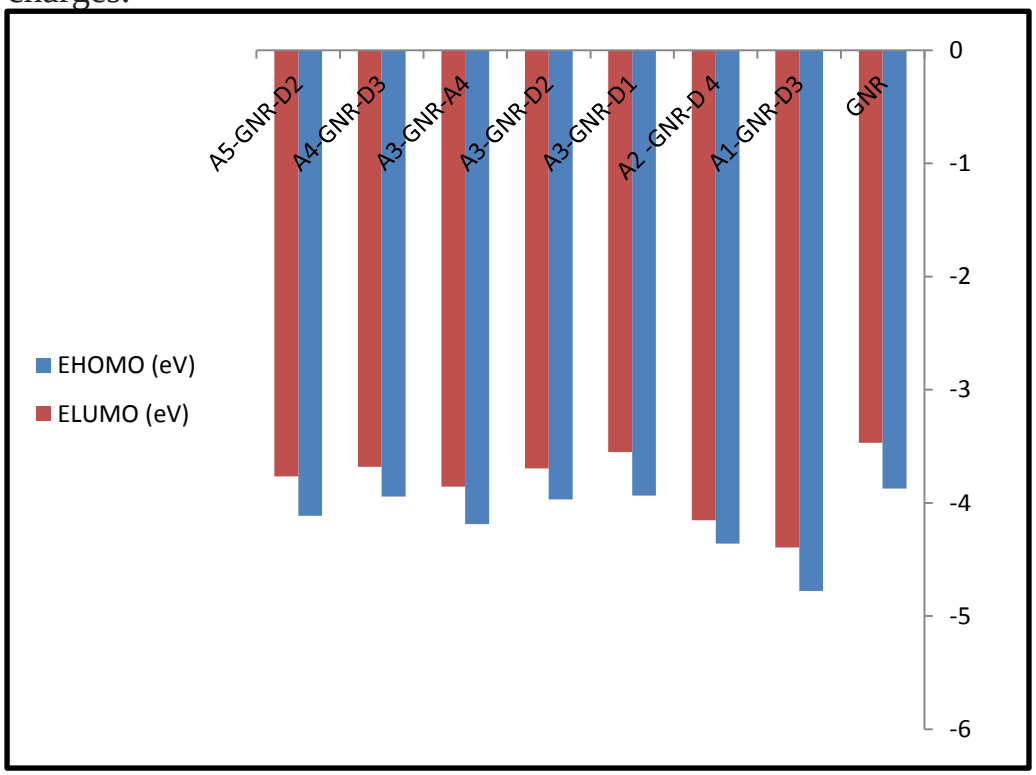

Figure (3.4): Energies of HOMO and LUMO for the studied structures.

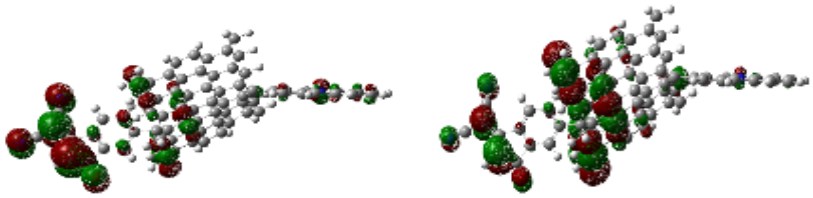

A1-GNR-D3

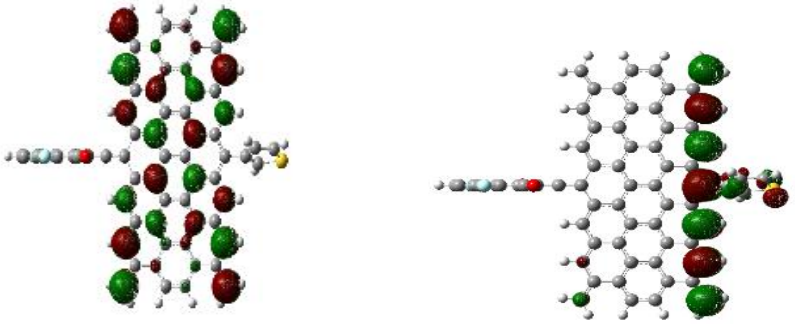

A2-GNR-D4

A3-GNR-D1

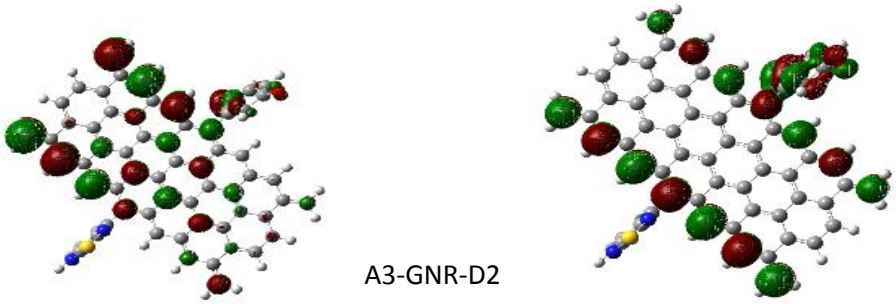

A3-GNR-D2

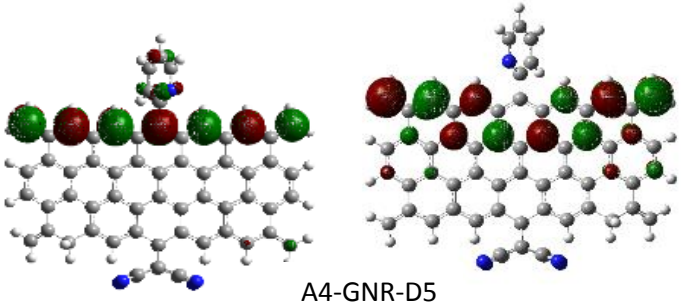

A4-GNR-D5

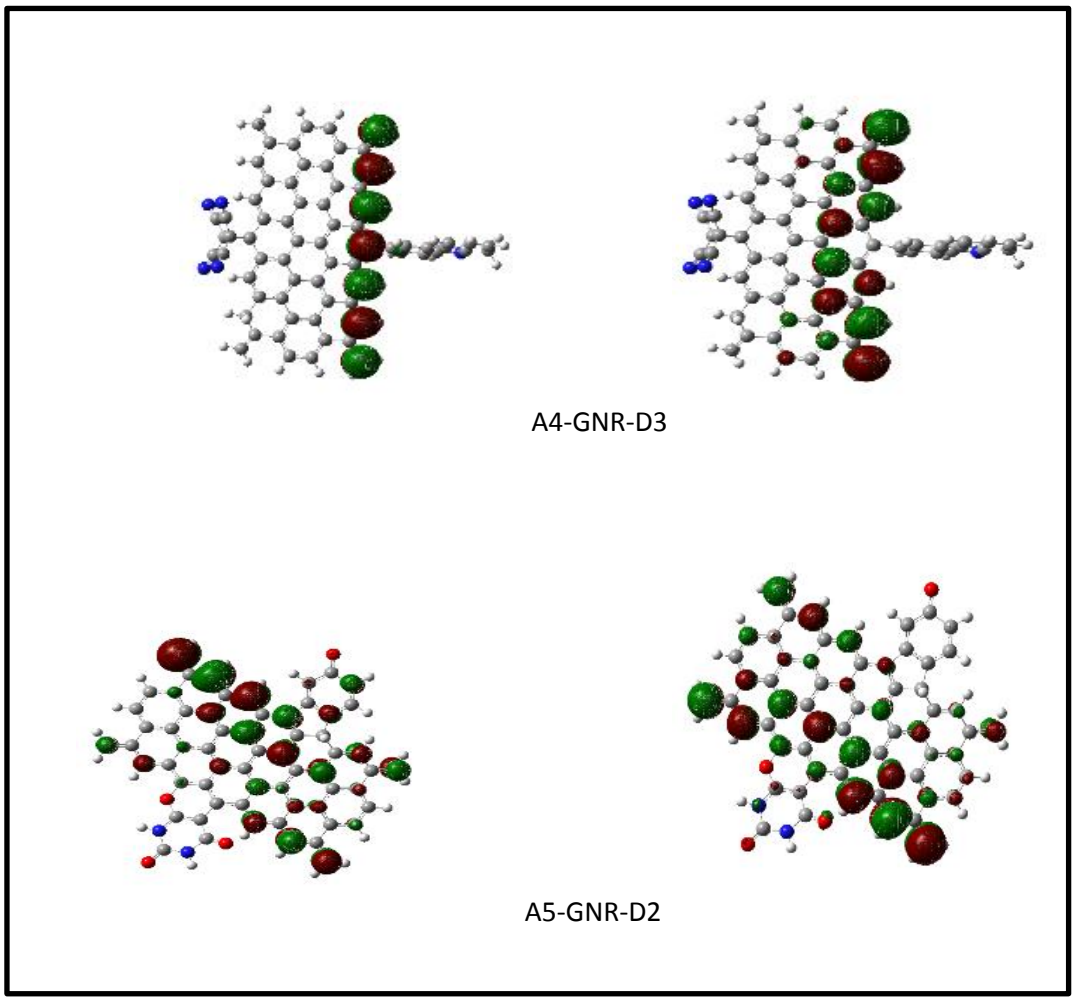

Figure (3.5): Shapes of HOMO(left) and LUMO(right) distribution for the studied structures.

Fermi energy E_F in Table 3.6 is the theoretical value of Fermi level and it was computed as the distance between the conduction band and the valence band.

Figure 3.6 declares the energy gap map for the studied Donor-GNR-Acceptor structures. Figure 3.6 showed the GNR has the largest value of energy gap compared with the designed Donor-GNR-Acceptor structures, in which makes it attractiveness and the grain of the GNR changes the value of the energy gap. A2-GNR-D4, A4-GNR-D3 and A3-

GNR-D2 have the lowest values of energy gap. Generally, the variant of E_g for the structures allow leads to different applications in electronic field.

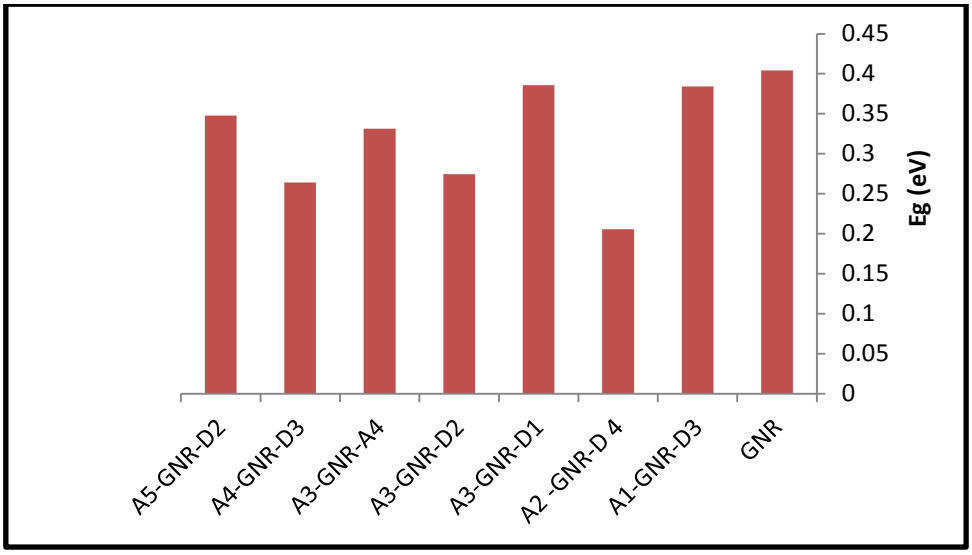

Figure (3.6): Energy gap of the structures.

3.2.1.2 Ionization Energy and Electron Affinity

Table 3.7 shows some electronic properties of the studied Donor-GNR-Acceptor molecules involved the ionization energy IE and electronic affinity EA calculated according to Koopmans theorem. As we found the highest value of ionization energy at the next fitting A1-GNR-D3 equal to 4.394 eV in which this structure needs to a large energy to donating an electron in compared with the others and the highest value of electron affinity at the next fitting A1-GNR-D3 equal to 4.778 eV in which it has high ability to accepting an electron compared with other structures. In general, all studied Donor-GNR-Acceptor molecules have values of electron affinity higher than for the base GNR. Figures 3.7 and 3.8 illustrate the IE and EA for the structures under study, respectively.

Table 3.7: Ionization energy and electron affinity for Acceptor -GNR-donor structures.

Structures	IE (eV)	EA (eV)
GNR	3.874574	3.470219
A1-GNR-D3	4.394304	4.778524
A2 -GNR-D 4	4.360291	4.154575
A3-GNR-D1	3.937432	3.551852
A3-GNR-D2	3.765186	4.112943
A4-GNR-D5	3.69607	3.970629
A4-GNR-D3	3.945051	3.681104
A5-GNR-D2	3.856615	4.187773

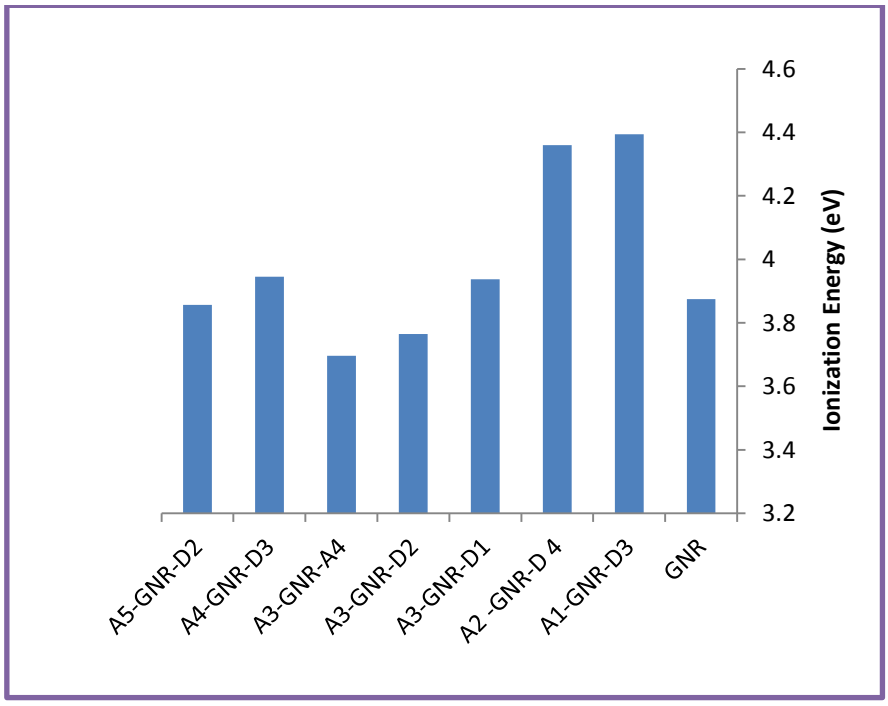

Figure (3.7): Ionization energy of the studied structures.

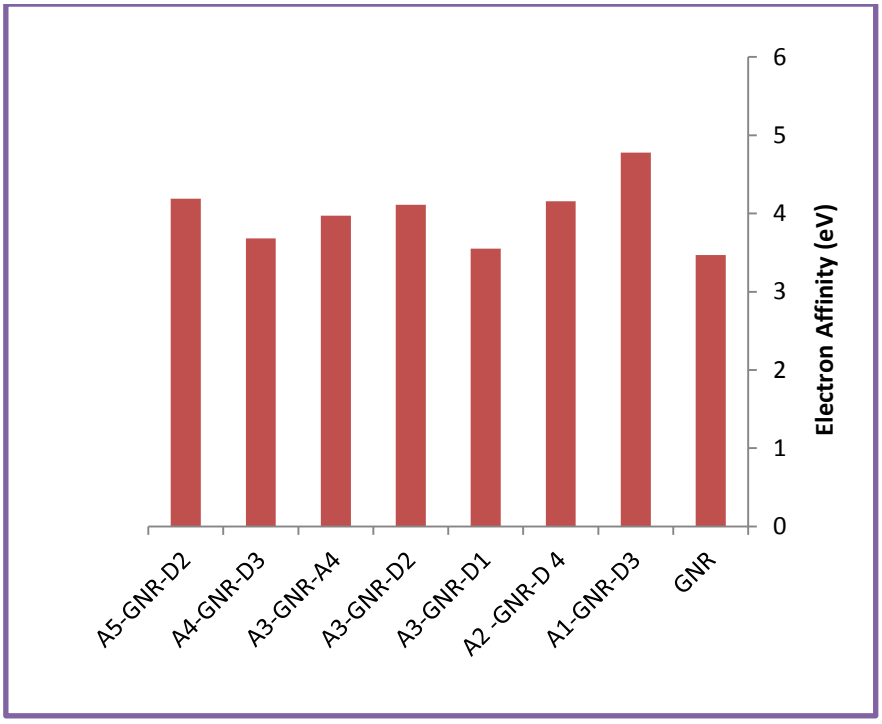

Figure (3.8): Electron Affinity of the studied structures.

3.2.1.3 Global Quantum Chemical Parameters

Some calculated global quantum chemical properties for the studied Donor-GNR-Acceptor molecules such as electrochemical hardness H, electronic softness S and electrophilic index W are presented in Table3.8.By close inspection to Figure 3.8 it was found that the Hardness was decreased when adding the donor and acceptor molecules to the graphene nanoribbon, which means that there was binding with the GNR effect or change the value of separation between the two edges of the conduction band and the valence band of the GNR. On the other hand, the constructed Donor-GNR- Acceptor molecules are more soft than the GNR, they are all have electronic softness higher than that for GNR. Softness was increases when the graphene nanoribbon is attached to the acceptor molecules on one hand and the donor molecules on the other hand. This result refers that small excitation energy was required for the

constructed Acceptor -GNR-Donor molecule in compared with GNR to an electron to transfer from valence to conduction band. Table 3.8 showed also an influence of donor and acceptor molecules on the behavior of electrophilicity of GNR, electrophilic index increased when by adding the donors and acceptors molecules. This result indicates that the constructed Donor-GNR-Acceptor molecules have high activity to interact with other molecules or species in the surroundings compared with the GNR. Figures 3.9 to 3.11 illustrate the electrochemical hardness, electronic softness and electrophilic index for the studied structures, respectively.

Table 3.8: Global Quantum Chemical Parameters of the studied Structures.

Structures	H (eV)	S $(eV)^{-1}$	W(eV)
GNR	0.202178	2.473372	33.35307
A1-GNR-D3	0.19211	2.60268	54.74788
A2-GNR-D4	0.102858	4.86109	88.11084
A3-GNR-D1	0.19279	2.593496	36.36689
A3-GNR-D2	0.137279	3.642205	53.52063
A4-GNR-D5	0.165579	3.0179708	48.85297
A4-GNR-D3	0.131973	3.788644	55.08521
A5-GNR-D2	0.173878	2.875575	44.61807

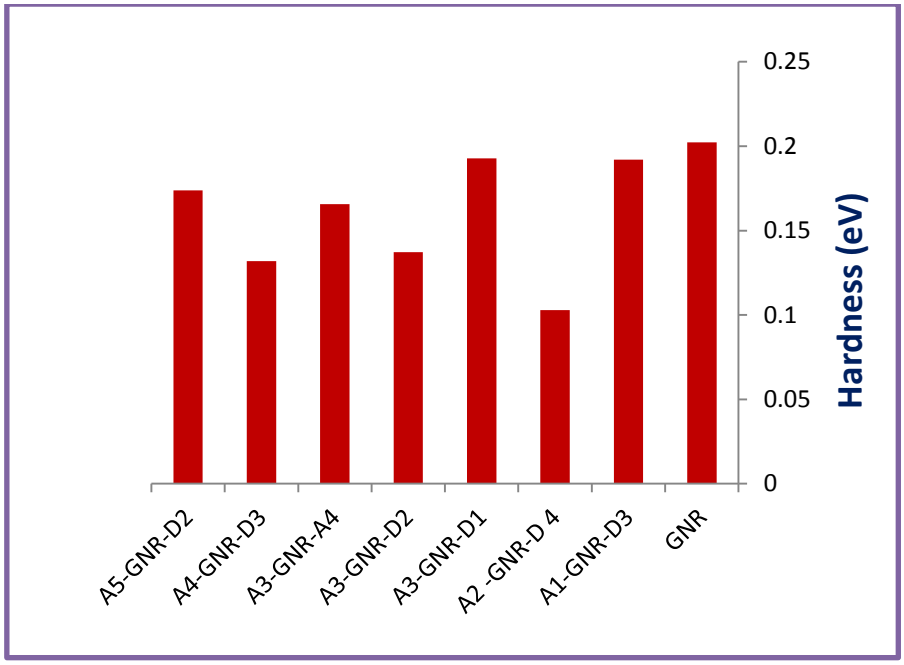

Figure (3.9): Electrochemical hardness of the studied structures.

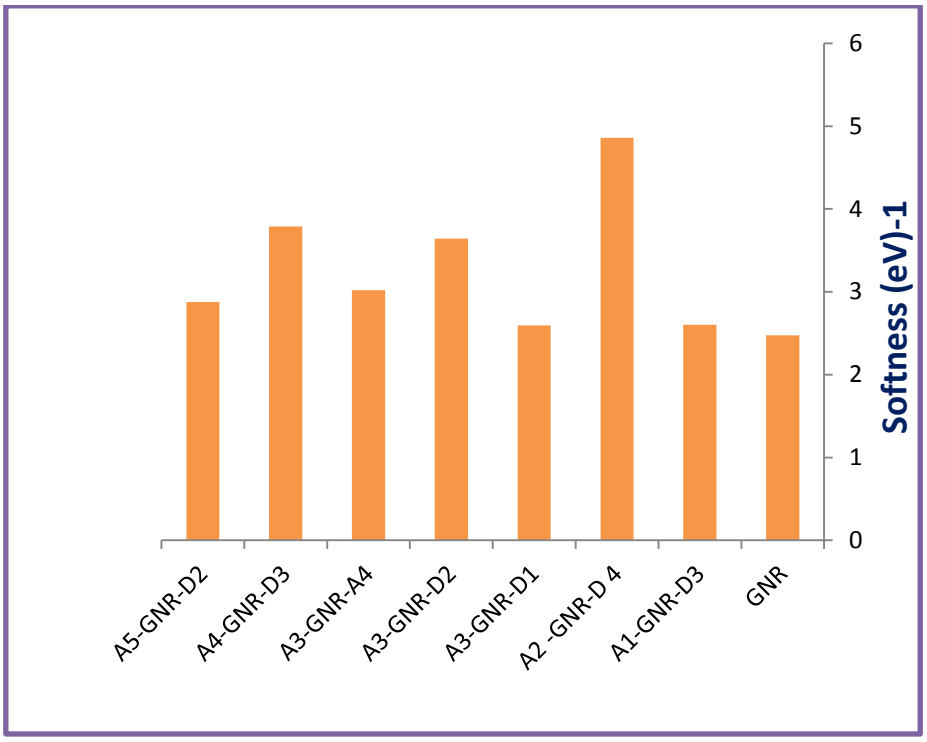

Figure (3.10): Electronic softness S of the studied structures.

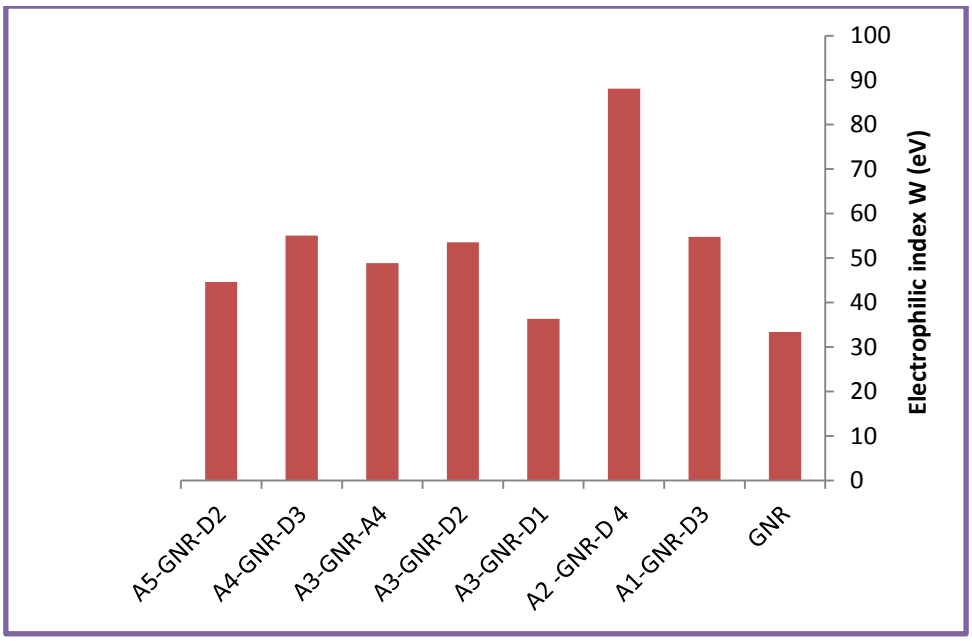

Figure (3.11): Electrophilic index W of the studied structures.

3.2.1.4 Electrostatic Potential

Figure 3.12 represents the 3-D shapes and 2-D contours of the electrostatic potential ESP distribution for the GNR and it is adducting Donor-GNR-Acceptor. As seen, highly symmetric of ESP distribution was observed for the reference GNR due to symmetrical distribution of charges in GNR of zeroth dipole moment. In the other structures, it is clear the effect of presence of both donors and acceptors on the distribution of the ESP, the electrostatic potential was dragged towards the areas of high concentration of charges in each Donor-GNR-Acceptor molecule. The map of ESP distribution leads to understanding the behavior of the molecules with and without different types of atoms and molecules in the surrounding space of each molecule.

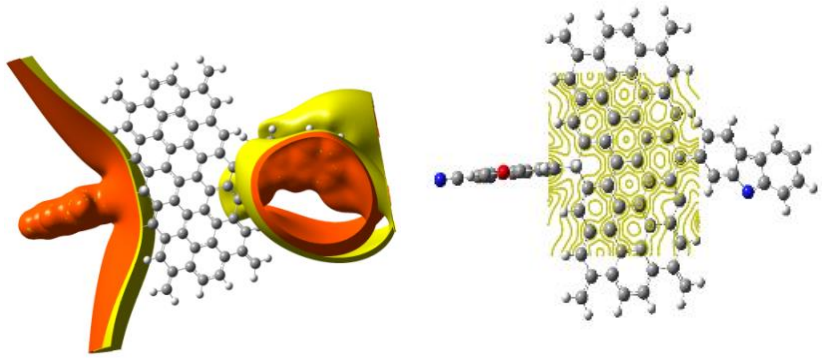

A1-GNR-D3

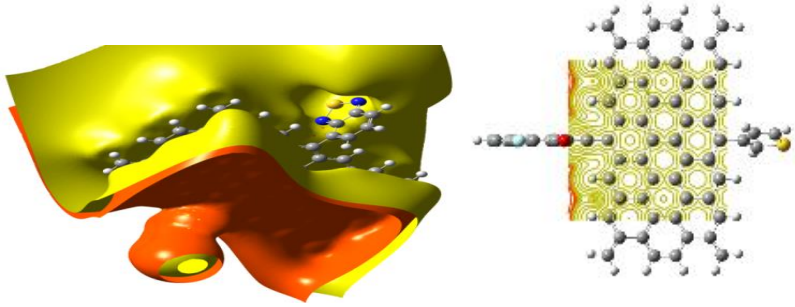

A2-GNR-D4

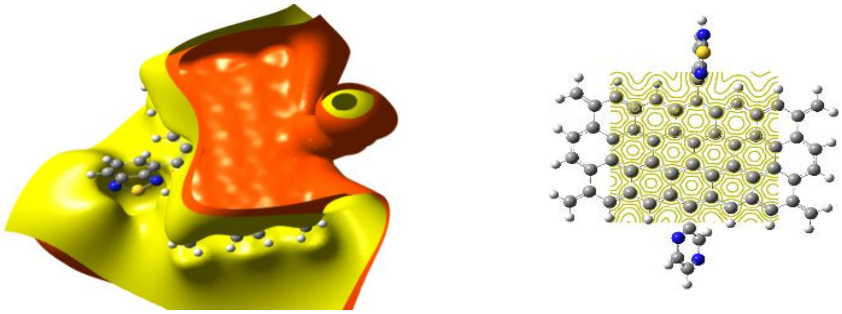

A3-GNR-D1

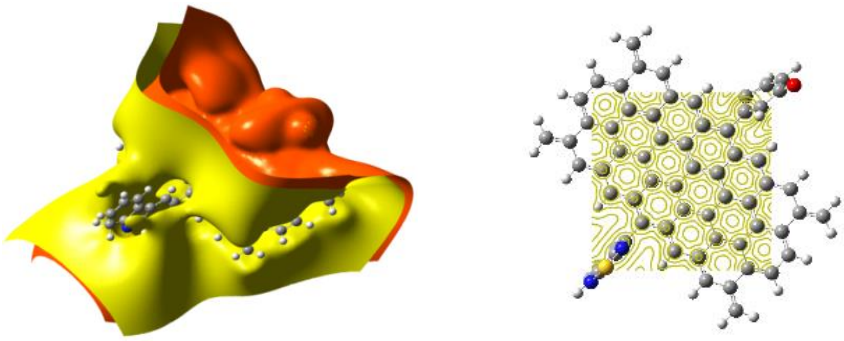

A3-GNR-D2

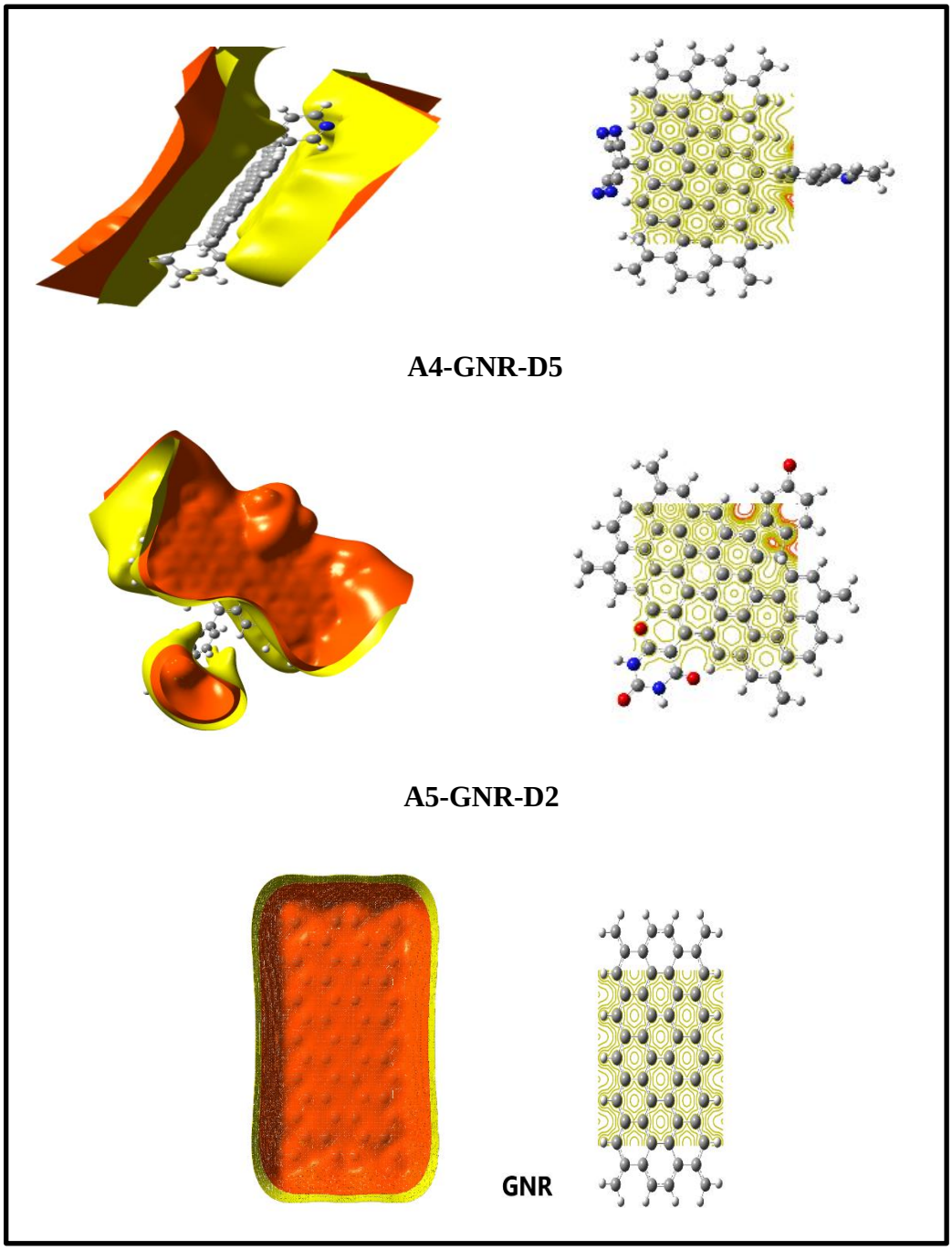

Figure (3.12): ESP distribution for the studied structures.

3.2.1.5 Density of States DOS

Figure 3.13 illustrates the spectra of the density of states DOS for the structures under study. As seen, the DOS spectra for the D-GNR-A structures were distributed according to number of the degeneracy in each D-GNR-A structure due to presence different types of donors and acceptors in the structures.

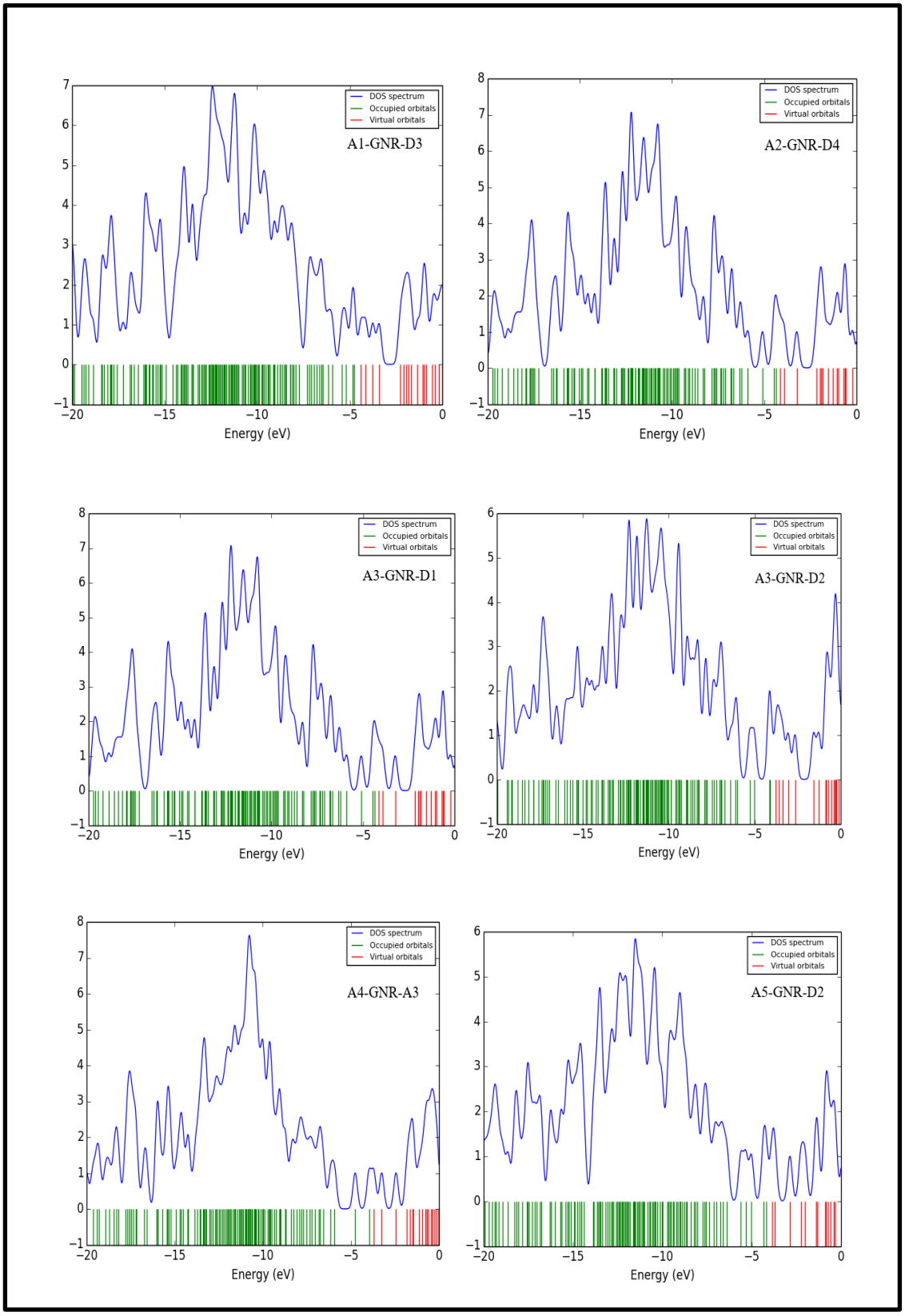

Figure (3.13): The density of states DOS distribution for the A-GNR-D structures.

Generally, the number of degeneracy of states in HOMO is greater than the degeneracy of states in LUMO, this give an idea for low probability for direct transition of an electron from valence band to conduction band and most probability of an electron transition is indirect. From Figure 3.13, one can observed the highly degeneracy of states is in A4-GNR-A3 structure at the range of energy levels between -10 eV and -13 eV.

3.2.2 Molecular Polarizability

Table 3.9 declares the results of the dipole moments in Debye and molecular polarizability in a.u., for the studied structures Donor-GNR-Acceptor molecules. The dipole moment for GNR of zero value refers to D_{6h} group symmetry and therefore GNR has highly symmetrical distribution in the space.

Table 3.9: Total dipole moment and polarizability for Donor-GNR-Acceptor molecules.

Molecules	Total dipole moment (Debye)	Polarizability (a. u)			
		α_{xx}	α_{yy}	α_{zz}	α_{ave}
GNR	0.000	131.144	1530.172	1279.221	980.179
A1-GNR-D3	16.1552	298.312	2011.941	2431.022	1580.425
A2-GNR-D4	19.2104	311.867	2275.847	2677.548	1755.087
A3-GNR-D1	2.3588	304.016	1722.254	1566.903	1197.724
A3-GNR-D2	8.6396	333.993	1973.014	2049.388	1452.132
A4-GNR-D5	7.6818	268.851	1122.002	2216.388	1202.414
A4-GNR-D3	7.7910	274.346	1171.320	2298.101	1247.922
A5-GNR-D2	9.3893	213.733	1883.644	2196.087	1431.155

The dipole moment for GNR is zero refers to D_{6h} group symmetry and therefore GNR has highly symmetrical distribution in the space. The other structures have different values of dipole moment in which refers to their low symmetric distribution these structures have, and this give D-GNR-A structures high ability to an electron transfer in comparison with the base GNR.

Results and Discussion-Part Two

3.3 Introduction

Current part included narrow Graphene Nano Ribbon GNR of length 20.905 nm and width 5.13 nm named GNR1 as drawn in Figure 3.14 and compared with GNR studied in part one. The electronic states (two frontier molecular orbitals) HOMO and LUMO, and energy gap Eg for GNR1 were computed and compared with those for GNR. GNR1 has also low value of energy gap (0.842 eV). Energy gap for GNR1 is the higher than for GNR (0.404 eV). The calculations of global quantum parameters for GNR1 showed the electronic softness for GNR1 equals 0.5/eV, this value is less than that GNR (0.61/eV). That means the dimensions of GNR make from these structures to have large/small electronic soft, and therefore, small/high excitation energy was required for charge transfer and different electronic applications can be recorded.

Figure 3.15 shows the distribution of wave functions for GNR1 compared with GNR represented by the shapes of HOMO and LUMO energies resultant from the linear combination of atomic orbitals contributed to form the molecular orbitals in the two structures. The positive charges (green color) and negative charges (red color) are distributed according to their values in the ribbon. HOMO for GNR1 is symmetrically distributed along the ribbon with almost contribution from 2p-carbon atoms, and LUMO for GNR1 has the same behavior as for z.

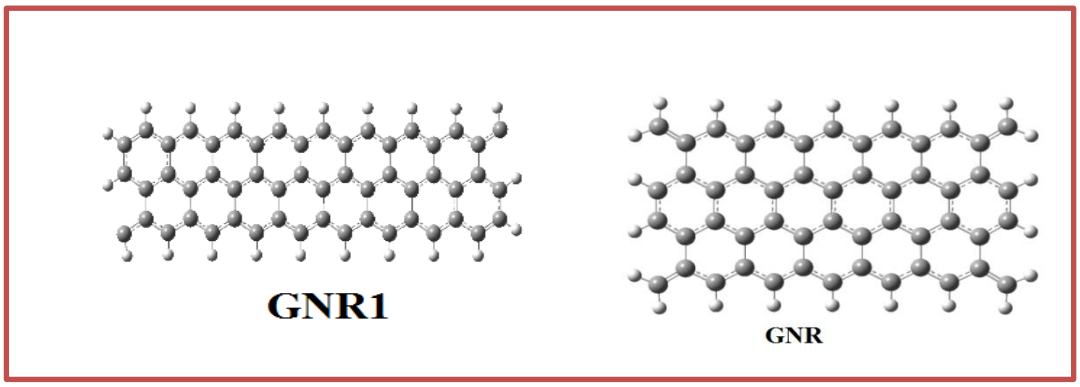

Figure (3.14): Relax structures for GNR1 and GNR.

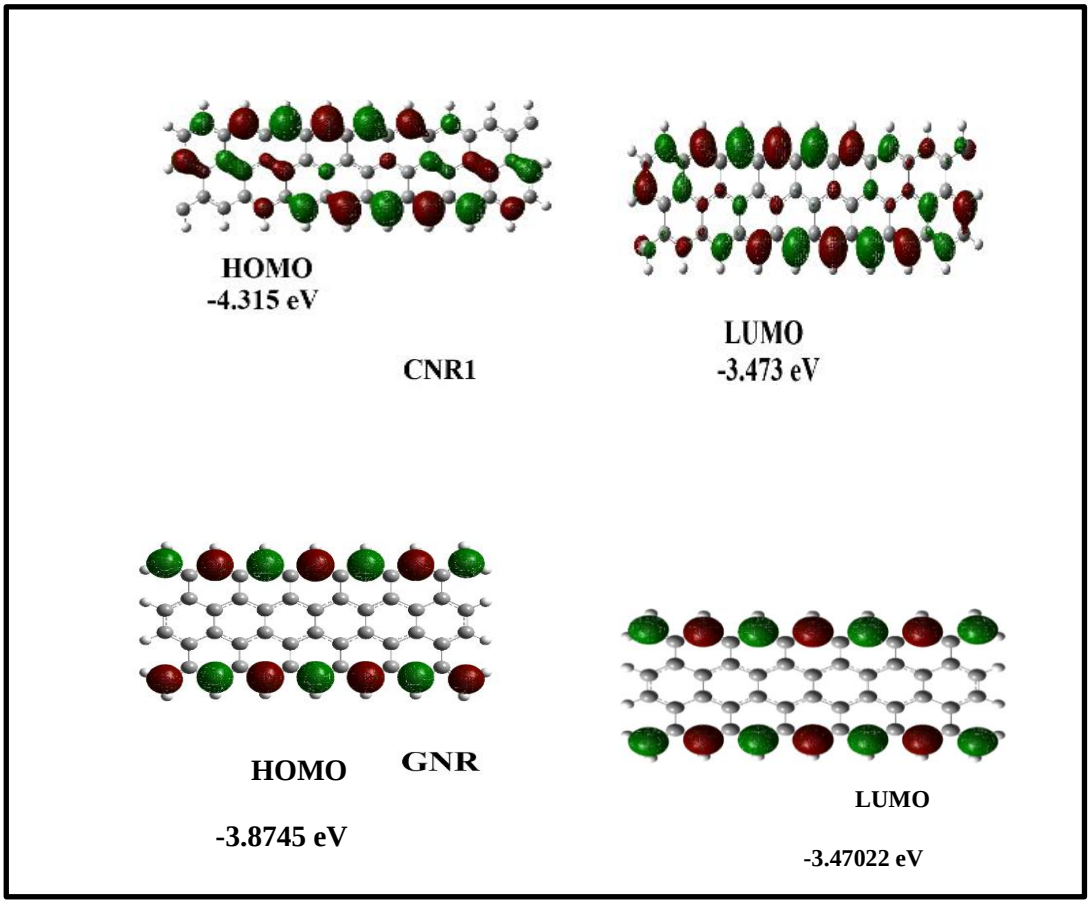

Figure (3.15): HOMO (left) and LUMO(right) shapes for GNR1 and GNR.

Figure 3.16 illustrates the density of states DOS for GNR1 and GNR. In both structures, the two frontier orbitals (occupied and unoccupied) are each near to other in which very small separation distance between the valence and conduction bands. GNR1 has separation between valence and conduction band larger than for GNR. This property

gave an electron can be easily transmission starting valence band towards conduction band. As seen, a spectrum of density of states in the two structures of GNR1 was more distributed in occupied orbitals due to high degeneracy was observed for states of occupied orbitals approaches 6 at (-11 eV) energy level, while the high degeneracy in DOS spectrum for GNR is 5 at the same energy level, and this may an indication that indirect transition can be recorded between the valence and conduction bands. In GNR1, the largest degeneracy of states was recorded between -9 eV and -15 eV, while in GNR the largest degeneracy of states was recorded between -9.5 eV and -12.5 eV.

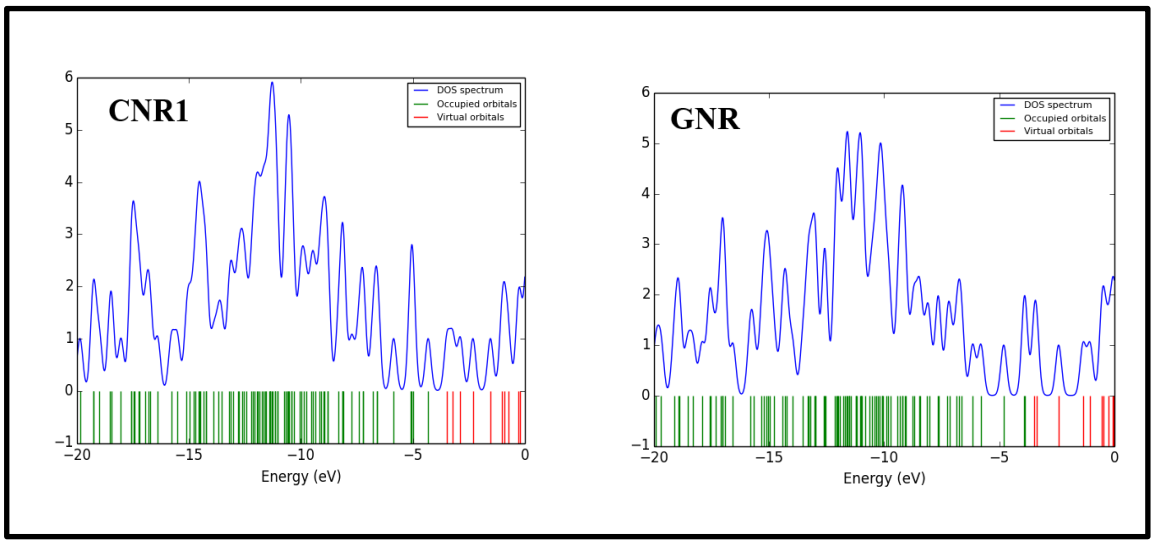

Figure (3.16): DOS for GNR1 and GNR.

The behavior of electrostatic potential ESP for GNR1 and GNR structures under study was shown in Figure 3.17. As seen, the potential was symmetrically distributed around the scattering region of pure Graphene Nano ribbons due to periodically of carbon atoms in the structures.

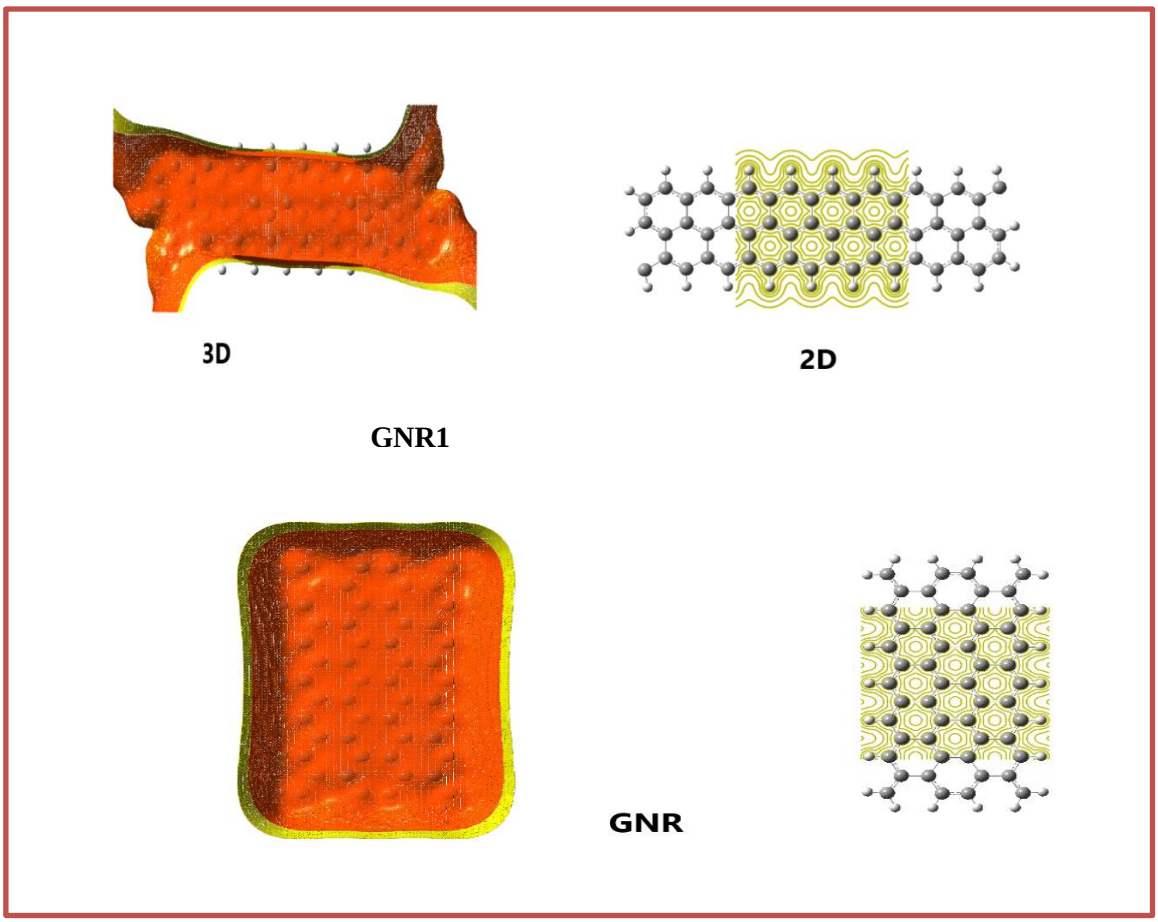

Figure (3.17): ESP distribution for GNR1 and GNR, (left=3D shapes and right=2D contours).

Table 3.10 illustrates the calculations of the molecular polarizability for GNR1 and compared with GNR included the total dipole moment D. M in Debye and molecular polarizability in a.u., Zeroth value of D. M for Graphene Ribbons is a picture of a high symmetry of the structures due to the characterization D_{6h}/C1 point group symmetry of GNR. In both structures, the rank of the components of molecular polarizability is as $\alpha_{zz} > \alpha_{yy} > \alpha_{xx}$ and this may an indication to good relax was obtained for the two GNR^s under the B3LYP/6-31G density functional theory.

Table 3.10: Total dipole moment and polarizability for GNR1 and GNR.

Structure	Total dipole moment (Debye)	Polarizability (a. u)			
		α_{xx}	α_{yy}	α_{zz}	α_{ave}
GNR	0.000	131.144	1279.221	1530.172	980.179
GNR1	0.000	119.434	456.018	775.982	450.478

3.4 Donor-GNR1-Acceptor

Figure 3.18 illustrates the relax structures for the second group of donors (D11-D33) and acceptors (A11 and A22) before they are connected graphene nanoribbon GNR1. Previously we noticed the dimensions of GNR1 were 20.905 nm length and 5.13 nm width.

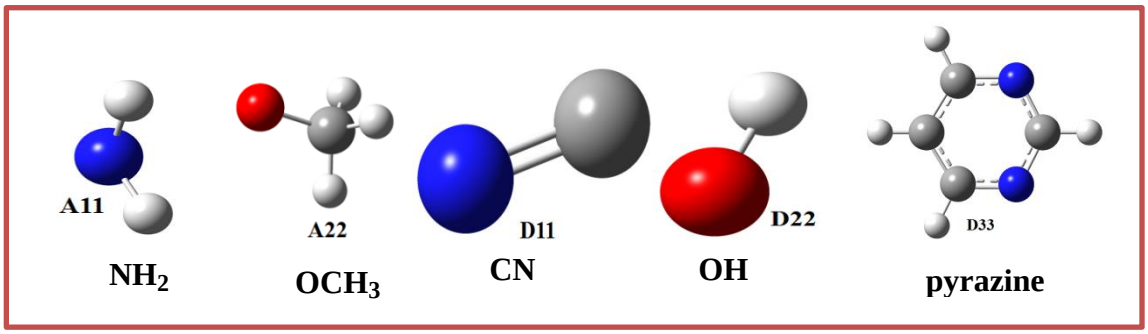

Figure (3.18): Relax structures of donors (D11-D33) and acceptors (A11 and A22).

Table 3.11: Geometric parameters for donors (D11-D33) and acceptors (A11 and A22).

Structures	Bond Length (nm)		Bond Angle (degree)	
	Bond	**Value**	**Angle**	**Value**
A11	C-N	1.0419	C-N-C	104.9979
A22	C-H	1.0843	H-C-H	108.9763- 110.8674
	C-O	1.4244	H-C-O	106.2042
D11	C-N	1.2592		
D22	O-C	0.9969		
D33	C-N	1.3509	N..C..N	126.0055
	C-H	1.0824	N..C-H	116.9974
	C..C	1.3981	C..N..C	116.5428
			N..C..C	121.8841
			C..C..C	117.1407

SCF calculations for the ground state energy with full minimization of mentioned donors and acceptors are carried out to find the standard optimized parameters involved the bond lengths in nm and bond angles in degrees, as listed in Table 3.11.

3.4.1 Ground State Energies

Table 3.12 listed the SCF calculations for the second group of donors and acceptors and graphene nanoribbon GNR1 computed from the full minimization under the employing of DFT-B3LYP/6-31G level of theory. These calculations are included the total energy E_T in a.u., high occupied molecular orbital energy E_{HOMO}, lower unoccupied molecular orbital energy E_{LUMO} and energy gap E_g in eV. The total ground state energy for suggested donors and acceptors in Table 3.12 is calculated depending on the number of electrons in each donor and acceptor.

The solution of SCF equations leads to compute of the energy of the two edges molecular orbitals E_{HOMO} and E_{LUMO}. The final molecular orbitals are computed from the linear combination of atomic orbitals based on Molecular Orbital MO theory. LUMO-HOMO gap for GNR1 is 0.842 eV, the studied donors and acceptors have values of energy gap depending on the type of the donor or acceptor. This variety in energy gap is required to choose numeral of donors and acceptors to help towards determining the meaningfully of the Donor-GNR1-Acceptor applications.

Table 3.12: Ground state energies for donors (D11-D33) and acceptors (A11 and A22).

Structure	E_T (a.u)	E_{HOMO} (eV)	E_{LUMO} (eV)	E_g (eV)
A11	-55.8529	-7.54833	-2.73933	4.809
A22	-114.379	-12.0776	-3.62478	8.452825
D11	-92.6371	-9.10208	-7.72139	1.380686
D22	-75.7085	-8.18643	-4.23811	3.948316
D33	-264.234	-6.77663	-1.36327	5.413356
GNR1	-2070.43	-4.31539	-3.47294	0.842453

3.4.2 Some Electronic Properties

In this section, some electronic variables of the compounds under study were determined depending on the values of the frontier molecular orbitals HOMO and LUMO, and calculated according to Koopmans theorem. These variables represent the electronic properties of the compounds. They are the Ionization Energy, Electron Affinity,

Electronegativity, Quantum Chemical Parameters (Electrochemical Hardness and Electronic Softness), Electrophilic Index and net electrophilicity.

3.4.2.1 Ionization Energy and Electron Affinity

Ionization energy IE and electron affinity EA for the second group of donors and acceptors were computed from the SCF calculations as vertical energies by employing the Koopmans theorem. Table 3.13 illustrates IE and EA for the donors, acceptors and GNR1.

Table 3.13 illustrates, the suggested acceptors have high values of ionization energy comparing to donors, and this indicates that the donors have high capability to donating an electron to become cations, the lowest value of ionization is for D33 donor in comparison with D11 and D22. Alternatively, A22 acceptor has high value of an electron affinity compared with A11 acceptor, this refers to that A22 perform high capability to accepting an electron to become anion in compared with A11. Generally, low ionization energy for a molecule high ability for the molecule to donating electrons. On the other hand, molecules with large values of electron affinity means the molecules have high ability to accept electrons. Table 3.13 presented different values of ionization energy and electron affinity for the studied donors and acceptors and this be responsible to allow building structures of Donor-GNR1-Acceptor.

Table 3.13: IE and EA in eV for donors (D11-D33) and acceptors (A11 and A22).

Structure	IE (eV)	EA (eV)
A11	7.548331	2.739331
A22	12.0776	3.624777
D11	9.10208	7.721393
D22	8.186429	4.238113
D33	6.776627	1.363271
GNR1	3.47294	4.315392

3.4.2.2 Global Quantum Chemical Parameters

Table 3.14 explains the quantum chemical parameters for the second group (donors and acceptors) and GNR1. These parameters included the electrochemical hardness H, electronic softness S and electrophilic index W. The result showed the values of electrochemical hardness for donors and acceptors are larger than for GNR1. While these donors and acceptors have electronic softness smaller than for GNR1. The results in Table 3.14 give one to build Donors-GNR1-Acceptors.

Table 3.14: Global quantum chemical parameters for donors (D11-D33) and acceptors (A11 and A22).

Structure	H (eV)	S $(eV)^{-1}$	W(eV)
A11	2.4045	0.207943	5.501976
A22	4.226413	0.118304	7.292376
D11	0.690343	0.724278	51.24793
D22	1.974158	0.253273	9.774373
D33	2.706678	0.184728	3.059929
GNR1	1.18701	0.421226	18.00046

3.4.2.3 Molecular Polarizability

Table 3.15 presents the total dipole moment in Debye and the average molecular polarizability α_{ave} in a.u., with its components α_{xx}, α_{yy} and α_{zz} for D11-D33 donors and A11-A22 acceptors. In Table 3.15 the components of molecular polarizability are in the rank:

$$\alpha_{xx} < \alpha_{yy} < \alpha_{zz}$$

As well as, the computed molecular polarizability depend on the type of atoms in each structure of donor and acceptor. Due to its periodically in space the GNR1 has high symmetric distribution with zero total dipole moment, the point group of GNR1 is D6h. Different values of dipole moment were recorded for donors and acceptors because of their symmetrical distribution in space. Approximately, they are all asymmetric in space with C2v point group. Generally, molecules with large values can appear charge transfer. Different structures of D-GNR1-A were constructed and studied in current study found depend on characterization of the donors and acceptors such as the molecular polarizability.

Table 3.15: Molecular polarizability for donors (D11-D33) and acceptors (A11 and A22).

Structure	Total dipole moment (Debye)	Polarizability (a. u)			
		α_{xx}	α_{yy}	α_{zz}	α_{ave}
A11	2.2727	4.632	7.048	4.632	7.368333
A22	2.4393	12.617	14.281	12.617	13.857
D11	0.0921	3.527	7.925	3.527	9.561667
D22	1.9774	1.062	2.203	1.062	3.22665
D33	2.6133	18.741	56.071	18.741	45.327
GNR1	1.3313	0	0	0	0

3.4.3 Electronic Properties of Donor-GNR1-Acceptor

Figure 3.19 illustrates the relax structures of five constructed Donor-GNR1-Acceptor were optimized at B3LYP/6-31G/DFT. The structures in present section included D11-GNR1-A11, D11-GNR1-A22, A11-GNR1-A22, D22-GNR1-A22 and A22-GNR1-D33. The minima energy for the studied structures was calculated for the convergence of both displacement and force with virial ratio equals 0.0054.

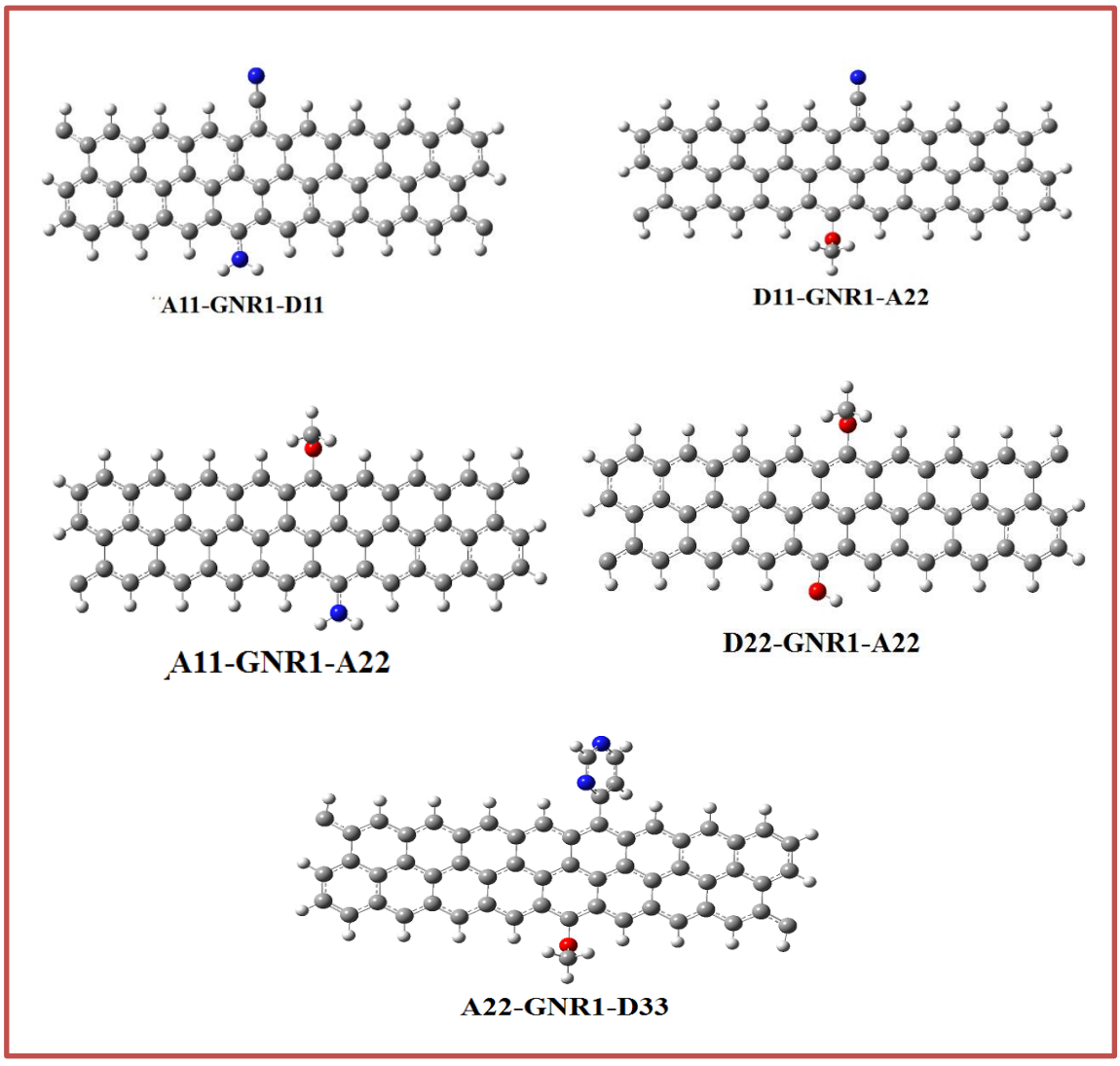

Figure (3.19): Relax structures of Donor-GNR1-Acceptor molecules.

3.4.3.1 LUMO-HOMO Gap

Table 3.16 explains the calculations of the SCF obtained from the relaxation of the structures Donor-GNR1-Acceptor, these calculations included the high occupied molecular orbital energy E_{HOMO}, lower unoccupied molecular orbital energy E_{LUMO}, Fermi energy E_F and the energy gap E_g in eV.

Table 3.16: E_{HOMO}, E_{LUMO}, E_F, and E_{gap} for Donor-GNR1-Acceptor.

Structures	E_{HOMO} (eV)	E_{LUMO} (eV)	E_F (eV)	E_g (eV)
D11-GNR1-A11	-4.33526	-3.54342	-3.93934	0.79184
D11-GNR1-A22	-4.51947	-3.73036	-4.12491	0.789119
A11-GNR1-A22	-4.04981	-3.28246	-3.66613	0.76735
D22-GNR1-A22	-4.2626	-3.45035	-3.85647	0.812248
D33-GNR1-A22	-4.38532	-3.56138	-3.97335	0.823949

The SCF total energy for the structures of Donor-GNR1-Acceptor was computed according to the number of iterations in each cycle through the way out of SCF calculations.

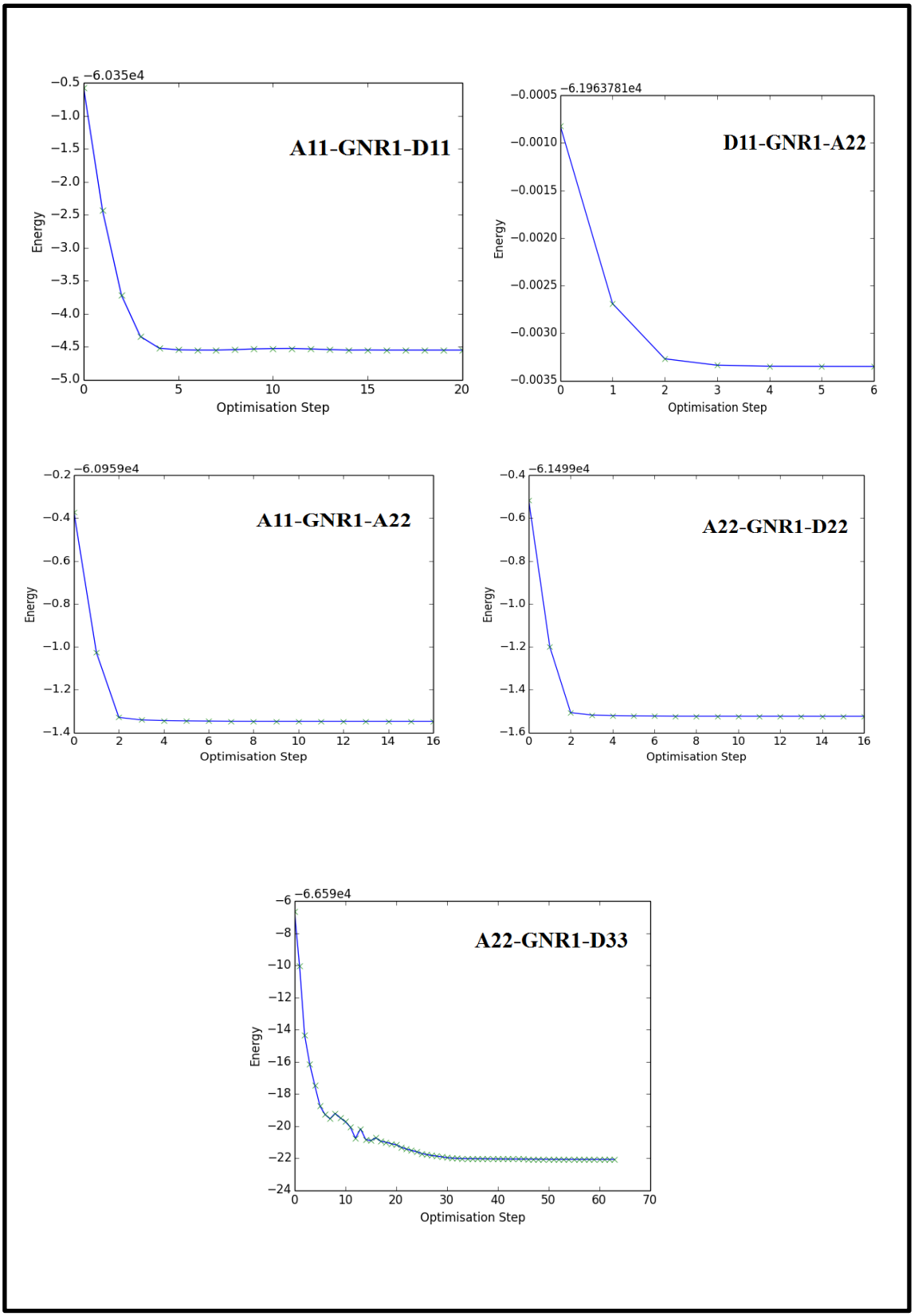

Figure (3.20): Relationship of SCF energy with optimization steps for Acceptor-GNR1-Donor.

Figure 3.20 illustrates the relationship between the SCF total energy and the number of optimization steps for the studied structures in which the limitations are determined depending on the types of both donors and acceptors in each Donor-GNR1-Acceptor.

Figure 3.21 presents the E_{HOMO} and E_{LUMO} for the Donor-GNR1-Acceptor. As seen in Table 3.16, the values of HOMO energy for all structures are approximately close to other and they lie in the range -4 eV to -4.5 eV. The LUMO energy for the structures also all lie in the range -3.2 eV to -3.7 eV. Figure 3.22 shows the 3-D distribution of HOMO and LUMO for Donor-GNR1-Acceptor structures, where the green color represents the positive charges and the red color represents the negative charges. The two wave functions HOMO and LUMO for the studied structures were distributed depending on the types atoms in both donors and acceptors in each structure and according to the linear combination of atomic orbitals.

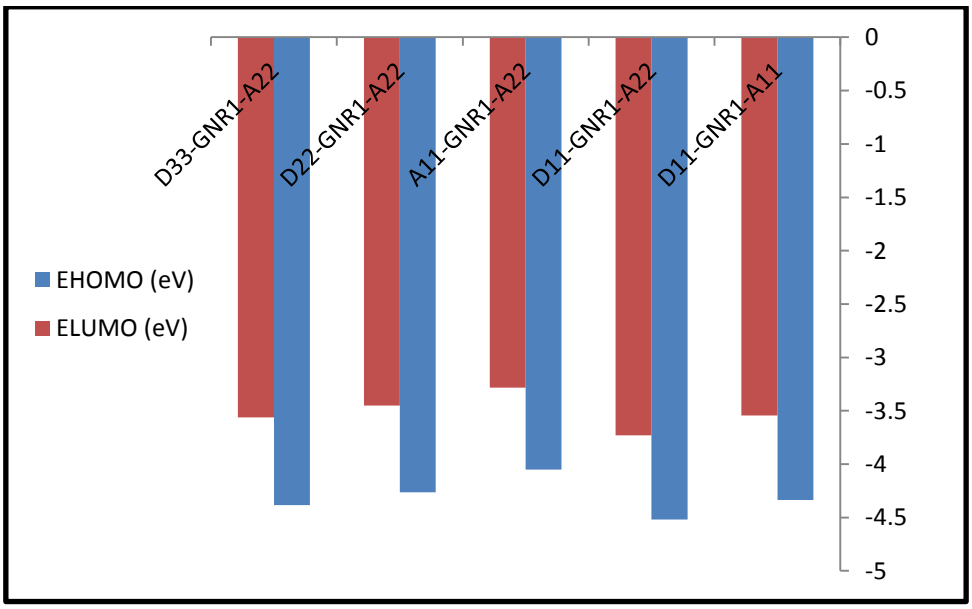

Figure (3.21) : E_{HOMO} and E_{LUMO} for Donor-GNR1-Acceptor.

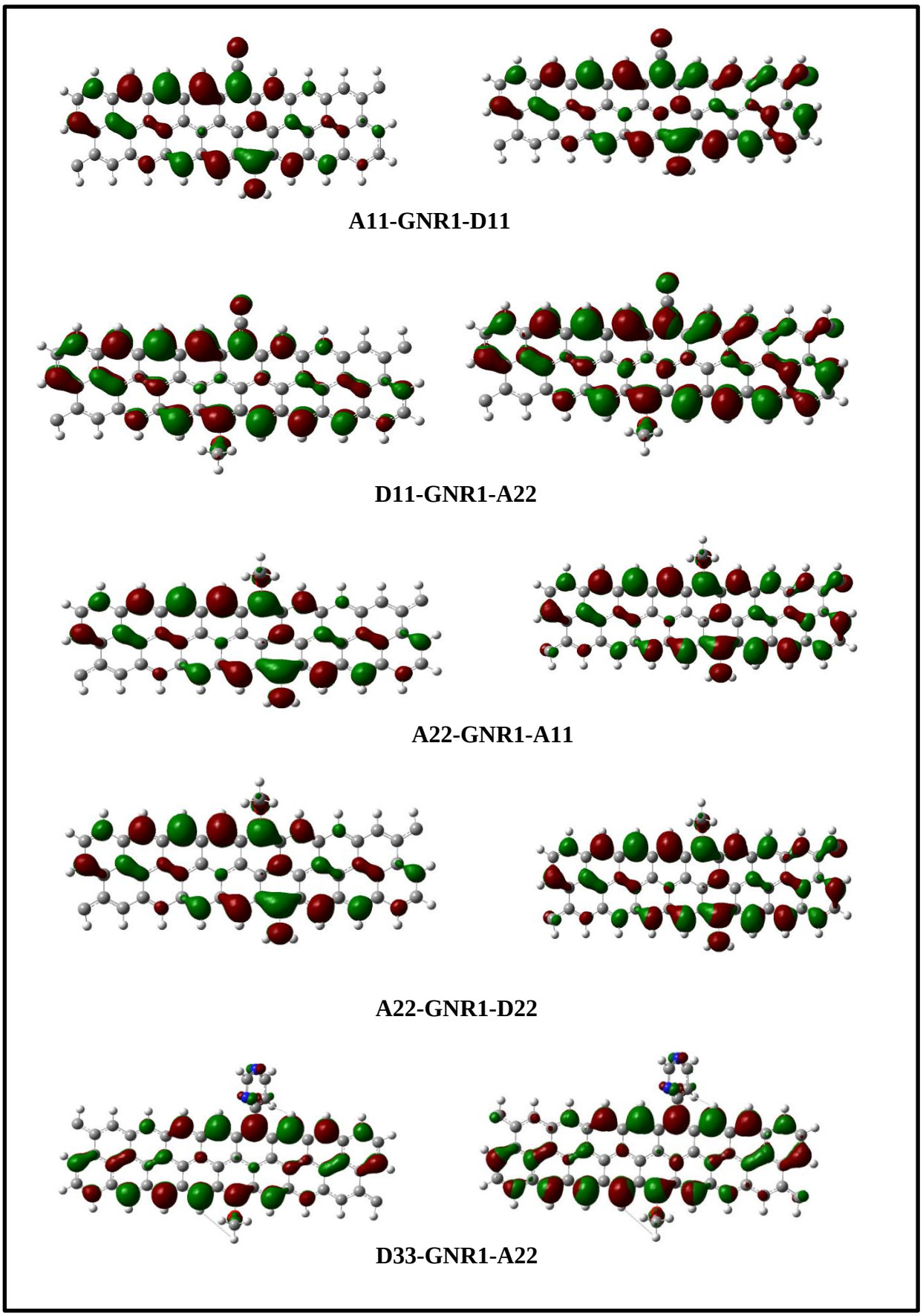

Figure (3.22) : HOMO(left) and LUMO(right) distribution for Donor-GNR1-Acceptor.

The theoretical value of Fermi energy E_F in Table 3.16 showed the structure A11-GNR-A22 has the lowest value as E_F is the midpoint of the separation between the conduction and valence band. LUMO-HOMO gap results for the Donor-GNR1-Acceptor in Figure 3.23 showed that all Donor-GNR1-Acceptor have energy gap lower than that for the pure GNR but A11-GNR-A22 has the lowest value. Presence of donors and acceptors in the GNR reduces the energy gap. In summary, the rank of energy gap for the group of Donor-GNR1-Acceptor structures is as:

A11-GNR1-A22 < D11-GNR1-A22 < D11-GNR1-A11 < D22-GNR1-A22 < D33-GNR A22.

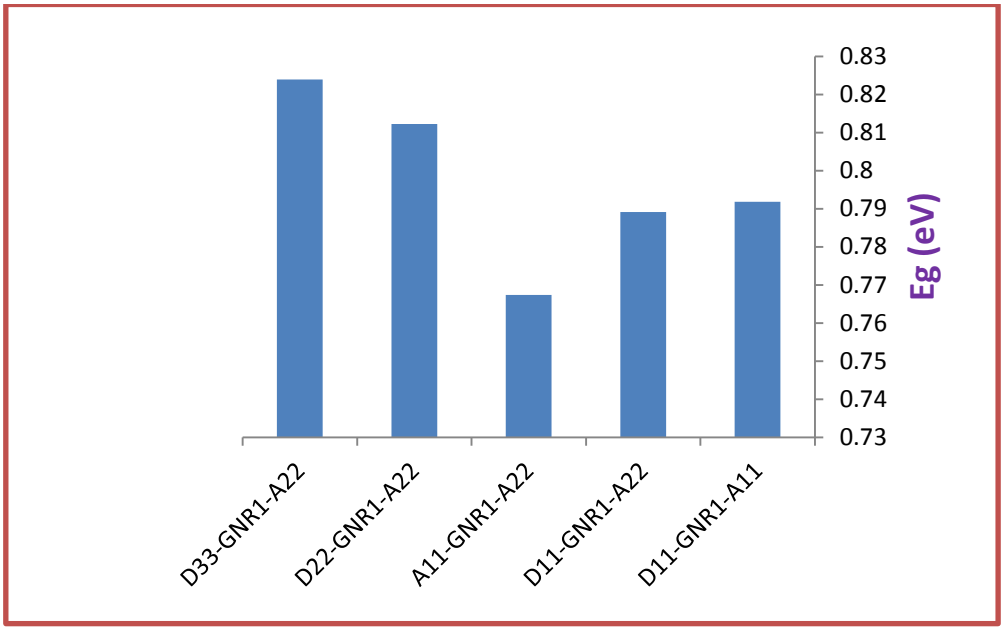

Figure (3.23) : Energy gap of Donor-GNR1-Acceptor.

3.4.3.2 Ionization Energy and Electron Affinity

Table 3.17 explains the calculated values of ionization energy IE and electronic affinity EA for the studied Donor-GNR1-Acceptor structures based on Koopmans theorem. The result showed

A11-GNR1-A22 structure has the lowest IE in which it needs small energy to donate an electron to become cation in comparison with the others, while D11-GNR1-A22 needs high energy for donating an electron due to that this structure has the highest value of EA, D11-GNR1-A22 structure can easily accepting an electron to become anion in comparison with the others. Figures 3.24 and 3.25 declare the IE and EA for the studied Donor-GNR1-Acceptor structures, respectively.

Table 3.17: Ionization energy and electron affinity for Donor-GNR1-Acceptor.

Structures	IE (eV)	EA (eV)
D11-GNR1-A11	4.335257	3.543416
D11-GNR1-A22	4.519475	3.730356
A11-GNR1-A22	4.049813	3.282463
D22-GNR1-A22	4.262603	3.450355
D33-GNR1-A22	4.385325	3.561376

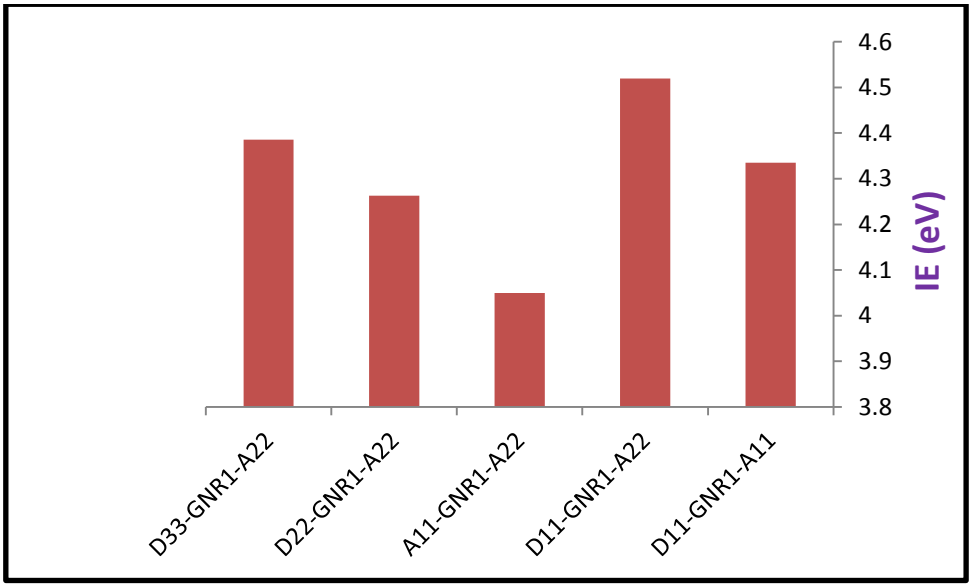

Figure (3.24) : Ionization energy of Donor-GNR1-Acceptor.

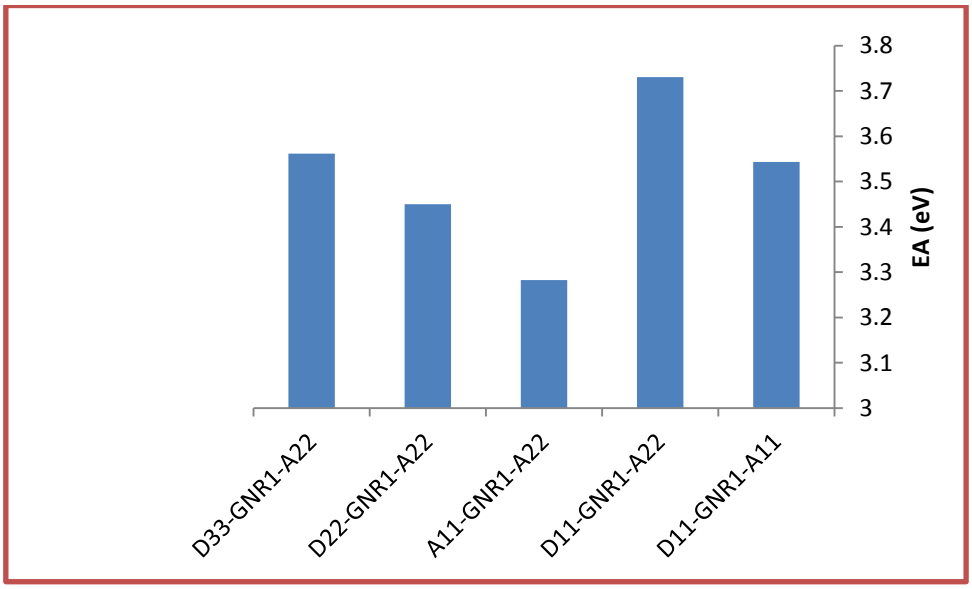

Figure (3.25) : Electron Affinity of Donor-GNR1-Acceptor.

3.4.3.3 Global Quantum Chemical Parameters

Some global quantum chemical properties for second group of Donor-GNR1-Acceptor were calculated and listed in Table 3.18 included the electrochemical hardness H, electronic softness S and electrophilic index W. Table 3.18 showed the electrochemical Hardness was reduced with the addition of donors and acceptors GNR1, this refers to effect of type of donors and acceptors on the gap between the conduction and valence band of the GNR1. The result showed all structures of Donor-GNR1-Acceptor have electrochemical hardness less than 0.451 eV, as shown in Figure 3.26. Alternatively, the constructed Donor-GNR1-Acceptor have electronic soft greater than for GNR1, S for such structures more than 1 eV, as in Figure 3.27. In other words, electronic softness was increased with adding the donors and acceptors to GNR1. This result is a sign to small excitation energy was required for the constructed Donor-GNR1-Acceptor to an electron to transfer from

valence to conduction band in compared with GNR1. Instead, Table 3.18 showed the power of donors and acceptors on increasing the electrophilic index of GNR1, electrophilic index was increased due to the addition of the donors and acceptors. D11-GNR1-A22 has the largest value of electrophilic in which this structure has high activity to act together with other molecules in the surroundings space in comparison with the others. Figure 3.28 shows the electrophilic index for the studied Donor-GNR1-Acceptor.

Table 3.18: Global quantum chemical parameters for Donor-GNR1-Acceptor.

Structures	H (eV)	S $(eV)^{-1}$	W(eV)
D11-GNR1-A11	0.39592	1.262881	19.59786
D11-GNR1-A22	0.39456	1.267236	21.56193
A11-GNR1-A22	0.383675	1.303186	17.51556
D22-GNR1-A22	0.406124	1.231151	18.3102
D33-GNR1-A22	0.411975	1.213667	19.16079

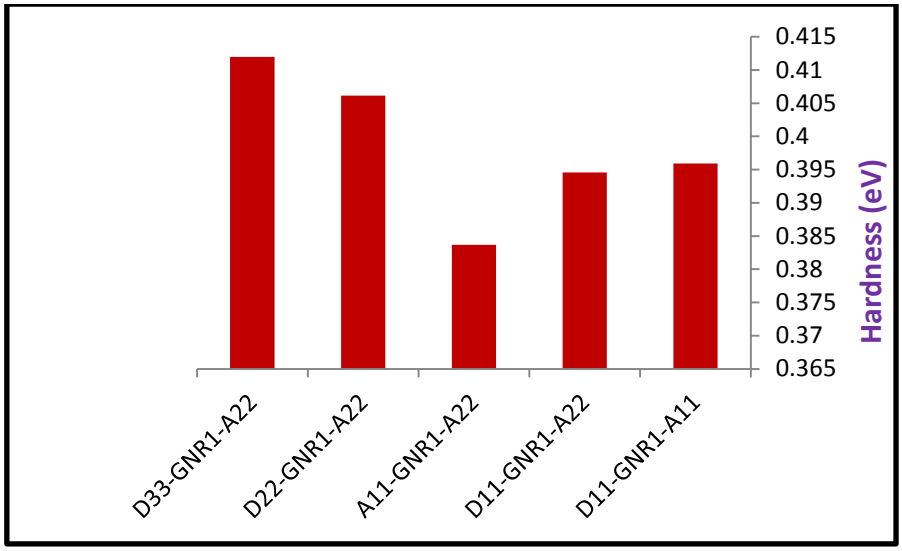

Figure (3.26): Electrochemical hardness of Donor-GNR1-Acceptor.

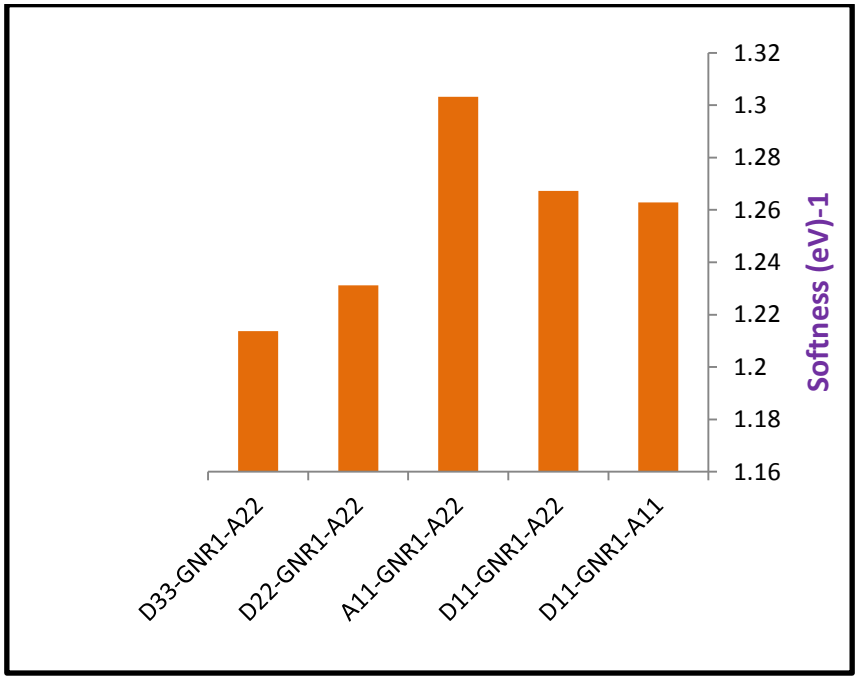

Figure (3.27): Electronic softness of Donor-GNR1-Acceptor.

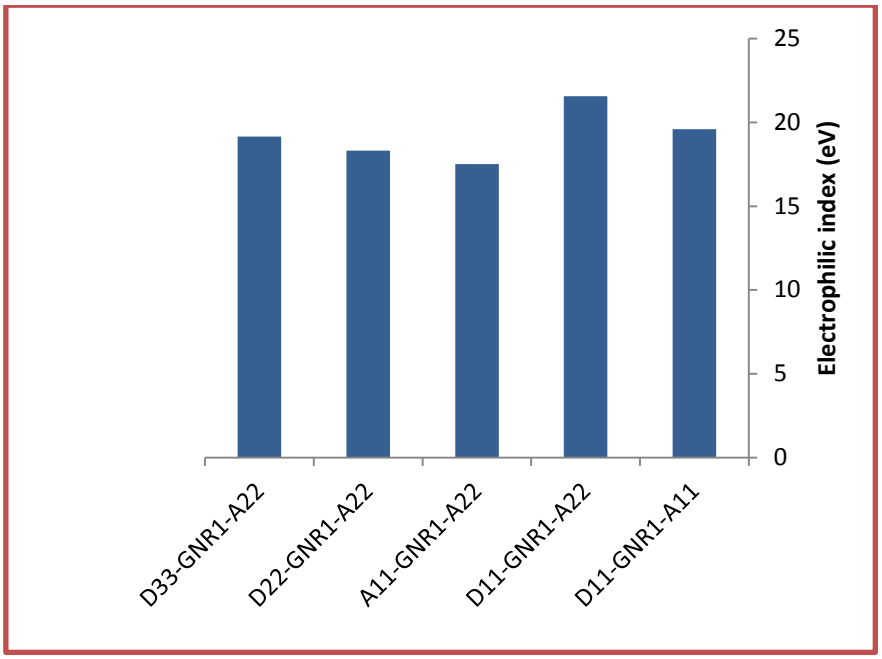

Figure (3.28): Electrophilic index of Donor-GNR1-Acceptor.

3.4.3.4 Electrostatic Potential

Total SCF of electrostatic potential ESP for the second group of Donor-GNR1-Acceptor was drawn in Figure 3.29. This figure showed, an influence of existence of donors and acceptors on the ESP distribution of GNR1, ESP was drawn in the direction of the parts of atoms of high electronegativity in each donor-GNR1-Acceptor. These distribution principals to considerate the actions of the structure with and without different types of atoms, molecules in the surrounding space of each Donor-GNR1-Acceptor. D11-GNR1-A22 structure appears highly distribution of ESP in the areas near the molecules OCH_3 and CN due to high electronegativity for oxygen and nitrogen atoms. For the other Donor-GNR1-Acceptor, the picture of ESP is clear at the areas near the adding subgroups as donors and acceptors.

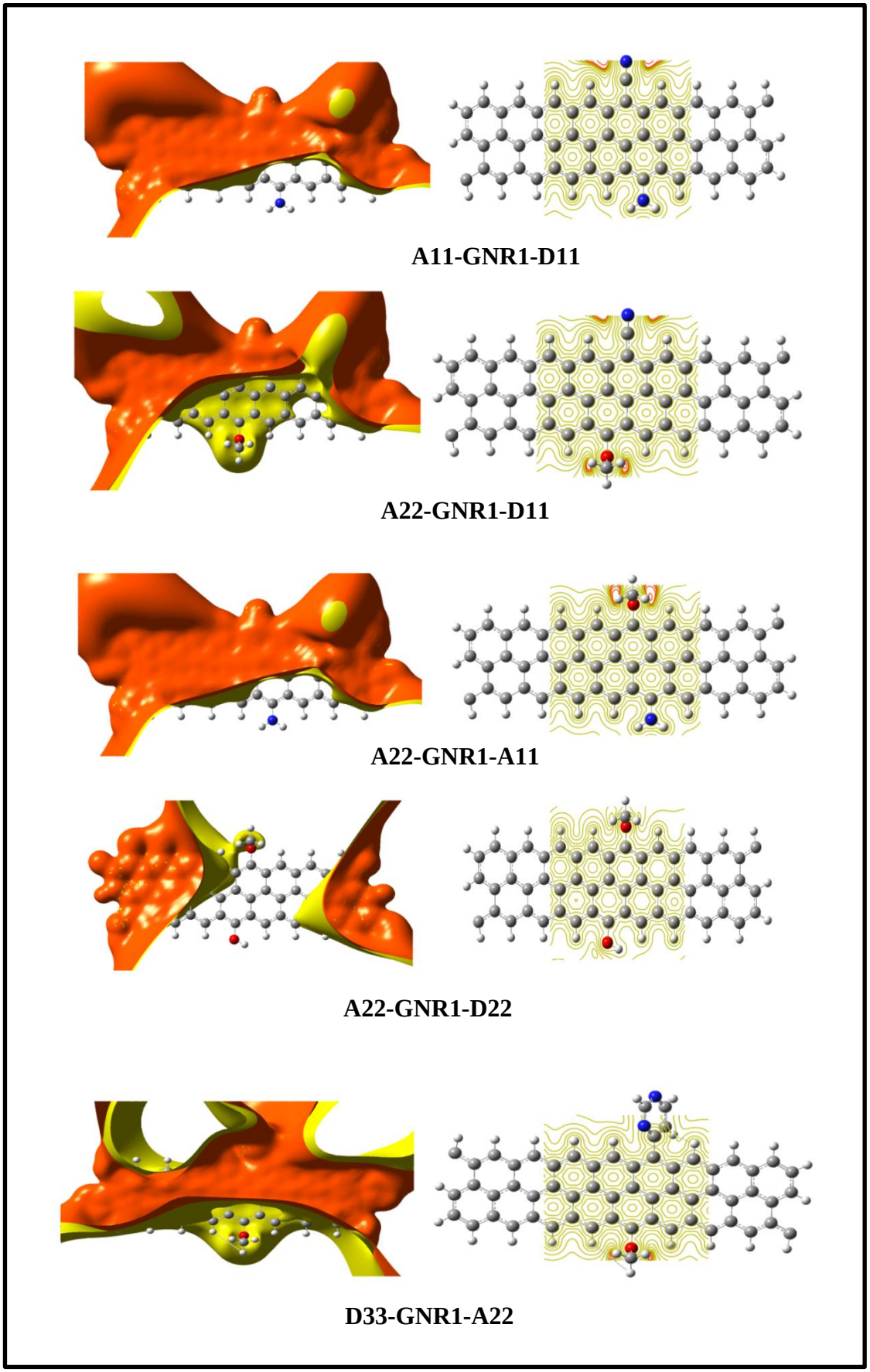

Figure (3.29): ESP distribution of Donor-GNR1-Acceptor.

3.4.3.5 Density of States

Figure 3.30 explain the density of states DOS spectra for studied Donor-GNR1-Acceptor. As seen, the DOS spectra for the Donor-GNR1-Acceptor were spread according to number of the degeneracy in each structure because of the occurrence different types of donors and acceptors in the GNR1. Commonly, the number of degeneracy of states in HOMO for the structures is greater than the degeneracy of states in LUMO and this result provide an indication for low probability for direct transition of an electron from valence to conduction band and the greatest probability of an electron transition is indirect transition. Figure 3.30 observed the highly degeneracy of states is in D11-GNR1-A22 at the range of energy levels between -10 eV and -13 eV.

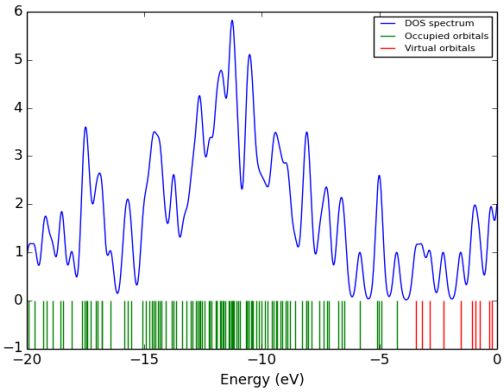

A11-GNR1-D11

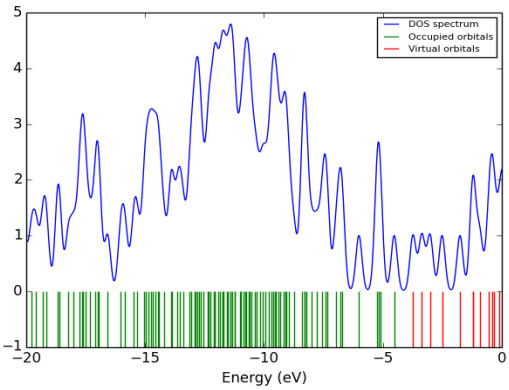

D11-GNR1-A22

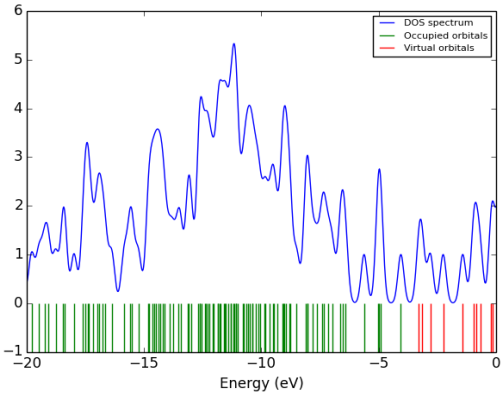

A11-GNR1-A22

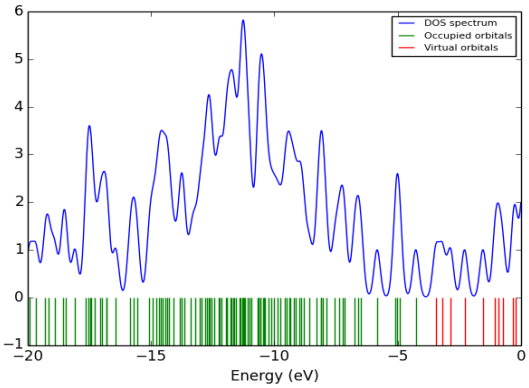

D22-GNR1-A22

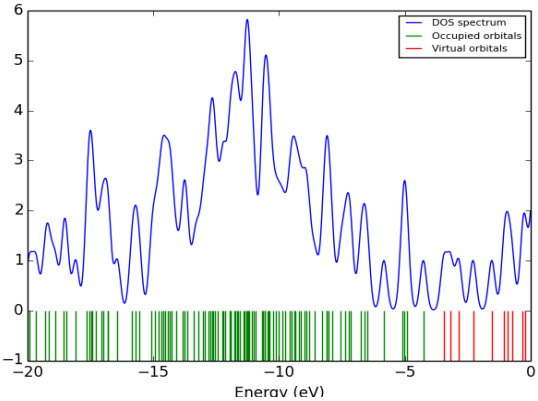

A22-GNR1-D33

Figure (3.30) : DOS distribution of Donor-GNR1-Acceptor.

Results and Discussions-Part three

3.5 Gas Sensing

3.5.1 Introduction

Before the starting of discussion of the sensing of Donor-Graphene Nano Ribbon-Acceptor for gas, we choose the appropriate structure D11-GNR1-A22 due to its suitable properties such as electron affinity and electrophilic index, therefore, the two subgroups, methoxide OCH_3 and cyanide CN are connected to first GNR and then relaxation process for the D11-GNR-A22 was done for comparing between the two structures D11-GNR1-A22 and D11-GNR-A22. Figure 3.31 shows the relax of the two structures.

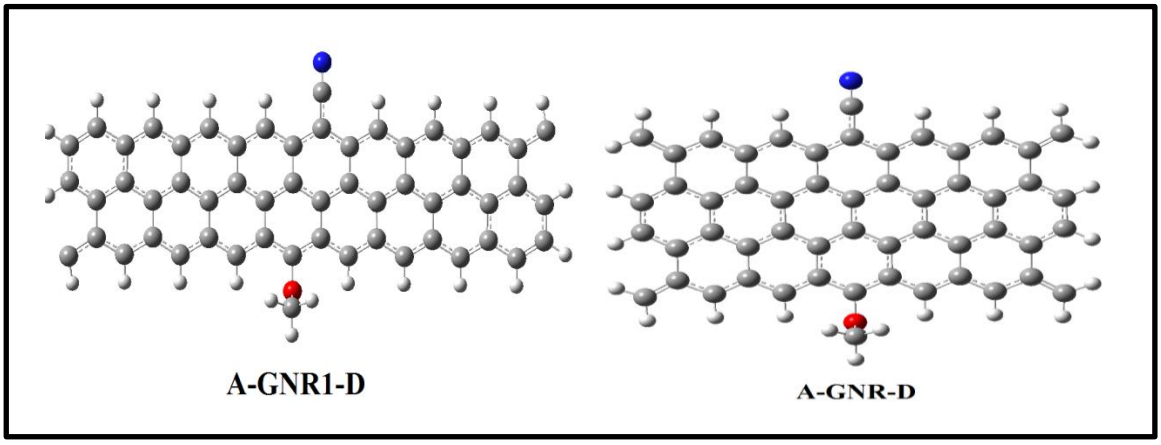

Figure (3.31): Relax structures GNR and GNR1 with OCH_3 and CN.

Table 3.19 explains the electronic properties from the SCF calculations for D11-GNR-A22 included the E_T, E_{HOMO}, E_{LUMO}, E_F and E_g with the values of these electronic properties for D11-GNR1-A22 from previous section.

LUMO-HOMO gap for D11-GNR-A22 is less than that for D11-GNR1-A22, as in Figure 3.32. This result refers to D11-GNR-A22 structure can take place in the field of conducting materials comparing with D11-GNR1-A22 structure of energy gap can put it in the range of

semiconductor materials. The difference in energy gap enable to decide which one of these two structures can performed in limit field of materials.

Figure 3.33 declares the shapes of distribution of the two wave functions HOMO and LUMO for the two structures. As seen, approximately there is no clear difference can have recorded in the shapes of HOMO and LUMO for the two structures, this due to these wave functions are built from the same atomic orbitals in the two structures.

Table 3.19: SCF calculations for D11-GNR1-A22 and D11-GNR-A22.

Structure	**E_T (a. u)**	**E_{HOMO} (eV)**	**E_{LUMO} (eV)**	**E_F (eV)**	**E_g (eV)**
D11-GNR-A22	**-2201.062**	**-4.0835**	**-3.7061**	**-3.8948**	**0.37741**
D11-GNR1-A22	**-2277.127**	**-4.5194**	**-3.7303**	**-4.1249**	**0.78911**

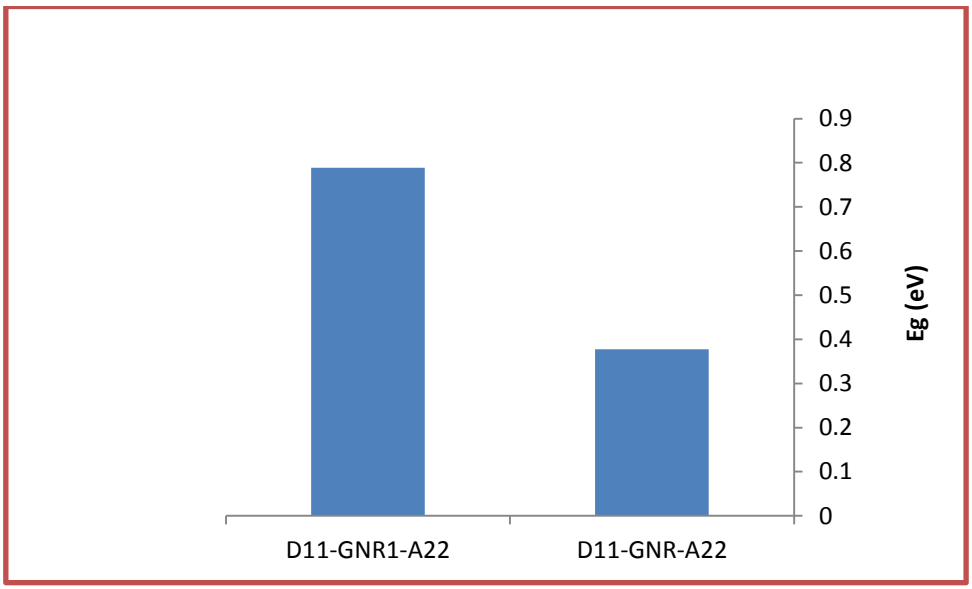

Figure (3.32) : E_{gap} for D11-GNR-A22 and D11-GNR1-A22.

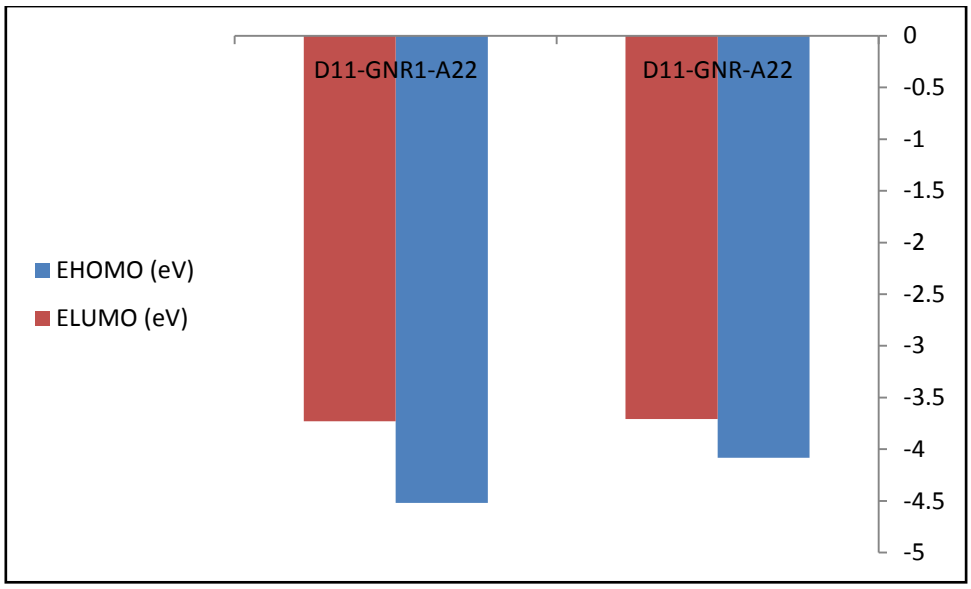

Figure (3.33): HOMO and LUMO distribution for D11-GNR-A22 and D11-GNR1-A22.

3.5.2 Ionization Energy and Electron Affinity

Table 3.20 shows the IE and EA values for the two structures D11-GNR-A22 and D11-GNR1-A22 calculated according to Koopmans theorem. Few variance was observed in both IE and EA for the two structures, this result is because of these two electronic properties depending on the same donor and acceptor in the two structures. Figure 3.34 shows the IE and EA for D11-GNR-A22 and D11-GNR1-A22.

Table 3.20: IE and EA for D11-GNR1-A22 and D11-GNR-A22.

Structures	IE (eV)	EA (eV)
D11-GNR-A22	4.083555	3.706138
D11-GNR1-A22	4.519475	3.730356

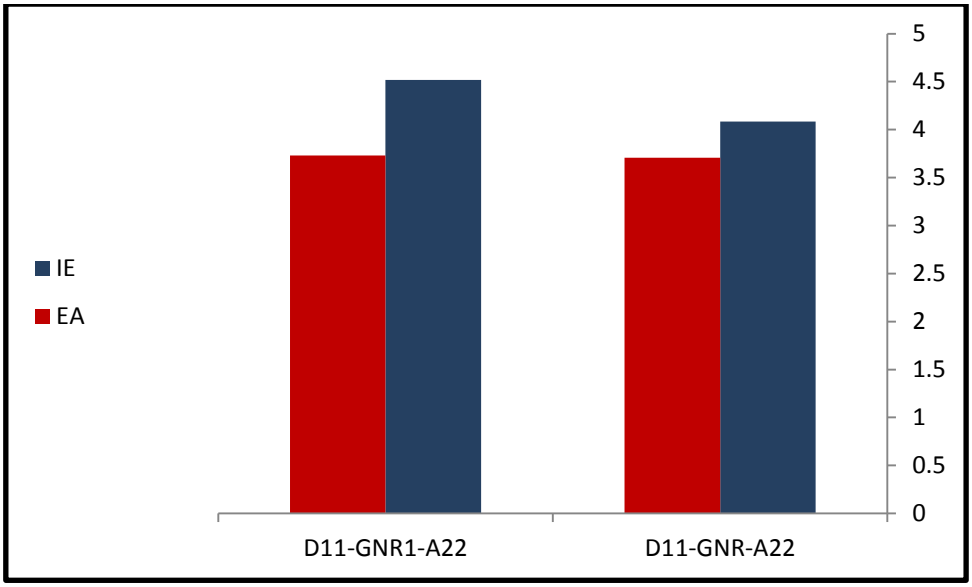

Figure (3.34): IE and EA for D11-GNR-A22 and D11-GNR1-A22.

3.5.3 Quantum Chemical Parameters

Table 3.21 declares the calculated values of some quantum chemical parameters included H, S and W for D11-GNR-A22 and comparing them with those for D11-GNR1-A22. The result showed the D11-GNR-A22 has electrochemical hardness lower than for D11-GNR1-A22 and it has electronic softness greater than for D11-GNR1-A22, as in Figures 3.35 and 3.36. These results show small excitation energy required for an electron to transfer from valence to conduction band. Instead, D11-GNR-A22 has high index of electrophilic to interacts with other molecules in the space in compared with D11-GNR1-A22. Figure 3.37 shows the W for D11-GNR-A22 and D11-GNR1-A22, respectively.

Table 3.21: Quantum chemical parameters for D11-GNR1-A22 and D11-GNR-A22.

Structures	H (eV)	S $(eV)^{-1}$	W(eV)
D11-GNR-A22	0.1887	2.6495	40.1938
D11-GNR1-A22	0.3945	1.2672	21.5619

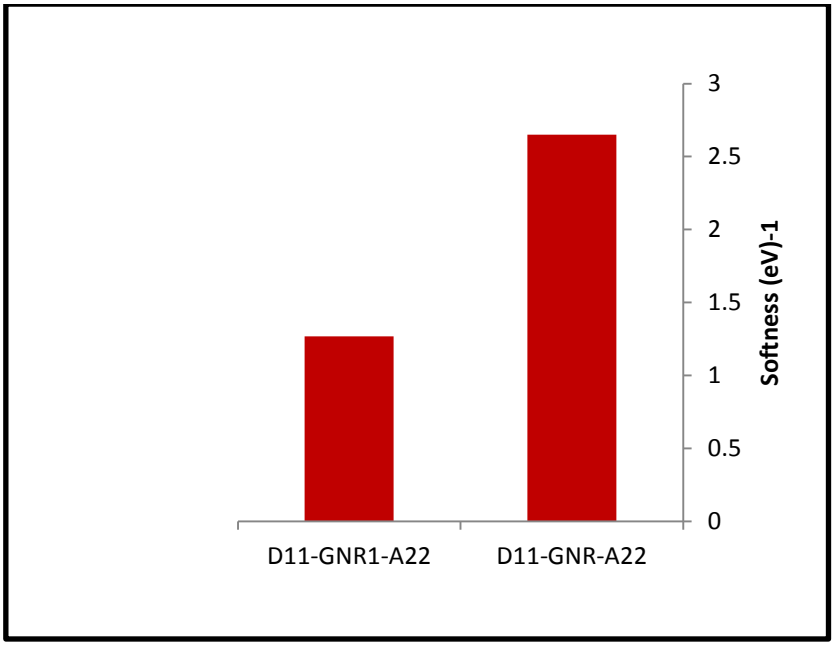

Figure (3.35): Hardness for D11-GNR-A22 and D11-GNR1-A22.

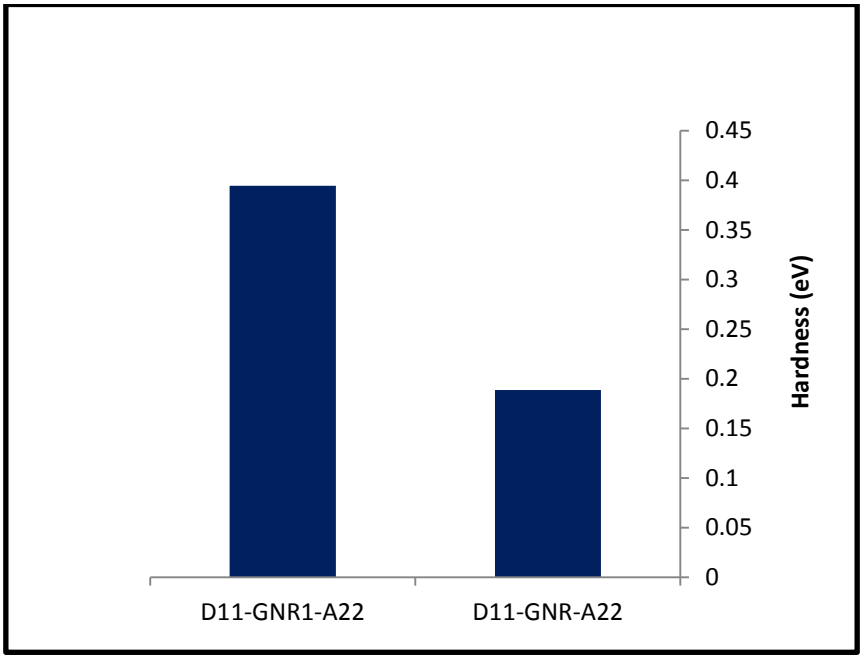

Figure (3.36) : Softness for D11-GNR-A22 and D11-GNR1-A22.

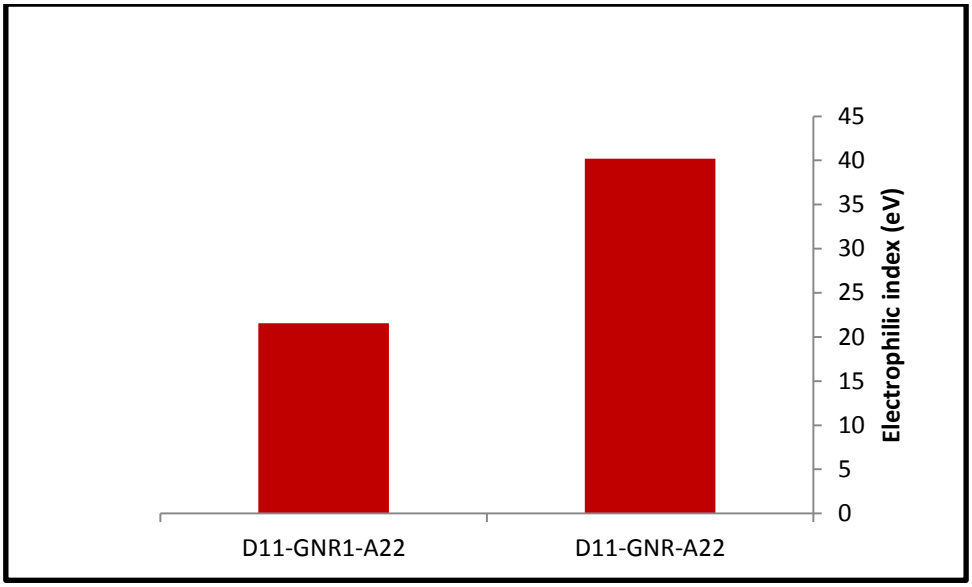

Figure (3.37): electrophilic **index W for D11-GNR-A22 and D11-GNR1-A22.**

3.5.4 Molecular Polarizability

Table 3.22 illustrates the molecular polarizability values for D11-GNR-A22 and D11-GNR1-A22. It is clear that the two structures have asymmetric formation with high dipole moment but D11-GNR-A22 has the highest. Also, D11-GNR-A22 has higher polarizability in comparison with D11-GNR1-A22. These results assistance to estimate the ability of the structures for gas sensing.

Table 3.22: Molecular Polarizability for D11-GNR1-A22 and D11-GNR-A22.

Structures	Total dipole moment (Debye)	Polarizability (a. u)			
		α_{xx}	α_{yy}	α_{zz}	α_{ave}
D11-GNR-A22	7.269	150.336	405.829	2107.770	887.978
D11-GNR1-A22	5.808	137.661	312.567	1802.987	751.071

3.6 D11-GNR-A22 / Gases

DFT calculations were used to estimate the sensitivity of D11-GNR-A22 structure for three types of gases. These gases are toxic and they are sarin , hydrogen sulfide and ammonia located at the surface of D11-GNR-A22, again a relaxation structure and electronic properties are computed, and other significant parameter is the adsorption energy was calculated to conclude the capability of sensing toxic gases via D11-GNR-A22 structure. Figure 3.38 illustrates the relax structure for D11-GNR-A22 / Gas.

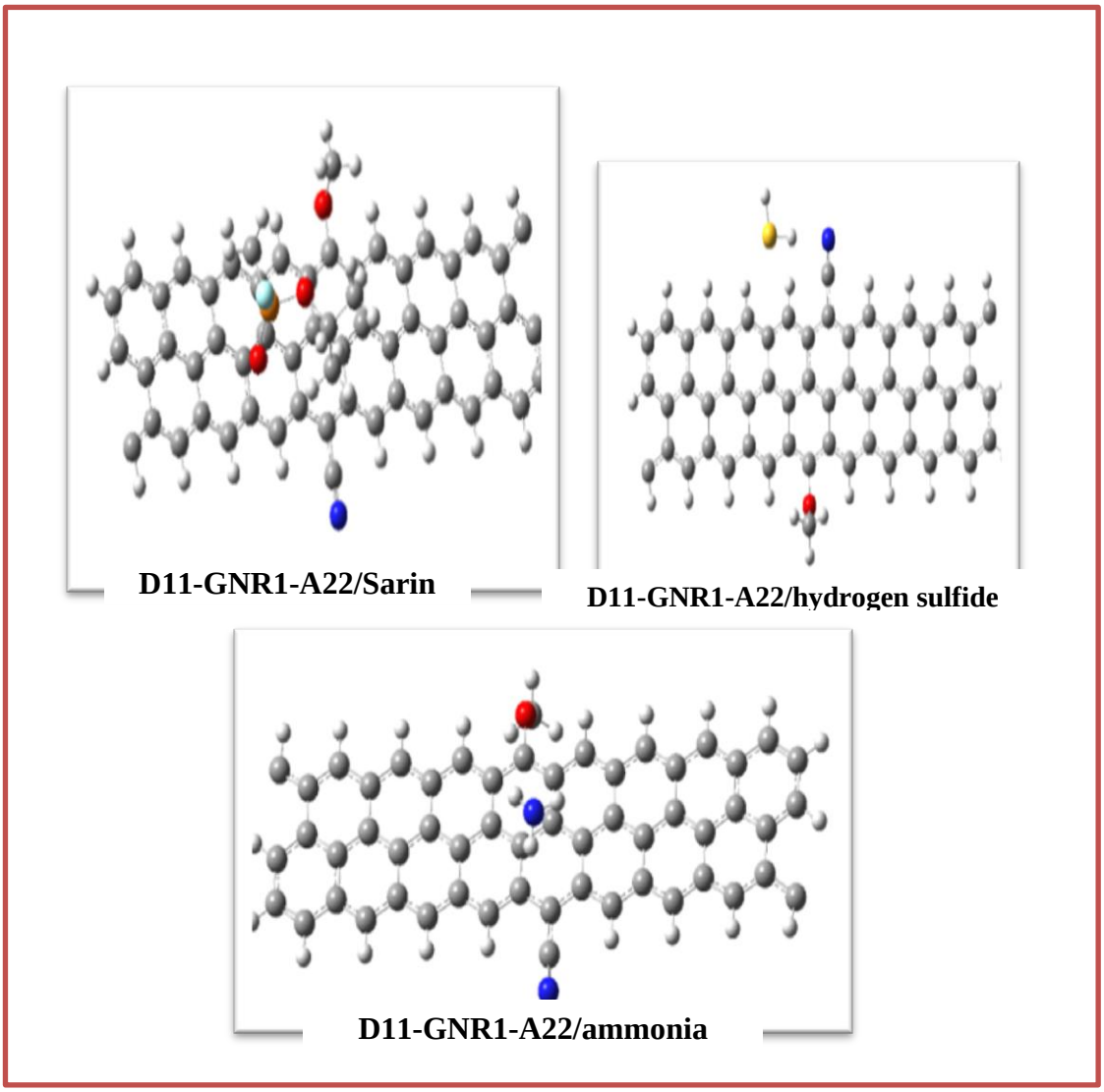

Figure (3.38) : Relax structure for D11-GNR-A22 / Gases.

The three gases sarin, hydrogen sulfide and ammonia are located at different distances on the surface of the D11-GNR1-A22 structure and in each one the relax was done to determine the stability of the system from the calculation of the minima ground state energy. Table 3.23 illustrates the distance and adsorption energy for the three gases, firstly study sensitivity of gases by the equation [111]:

S=[abs (Eg(1)-Eg(0))/Eg(0)]*100% (3-2)

Where Eg(1) energy gap when gas presence, Eg(0) energy gap when gas absence and S is sensitivity.

The theoretical model that describe adsorption energy following this equation[111]:

EAd=E(Gas+Rib.)-(E(Gas)+E(Rib.)) (3.3)

Where EAd represent adsorption energy, E(Gas+Rib.), E(Gas) and EE(Rib.) are total energy for mixture adsorption, gas molecule and isolated nano-ribbon, respectively.

Table 3.23: Adsorption energy and relax distance for D11-GNR-A22 / gas

Gases	Adsorption energy eV	Distance of relax nm	Sensitivity
Sarin	0.027	4.7	0.52103
Hydrogen sulfide	-0.797	3.1	0.14443
Ammonia	-0.0011	3.8	0.27587

The result in Table 3.23 showed the high sensitivity was recorded for the structure D11-GNR-A22 to sarin gas but at long distance 4.7 nm, means a small amount of energy transfer between the sarin and the structure. Decreasing the distance between the sarin gas and the structure may increase the adsorption energy but this also require forming bond

between the carbon atom in the ribbon and the atoms in sarin gas. On the other hand, the structure D11-GNR-A22 has low sensitivity for hydrogen sulfide gas at 3.1 nm and ammonia gas at 3.8 nm. In general, the sensitivity of D11-GNR-A22 structure was observed but in low amount.

Table 3.24 illustrates the calculations of UV-Vis for D11-GNR-A22 / gas (Sarin-Hydrogen sulfide-ammonia) included the absorption energy, maximum wave length and transition characters. These calculations were computed from the TD-DFT method. The result showed that the structure D11-GNR-A11/ sarin was appeared main band at 585 nm matches to absorption energy 2.16 eV with electronic transitions between the electronic states H-3→LUMO, H-5→LUMO and HOMO→LUMO. While the structure D11-GNR-A11/ hydrogen sulfide appeared two main bands, the first at 475 nm matches to absorption energy 2.24 eV with electronic transitions between the electronic states H-4→LUMO, H-5→LUMO, H-4→L+1 and H-2→L+1. And the second band appeared at 610 nm corresponding to absorption energy 2 eV. Above electronic transitions can be careful as $\pi \rightarrow \pi^*$ transitions. The structure D11-GNR-A11/ ammonia appeared main band at 550.45 nm matches to absorption energy 1.8202 eV with electronic transitions between the electronic states HOMO→LUMO(84%), H-2→LUMO (8%), H-5→LUMO (6%). In general, the electronic transitions are almost indirect transitions in UV-Vis range of electromagnetic radiation. Figures 3.39, 3.40 and 3.41 illustrates the UV-Vis spectrum for D11-GNR-A22/sarin, D11-GNR-A22/hydrogen sulfide and D11-GNR-A22/ammonia respectively.

Table 3.24: UV-Vis Calculations for D11-GNR-A22 / gas

Gas	Absorption Energy eV	Maximum Wave Length nm	Transition Character HOMO→LUMO
Sarin	2.16	585	H-3→LUMO (87%) H-5→LUMO (8%) HOMO→LUMO(3%)
Hydrogen sulfide	2.24	475	H-4→LUMO (87%) H-5→LUMO (3%) H-4→L+1(5%) H-2→L+1(4%)
	2.002	610	H-6→LUMO (12%) H-2→LUMO (84%) H-5→L+1(2%)
Ammonia	1.8202	550.45	HOMO→LUMO(84%) H-2→LUMO (8%) H-5→LUMO (6%)

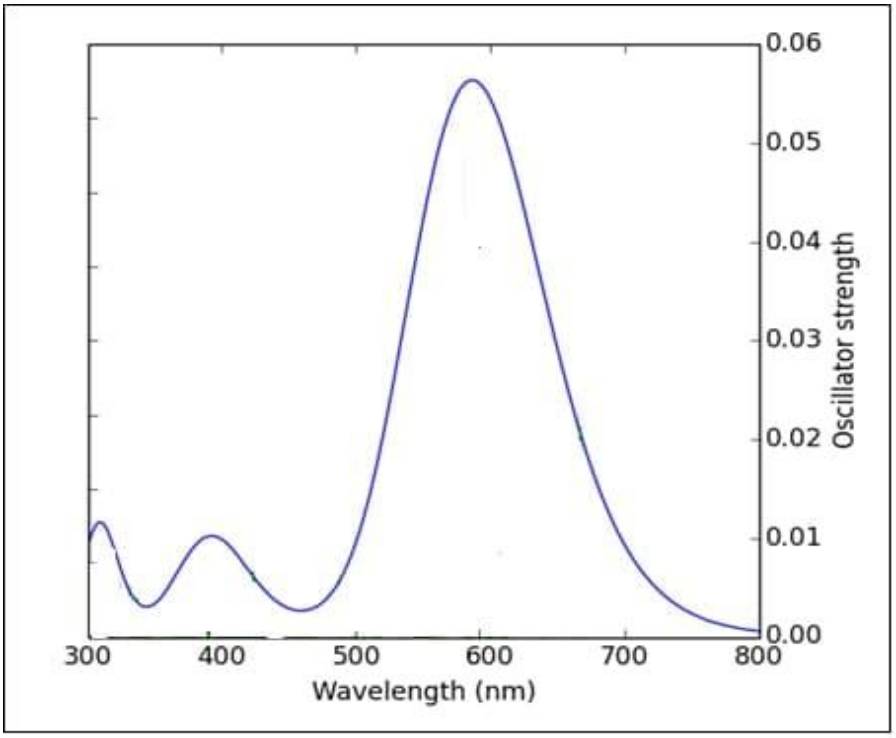

Figure (3.39): UV-Vis spectrum for D11-GNR-A22/sarin.

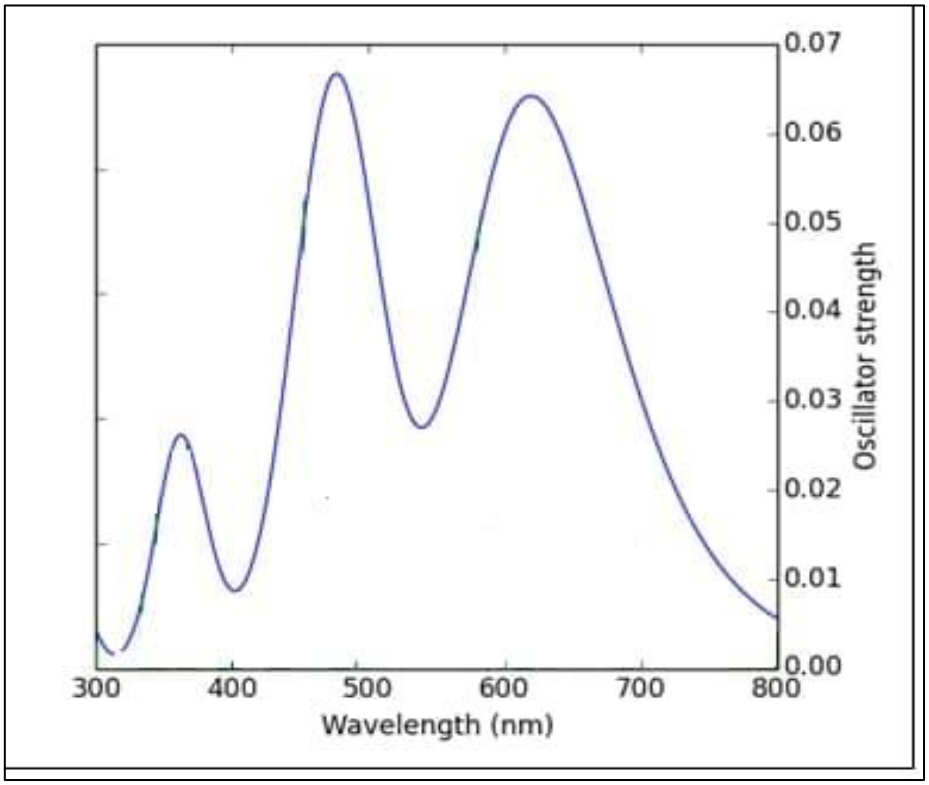

Figure (3.40) : UV-Vis spectrum for D11-GNR-A22/hydrogen sulfide.

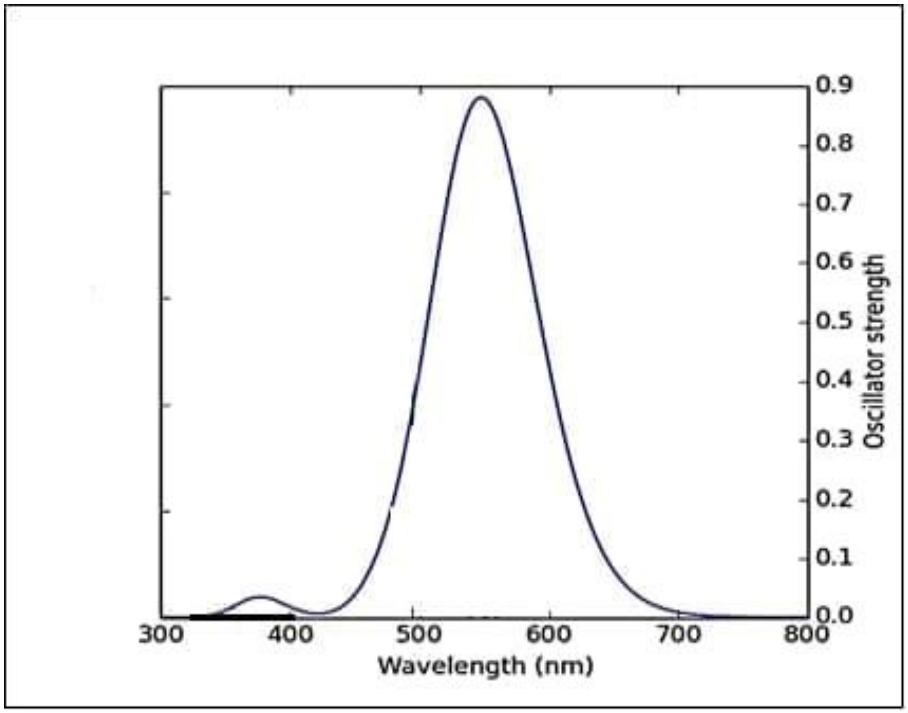

Figure (3.41) : UV-Vis spectrum for D11-GNR-A22/Ammonia.

Chapter Four
Conclusions and Suggestions for Future Work

4.1 introduction

In this study, the hybrid functional B3LYP with 6-31G basis sets under the theoretical methodology density functional theory has been employed.

4.2 Conclusions

4.2.1 D-GNR-A

1- The calculated values of geometrical parameters, total energy and viral ratio of the compounds are in a good agreement with experimental data and other theoretical studies.

2- Approximately, all the studied compounds showed change of LUMO and HOMO, which can play significant role in electronic properties. The effect of symmetry and distribution of aromatic rings has also an influence on the calculation of HOMO and LUMO.

3- Optimized structures depend on the positions and type of donor and acceptor molecules .

4- Energy gap is a useful global property where , the small energy gap calculated for pure graphene nanoribbon was reduced by adding donors and acceptors to the ribbon depending on the type of the donor and acceptor.

5- Dipole moment has effects which be related to the reactive positions of atoms because it describes properties of the whole molecules and for active sites.

6- Donor-GNR-Acceptor have low value of global electrochemical hardness and high electronic softness than those for pure GNR, the index of electrophilic for the GNR in case of presence of donors and acceptors is greater than that for pure GNR, therefore, donor-

GNR-acceptor can easily interact with surrounding species in comparison with pure GNR.

7- The electrophilicity increases when adding the donor and acceptor molecules and it is still the good descriptor, which may predict the reactive molecules with other atoms, molecules and groups. The electrophilicity is increasing from (33.353 eV) for graphene nanoribbon to (88.110)for A2-GNR-D4.

4.2.2 D-GNR1-A

Different width of graphene nano ribbon was studied, the results show that the dimensions of GNR make from these structures to have different electronic properties and different electronic applications can be recorded. Different structures of Donor-GNR1-Acceptor were constructed and studied in current thesis depending on characterization of the donors and acceptors, this result indicates that the constructed Donor-GNR-Acceptor molecules have high activity to interact with other molecules or species in the surroundings compared with the GNR.

4.2.3 Gas Sensing

As for the sensing of the graphene nanoribbon acceptor for the gas donor. The results refer to the two structure have different energy gap and other electronic properties that difference allow to decide which one of these two structures can performed in limit field of materials. The sensitive of D-GNR1-A structure was observed in low amount. The result showed that the electronic transitions are almost indirect transitions in UV-Vis range of electromagnetic radiation, The result showed the low sensitivity was recorded for the structure D11-GNR-A22 to sarin gas but at long distance 4.7 nm, means a small amount of energy transfer between the sarin and the structure. Decreasing the distance between the sarin gas

and the structure may increase the adsorption energy but this also require forming bond between the carbon atom in the ribbon and the atoms in sarin gas. On the other hand, the structure D11-GNR-A22 has low sensitivity for hydrogen sulfide gas at 3.1 nm and ammonia gas at 3.8 nm. In general, the sensitivity of D11-GNR-A22 structure was observed but in low amount.

4.3 Suggestions for Future Works

1- Study the electric and thermal properties of the studied structures
2- Test other types of donor acceptor molecules and make comparison with current study.
3- Investigating the effect of doping on studied structures
4- Use Graphene-like materials and studying its structural and electronic properties .
5- Using other types of toxic gases and checking sensitivity of these gases by the structures under study to these gases.

References

References

[1] Gryn'ova, Ganna, Kun-Han Lin, and Clémence Corminboeuf. **"Read between the molecules: computational insights into organic semiconductors".** Journal of the American Chemical Society 140.48 , PP.16370-16386, (2018).

[2] Vanin, M., **"Electronic and chemical properties of graphene-based structures: A density functional theory study".** Kgs. Lyngby, Denmark: Technical University of Denmark (DTU), (2011).

[3] Pauling, L., **"The Nature of the Chemical Bond".** Ithaca, NY: Cornell university press, Vol. 260, PP. 3175-3187, (1960).

[4] Harris, P. J.**, "Transmission electron microscopy of carbon: a brief history".** Journal of Carbon Research, Vol.4, PP.41-42, (2018).

[5] Seager, S. L., and Slabaugh, M. R. , **"Chemistry for today: General, organic, and biochemistry".** Cengage Learning, (2013).

[6] Smith, M. B. , **"March's advanced organic chemistry: reactions, mechanisms, and structure".** John Wiley and Sons, (2020).

[7] Allen, M. J., Tung, V. C., and Kaner, R. B. , **"Honeycomb carbon: a review of graphene".** Chemical reviews, Vol.110, PP.132-145, (2010).

[8] Dalosto, S. D., and Levine, Z. H. ,**"Controlling the band gap in zigzag graphene nanoribbons with an electric field induced by a polar molecule".** The Journal of Physical Chemistry C, Vol.112, PP.8196-8199, (2008).

[9] Neto, A. C., Guinea, F., and Peres, N. M. , **"Drawing conclusions from graphene".** Physics World, Vol.19, P.33, (2006).

[10] Novoselov K. S., Jiang D. , Schedin F., Booth T. J., Khotkevich V. V., Morozov S. V. and Giem A. K. , **"Graphene a Miracle Material",** Reviews of Modern Phy., Vol.81, (2009).

[11] Novoselov, K. S., Geim, A. K., Morozov, S. V., Jiang, D., Katsnelson, M. I., Grigorieva, I., and Firsov, A. A. , **"Two-dimensional gas of massless Dirac fermions in graphene".** nature,Vol. 438, PP.197-200, (2005).

[12] Stankovich, S., Dikin, D. A., Dommett, G. H., Kohlhaas, K. M., Zimney, E. J., Stach, E. A., and Ruoff, R. S. , **"Graphene-based composite materials".** nature, Vol.442, PP.282-286, (2006).

[13] Novoselov, K. S., Geim, A. K., Morozov, S. V., Jiang, D., Zhang, Y., Dubonos, S. V., and Firsov, A. A. , **"Electric field effect in atomically thin carbon films".** science, Vol.306, PP.666-669, (2004).

[14] Novoselov, K. S., Geim, A. K., Morozov, S. V., Jiang, D., Katsnelson, M. I., Grigorieva, I., and Firsov, A. A. , **"Two-dimensional gas of massless Dirac fermions in graphene**". nature, Vol.438, PP.197-200, (2005).

[15] Zhang, Y., Tan, Y. W., Stormer, H. L., and Kim, P. (2005). **"Experimental observation of the quantum Hall effect and Berry's phase in graphene".** Nature, Vol.438, PP.201-204, (2005).

[16] Lakshmi, S., Dutta, S., and Pati, S. K. **,"Molecular electronics: effect of external electric field".** The Journal of Physical Chemistry C, Vol.112, PP. 14718-14730, (2008).

[17] Nair, R. R., Blake, P., Blake, J. R., Zan, R., Anissimova, S., Bangert, U., and Latychevskaia, T. , **"Graphene as a transparent conductive support for studying biological molecules by transmission electron microscopy".** Applied Physics Letters, Vol.97, PP.152-153, (2010).

[18] Rooney, A. , **"Characterization of buried interfaces in van der Waals materials by cross sectional scanning transmission electron microscopy".** The University of Manchester (United Kingdom), (2017).

[19] Meyer, J. C., Geim, A. K., Katsnelson, M. I., Novoselov, K. S., Booth, T. J., and Roth, S. , **"The structure of suspended graphene sheets".** Nature, Vol.446, PP.60-63, (2007).

[20] Dutta, S., and Pati, S. K. **, "Novel properties of graphene nanoribbons: a review".** Journal of Materials Chemistry, Vol.20, PP.8207-8223, (2010).

[21] Eda G., Fanchini G., Chhowalla M., Nat. **"Nanotechnol".** Vol3, P.270, (2008).

[22] McAllister, M. J., Li, J. L., Adamson, D. H., Schniepp, H. C., Abdala, A. A., Liu, J., and Aksay, I. A. , **"Single sheet functionalized graphene by oxidation and thermal expansion of graphite".** Chemistry of materials, Vol.19, PP.4396-4404, (2007).

[23] Sun, C. Q. , **"Size dependence of nanostructures: Impact of bond order deficiency".** Progress in solid state chemistry, Vol.35, PP. 1-159, (2007).

[24] Wang Z. F., Li Q. X., Zheng H. X., Ren H., Su H. B., Shi Q. W. and Chen J. , Phys. Rev. B: Condens. **"Matter Mater".** Phys., Vol.75, P.113406, (2007) .

[25] Rao, C. N. R., Cheetham, A. K., and Thirumurugan, A., **"Hybrid inorganic–organic materials: a new family in condensed matter physics"**. Journal of Physics: Condensed Matter, Vol.20, P.083202, (2008).

[26] Bunch, J. S., Van Der Zande, A. M., Verbridge, S. S., Frank, I. W., Tanenbaum, D. M., Parpia, J. M., and McEuen, P. L., **"Electromechanical resonators from graphene sheets".** Science, Vol.315, PP. 490-493, (2007).

[27] Lamarsh, J. R., **"Introduction to nuclear reactor theory",** Addison-Wesley, (1966).

[28] Lamarsh, J. R., and Baratta, A. J. **,"Introduction to nuclear engineering ".** Vol. 3, P. 783. Upper Saddle River, NJ: Prentice hall, (2001).

[29] Nayak, T. R., Andersen, H., Makam, V. S., Khaw, C., Bae, S., Xu, X., and Ozyilmaz, B., **"Graphene for controlled and accelerated osteogenic differentiation of human mesenchymal stem cells"**. ACS nano, Vol.5, PP. 4670-4678,(2011).

[30] Tehrani, Z., Burwell, G., Azmi, M. M., Castaing, A., Rickman, R., Almarashi, J., and Guy, O. J., **"Generic epitaxial graphene biosensors for ultrasensitive detection of cancer risk biomarker"**. 2D Materials, Vol.1, P.025004, (2014).

[31] Aviram A and Ratner M A .chem.phys.lett,Vol.29, P. 277, (1994).

[32] Huda Bukheet Hassan, "**Density Function Theory B3LYP/6-31G**Calculation of Geometry Optimization and Energies of Donor-Bridge-Acceptor Molecular System**", International Journal of Current Engineering and Technology, Vol.4, P.4, (2014).

[33] Ramla A. A and Abbood H. I., "**Geometry Optimization and Energies of Donor-Bridge-Acceptor Molecular System:B3LYP/DFT Calculations**", Journal Of Kufa – Physics Vol.6, P.1, (2014).

[34] Jaafar T, A. and Abbood H. I., **"B3LYP/DFT Calculations of Donor-πbridge-Acceptor Molecular System",** IOSR Journal of Engineering , Vol. 04, Issue 09, (2014) .

[35] Timothy Hoan Vo,**. "Solution-Based Synthesis of Atomically Precise Graphene Nanoribbons".** The University of Nebraska-Lincoln, (2015).

[36] Ervasti M. M., Fan Z., Uppstu A., Krasheninnikov A. and Harju A. , **"Silicon and silicon-nitrogen impurities**" Vol.48, PP. 61-72, (2015).

[37] Abbood, H. I., and Mutashar, K. J., "**Study of the effect of the nanobridge length on the electroic properties of Donor-Nanobridge–Acceptor molecular system".** Journal of Kufa-physics, Vol.7, (2015).

[38] Gorczak-Vos, N., **"Mechanism and Dynamics of Charge Transfer in Donor-Bridge-Acceptor Systems",** (2016).

[39] Jayamurugan, G., Gowri, V., Hernández, D., Martin, S., Gonzalez-Orive, A., Dengiz, C., and Diederich, F. , **"Design and synthesis of**

Aviram–Ratner-type dyads and rectification studies in Langmuir–Blodgett (LB) films". Chem. Eur. J,Vol. 22, PP.10539-10547, (2016).

[40] Kozlov, O. V., Luponosov, Y. N., Solodukhin, A. N., Flament, B., Douhéret, O., Viville, P., and Pshenichnikov, M. S., **"Simple donor-acceptor molecule with long exciton diffusion length for organic photovoltaics"**. Organic Electronics, Vol.53, PP.185-190, (2017).

[41] Sisto, T. J., Zhong, Y., Zhang, B., Trinh, M. T., Miyata, K., Zhong, X., and Nuckolls, C., **"Long atomically precise donor–acceptor cove-edge nanoribbons as electron acceptors"**. Journal of the American Chemical Society, Vol.139, PP.5648-5651, (2017).

[42] Pour, M. M., Lashkov, A., Radocea, A., Liu, X., Sun, T., Lipatov, A., and Sinitskii, A., **"Laterally extended atomically precise graphene nanoribbons with improved electrical conductivity for efficient gas sensing"**, Vol.8, PP.1-9, (2017).

[43] Liu, Y. M., Hou, H., Zhou, Y. Z., Zhao, X. J., Tang, C., Tan, Y. Z., and Müllen, K., **"Nanographenes as electron-deficient cores of donor-acceptor systems".** Nature communications, Vol.9, PP.1-7,(2018).

[44] Huang, H., Strater, Z. M., Rauch, M., Shee, J., Sisto, T. J., Nuckolls, C., and Lambert, T. H. **"Electrophotocatalysis with a trisaminocyclopropenium radical dication.** ***Angewandte Chemie International Edition"*** , Vol.*58*, pp. 13318-13322, (2019).

[45] Shimizu, A., Ishizaki, Y., Horiuchi, S., Hirose, T., Matsuda, K., Sato, H., and Yoshida, J. I. , **"HOMO–LUMO Energy-Gap Tuning of π-Conjugated Zwitterions Composed of Electron-Donating**

Anion and Electron-Accepting Cation". The Journal of Organic Chemistry, (2020).

[46] Mutashar, K. J. , **"Characterization of Donor-Bridge-Acceptor Based on Aviram-Ratner Model".** Solid State Technology, Vol.63, PP.3547-3553, (2020).

[47] Mu, X., Wang, X., Quan, J., and Sun, M., **" Photoinduced Charge Transfer in Donor-Bridge-Acceptor in One-and Two-photon Absorption: Sequential and Superexchange Mechanisms"**. The Journal of Physical Chemistry C, Vol. 124, PP.4968-4981, (2020).

[48] Wan, X., Li, C., Zhang, M., and Chen, Y**., "Acceptor–donor–acceptor type molecules for high performance organic photovoltaics–chemistry and mechanism"**. Chemical Society Reviews, Vol. 49, PP. 2828-2842, (2020).

[49] Wang, Y., Shao, Y., Matson, D. W., Li, J., and Lin, Y. **,"Nitrogen-doped graphene and its application in electrochemical biosensing"**. ACS nano, Vol. 4, PP.1790-1798, (2010).

[50] Young, D. , **"Computational chemistry: a practical guide for applying techniques to real world problems"**. John Wiley and Sons, (2004).

[51] Griffiths, D. J. , **" Introduction to quantum mechanics"**. Prentice Hall, second edition (2010).

[52] Matthews P.T , **"Introduction to Quantum Mechanics"** Mc Graw-Hill, (1974).

[53] Schrödinger, E., **"SCHRÖDINGER 1926E"**. Annalen der Physik, Vol.81, P.109, (1926).

[54] Zhao, H. P., Feng, X. Q., and Gao, H. **, "Ultrasonic technique for extracting nanofibers from nature materials".** Applied physics letters, Vol.90, PP. 73-112, (2007).

[55] Richardson, T. H. (Ed.), **"Functional organic and polymeric materials: molecular functionality-macroscopic reality".** Wiley, , Richardson, TH, Ed., New York, P. 365. , (2000).

[56] Lin, S. K., **"Fundamentals of Quantum Chemistry: Molecular Spectroscopy and Modern Electronic Structure Computations",** ,PP. 291-292, (2001).

[57] Christopher, J. C., **"Essentials of computational chemistry: theories and models"**, (2004).

[58] Kenny Lipkowitz B., Larter R., Thomas Cundari R. and Boyd D.B. , **"Reviews in computational chemistry",** John Wiley and Sons, Inc.,Hoboken, New Jersey, (2005).

[59] Jensen, F., **"Polarization consistent basis sets: Principles".** The Journal of Chemical Physics, Vol.115, PP.9113-9125, (2001).

[60] Jensen F. **" Introduction to Computational Chemistry"**, John Wiley and Sons Ltd., the Atrium Southern Gate, Chichester, England, 2nd Edition, (2007).

[61] Cramer C. J. , **"Essentials of Computational Chemistry: Theories and Models"**, John Wiley and Sons Ltd., the Atrium, Southern Gate, Chichester England, 2nd Edition, (2004).

[62] Rogers, D. W. , **"Computational Chemistry using the PC."**, John Wiley and Sons, (2003).

[63] Cox, P. A**. "Introduction to quantum theory and atomic structure"**. New York: Oxford University Press, (1996).

[64] Valone, S. M., **"Quantal Density Functional Theory II. Approximation Methods and Applications"**, (2010).

[65] Maddala Sikder A. K., Agrawal G., Singh J. P. and Hazard H. J. , **"Mater",** Vol.84, PP.1-24, (2001).

[66] Kenny Lipkowitz B., Larter R., Thomas Cundari R., Boyd D. B **,"Reviews in computational chemistry",** John Wiley and Sons, Inc., Hoboken, New Jersey, (2005).

[67] Levine, I. N., Busch, D. H., and Shull, H., **"Quantum chemistry",** Vol. 6. Upper Saddle River, NJ: Pearson Prentice Hall , (2009).

[68] Sherrill, C. D., **"Introduction to Electronic Structure Theory"** , (2002).

[69] Koch W. and Holthausen M. C. . **"Achemist's Guide to Functional Theory"**, 2nd ed., Wiley- VCH Verilog, Germany, (2001).

[70] Chabinyc, M. L., Chen, X., Holmlin, R. E., Jacobs, H., Skulason, H., Frisbie, C. D., and Whitesides, G. M. , **"Molecular rectification in a metal− insulator− metal junction based on self-assembled monolayers"**. Journal of the American Chemical Society, Vol.124, PP. 11730-11736, (2002).

[71] Frank, J., **"Introduction to computational chemistry"**. Editorial Offices October, (1999).

[72] Hall, G. G. , "**The molecular orbital theory of chemical valency VIII. A method of calculating ionization potentials".** Proceedings of the Royal Society of London. Series A. Mathematical and Physical Sciences, Vol.205, PP. 541-552, (1951).

[73] Reimers, J. R., "**Computational methods for large systems: electronic structure approaches for biotechnology and nanotechnology**". John Wiley and Sons, (2011).

[74] Thiel, Walter. "**Semiempirical methods**" Modern methods and algorithms of quantum chemistry , PP. 261-283, (2000).

[75] Jasem Mohammed M**., "The Molecular Geometry and Electronic Structure of Some Macromolecules"**, Ph.D. Thesis, University of Basrah, (2005).

[76] Mohammed Merdan G. **, "Self-Consistent Field Calculation for the effect of Pressure and Temperature on some Properties of Greyt in Crystal",** M. Sc. Thesis, University of Babylon, (2005).

[77] Abd Ali Saeed K., "**A theoretical Study of the Structural Properties and its Correlation with the biological Activity of Stavudine and some Derivatives**", M. Sc. Thesis, University of Kufa, (2010).

[78] Matthews, P. T. **, "Introduction to quantum mechanics**", (1976).

[79] Dorsett, H., and White, A., "**Overview of molecular modelling and ab initio molecular orbital methods suitable for use with energetic materials**". Defense Science And Technology Organization Salisbury (Australia), (2000).

[80] Gotwals, R. R., and Sendlinger, S. C. **," A Chemistry Educator's Guide to Molecular Modeling".** The North Carolina School of Science and Mathematics, Durham, NC, (2007).

[81] Jones, R. O. , **"Introduction to density functional theory and exchange-correlation energy functional".** *Computational* Nanoscience: Do It Yourself, Vol.31, PP.45-70, (2006).

[82] Hutter, J. **, "Lecture notes in computational chemistry electronic structure theory".** Physical Chemistry Institute, University of Zurich, Winter thurerstrasse, Vol.190, P.8057, (2005).

[83] Reimers, J. R. , **"Computational methods for large systems: electronic structure approaches for biotechnology and nanotechnology".** John Wiley and Sons, (2011).

[84] Fitts, D. D., **"Principles of quantum mechanics: as applied to chemistry and chemical physics".** Cambridge University Press, (1999).

[85] Kenny Lipkowitz B.,Larter R., Thomas Cundari R. and Boyd D. B., **" Reviews in computational chemistry"**, John Wiley and Sons, Inc., Hoboken, New Jersey, Vol. 21, (2005).

[86] K. Xia, M. Zwierzycki, M. Talanana, P. J. Kelly, and Bauer G. , Journal of **" Physical Review B",** Vol.73, PP.1-6, (2006).

[87] Hohenberg P. and Kohn, Journal of **"Physical Review"** , Vol.136, PP.864-871, (1964).

[88] Zhan C., Nichols J. and Dixon D., Journal of **" Physical Chemistry A"**, Vol.107, PP.41-84, (2003).

[89] Sadasivam, K., and Kumaresan, R. **, "Theoretical investigation on the antioxidant behavior of chrysoeriol and hispidulin flavonoid compounds–A DFT study"**. *Computational and Theoretical Chemistry*, Vol.963, PP.227-235, (2011).

[90] Fleming, J., **"Frontier Orbitals and Organic Chemical Reactions"**, John Wiley, London, (1976).

[91] Kim, B. G., **"Mercury-containing species and carbon dioxide adsorption studies on inorganic compounds using density functional theory",** (2010).

[92] Naghavi, S. S., **"Theoretical study of correlated systems using hybrid functionals"**, (Doctoral dissertation, Ph. D. Thesis, Johannes Gutenberg-Universität, Mainz), (2010).

[93] Riahi, S. Eynollahi and Ganjali M. **"Journal of International Electrochemical Science",** Vol.4, PP.11-28, (2009).

[94] Hazim, A., Abduljalil, H. M., and Hashim, A. , **"Analysis of Structural and Electronic Properties of Novel (PMMA/Al 2 O 3, PMMA/Al 2 O 3-Ag, PMMA/ZrO 2, PMMA/ZrO 2-Ag, PMMA-Ag) Nanocomposites for Low Cost Electronics and Optics Applications"**. Transactions on Electrical and Electronic Materials, Vol.21, PP.48-67, (2020).

[95] Thangwane, S. C., **"Synthesis and characterization of substituted dithiocarbamates ligands and complexes as a source of metal (Pb, Ni and Co) sulphide nanoparticles"**, Doctoral dissertation, Vaal University of Technology, (2017).

[96] Sancho-García, J. C., and Pérez-Jiménez, A. J**. "A theoretical study of π-stacking tetracene derivatives as promising organic molecular semiconductors".** Chemical Physics Letters, Vol.499, PP.146-151, (2010).

[97] Fleming, I., **"Molecular orbitals and frontier orbitals Frontier Orbitals and Organic Chemical Reactions",** (Fleming, I., Ed.), John Wiley and Sons, New York, PP.5-32, (1976).

[98] Ferrer, J., Lambert, C., García-Suarez, V., Bailey, S., Hatef, S., and Manrique, D. **"GOLLUM version 1.0."** Lancaster University, (2014).

[101] Mazhir, S. N., Abbood, H. I., and Abdulridha, H. A., **"Electron Transport in Graphene-B/P compound Heterojunction Using LDA/SZ".** International Journal of Advanced Engineering Research and Science, Vol.3, PP. 236-762, (2016).

[102] Ali, A. M. , **"Investigations of some antioxidant materials by using density functional and semiempirical theories**". P. hD. Thesis, University of Basrah, College of Science, Department of Physics, (2009).

[103] M. J. Frisch, G. W. Trucks, H. B. Schlegel, G. E. Scuseria, M. A. Robb, J. R. Cheeseman, G. Scalmani, V. Barone, B. Mennucci, G. A. petersson, H. Nakatsuji, M. Caricato, X. Li, H. P. Hratchian, A. F. Izmaylov, J. Bloino, G. Zheng, J. L. Sonnenberg, M. Hada, M.Ehara, K. Toyota, R. Fukuda, J. Hasegawa, M. Ishid, T. Nakajima, Y. Honda, O. Kitao, H. Nakai, T. Vreven, J. A. Montgomery, Jr., J. E. Peralta, F. Ogliaro, M. Bearpark, J. J. Heyd, E. Brothers, K. N. Kudin, V. N. Staroverov, R. Kobayashi, J. Normand, K. Raghavacharii, A. Rendell, J. C. Burant, S. S. Iyengar, J. Tomasi, M.

Cossi, N. Rega, J. M. Millam, M. Klene, J. E. Knox, J. B. Cross, V. Bakken, C. Adamo, J. Jaramillo, R. Gomperts, R.E Stratmann, O. Yazyev, A. J. Austin, R. Cammi, C. Pomelli, J. W. Ochterski, R. L. Martin, K. Morokuma, V. G. Zakrzewski, G. A. Voth, P. Salvador, J. J. Dannenberg, S. Dapprich, A. D. Daniels, O. Farkas, J. B. Foresman, J. V. Ortiz, J. Cioslowski and D. J. Fox, **"Gaussian 09, revision A. 02 Gaussian, Inc"**, Wallingford CT., (2009.

[104] Pacheco, A. B. , **"Electronic Structure Calculations in Quantum Chemistry"**, (2011).

[105] McKinney W., **"Python for data analysis: Data wrangling with Pandas, NumPy, and IPython".** O'Reilly Media, Inc., (2012).

[106] Williams, T., and Kelley, C., **"GNU plot: an interactive plotting program",Molecular rectifiers**. Chemical physics letters, Vol.29, PP. 277-283, (1974).

[107] Reddy, S., Xu, X., Guo, T., Zhu, R., He, L., and Ramakrishana, S. **,"Allotropic carbon (graphene oxide and reduced graphene oxide) based biomaterials for neural regeneration".** Current Opinion in Biomedical Engineering, Vol.6, PP.120-129, (2018).

[108] Salman Jabour H**., "The Effect of Fluorine on the Structural, Electronic and Electrical Properties of Graphene Sheet by Using the Mathematical Hamiltonian Model",** PH.D Dissertation , University of Babylon, (2017).

[109] Gotwals R.R. and Send linger Shawn C., **"A Chemistry Educator's Guideto Molecular Modeling",** 1st Edition, North Carolina School of Science and Mathematics Center, USA, (2008).

[110] Palmieri, V., and M. J. N. T. Papi. **"Can graphene take part in the fight against COVID-19"**, Nano Today, Vol.33, P.100883, (2020).

[111] Huang Y., Yang H., Xiong T., Adekoya D., Qiu W., Wang Z., Zhang S., and Balogun M. S., **"Adsorption energy engineering of nickel oxide hybrid nanosheets for high areal capacity flexible lithium-ion batteries",** Energy Storage Materials, Vol. 25, PP. 41-51 , (2020).

الخلاصة

تركز الدراسة الحالية على دراسة تأثير مختلف الجزيئات القابلة والمانحة على الخصائص التركيبية والفيزيائية لشريط الكرافين النانوي المصمم وفقًا لنموذج افيرام- راتنر وفقا للتطبيقات الإلكترونية للتراكيب المصممة الجديدة. يتم تنفيذ جميع الحسابات من خلال استخدام نظرية دالية الكثافة B3LYP مع مجموعات أساس قياسية 6-31G.

الجزيئات المانحة والقابلة لديهم قيم مختلفة لفجوة الطاقة تعتمد على نوع كل منها. تم حساب بعض الخصائص الإلكترونية مثل طاقة التأين IE والالفة الإلكترونية EA والنعومة والصلابة ومؤشر الإلكتروفيليك (electrophilic) ، بوحدة الالكترون- فولت للجزيئات المانحة والقابلة و شريط الكرافين النانوي (GNR) قيد الدراسة. توفر القيم المختلفة لطاقة التأين والالفة الإلكترونية للجزيئات المانحة والقابلة المدروسة السماحية لبناء المانح- نانوريبون- القابل بشكل منهجي. تم إنشاء العديد من التراكيب من الجزيئات المانحة- نانوريبون - القابلة، يعتمد اختيار كل من المانح والقابل على سلوك كل منهما . أظهرت النتائج ان تراكيب Donor-GNR-Acceptor المصممة لها أقل قيمة لفجوة الطاقة مقارنةً بGNR، وجميع جزيئات Donor-GNR-Acceptor المدروسة لها قيم الفة إلكترونية أعلى من GNR الأساسي. يؤدي تغير Eg والالفة الإلكترونية للتراكيب إلى تطبيقات مختلفة في المجال الإلكتروني.

أظهرت النتائج أن الصلابة انخفضت عند إضافة جزيئات المانح والقابل إلى شريط الكرافين النانوي، وبعبارة أخرى ، فإن جزيئات Donor- GNR-Acceptor المصممة أكثر نعومة من GNR تم زيادة المؤشر electrophilic بإضافة جزيئات المانحة والقابلة. تشير هذه النتيجة إلى أن جزيئات Donor-GNR-Acceptor المصممة لها نشاط عالي للتفاعل مع الجزيئات أو الأنواع الأخرى في البيئة مقارنة مع GNR. كان تأثير وجود كل من المانح والقابل على توزيع الجهد الكهروستاتيكي واضحًا حيث تم سحب الإمكانات الكهروستاتيكية نحو مناطق التركيز العالي للشحنات في كل جزيء مانح - GNR - قابل. نلاحظ أن العزم ثنائي القطب لـ GNRهو صفر بينما التراكيب الأخرى لها قيم مختلفة للعزم ثنائي القطب والتي تشير إلى التوزيع المتماثل المنخفض لهذه التراكيب، وهذا يعطي تراكيب Accepter-GNR-Donor قدرة عالية على نقل الإلكترون بالمقارنة مع GNR الأساسي .

وبالنسبة للتحسس عن متلقي الكرافين النانوي الشريط المانح للغاز فتشير النتائج إلى أن التركيبين لهما فجوة طاقة مختلفة وخصائص إلكترونية أخرى يسمح هذا الاختلاف بتحديد أي من هذين التركيبين يمكن أن يؤدي في مجال الحد من المواد. لوحظ ان حساسية بنية Donor-GNR1-Acceptor انها منخفضة. كما وأظهرت النتيجة أن التحولات الإلكترونية هي تقريبًا انتقالات غير مباشرة في نطاق الأشعة المرئية وفوق البنفسجية للإشعاع الكهرومغناطيسي.

جمهورية العراق
وزارة التعليم العالي والبحث العلمي
جامعة بابل/ كلية العلوم
قسم الفيزياء

تأثير الجزيئات القابلة والمانحة على بعض الخصائص الفيزيائية لشريط الكرافين النانوي

رسالة مقدمة إلى قسم الفيزياء – كلية العلوم – جامعة بابل
وهي جزء من متطلبات نيل درجة الماجستير في العلوم /علوم الفيزياء

من قبل

رباب عبد الزهرة مسلم عبد الله

بإشراف

أ. م. د. نضال محمد عبيد الشريفي

أ. د. حامد ابراهيم عبود التميمي

١٤٤٣هـ

٢٠٢١ م